INVESTIGATION OF POWER CONVERTER TOPOLOGIES FOR STANDALONE DC SYSTEM

Thesis

Submitted in partial fulfillment of the requirements for the degree of

DOCTOR OF PHILOSOPHY

by

KHARE ANVIT

DEPARTMENT OF ELECTRICAL AND ELECTRONICS ENGINEERING
NATIONAL INSTITUTE OF TECHNOLOGY KARNATAKA,
SURATHKAL, MANGALORE - 575025

MARCH, 2024

DECLARATION

by the Ph.D. Research Scholar

I hereby ***declare*** that the Research Thesis entitled **INVESTIGATION OF POWER CONVERTER TOPOLOGIES FOR STANDALONE DC SYSTEM** which is being submitted to the ***National Institute of Technology Karnataka, Surathkal*** in partial fulfillment of the requirement for the award of the Degree of ***Doctor of Philosophy*** in **Department of Electrical and Electronics Engineering** is a ***bonafide report of the research work carried out by me***. The material contained in this Research Thesis has not been submitted to any University or Institution for the award of any degree.

177129177EE004, KHARE ANVIT

Department of Electrical and Electronics Engineering

Place: NITK-Surathkal.

Date: 12-03-2024

CERTIFICATE

This is to certify that the Research Thesis entitled **INVESTIGATION OF POWER CONVERTER TOPOLOGIES FOR STANDALONE DC SYSTEM** submitted by Khare Anvit,(Register Number: 177129177EE004) as the record of the research work carried out by him, is *accepted as the Research Thesis submission* in partial fulfillment of the requirements for the award of degree of **Doctor of Philosophy**.

Dr. A. Karthikeyan

(Research Guide)

12/3/2021

Prof. D.N. Gaonkar

(Chairman- DRPC, EEE dept.)

PROFESSOR AND HEAD
DEPARTMENT OF ELECTRICAL AND ELECTRONICS ENGINEERING
NATIONAL INSTITUTE OF TECHNOLOGY KARNATAKA
SRINIVASNAGAR, SURATHKAL, MANGALORE - 575 025, INDIA

Acknowledgements

I will be forever thankful to my guide Dr. A. Karthikeyan for giving me the opportunity of working under him.His patience, encouragement and constant guidance are the only reasons for the completion of this work. The availability of power electronics laboratory set-up developed by him has helped in my work, allowing me to concentrate on the main objectives of the research.

I am very thankful towards the members of my Research Progress Assessment Committee, Dr. CMC Krishnan and Dr. V. Murugan for their valuable suggestions.

The Electrical and Electronics Engineering Department of NITK has given me a conducive environment and excellent facilities for conducting this research. For this, I thank Prof. Dattatraya N. Gaonkar, HOD of the dept and also very thankful to the former HODs Prof. B.Venkatesa Perumal, Prof. K. N. Shubhanga and Prof. G. S. Punekar who have successively headed the department during the tenure of my doctoral research.

I ought to place on record my gratitude to my lab-mates -Dr. KK Prabhakaran, Dr. Krishna Abhilash, Dongara Ramesh, Preeti A.G . I also thank my fellow research scholars and friends- Vikas, Roopa, Aalam, Teena, Shiva, Vishnu, Rasa, Amal, Supradeep and Santosh at the Electrical Engineering Department, for their constant help and support. Also, I am thankful to staff members of the department for their support.

I will always be grateful to my family for their consistent encouragement and support over the course of my research work.

To conclude, I want to express my gratitude to God Almighty for giving me the strength and patience to successfully complete this research work.

NITK-Surathkal Khare Anvit

Abstract

The power distribution system, mainly powered by the utility grid, is under more strain due to constant rise in load demand. This conventional distribution system will cater to DC load at the end of the power chain. However, there are several power conversion stages involved before generating a DC output. Consequently, there will be power loss at various conversion points. Therefore, to address this situation, a standalone DC system using solar and wind energy sources together is suitable solution to cater for the DC load demand.

The solar and wind energy are known to be complementary in nature. However, combining these sources together necessitates use of appropriate power converters. In recent years, many researchers have put forth the numerous power conversion methods with these sources. These conversion stages comprises with the qualities of reliability and simplicity in operation. Therefore, various efforts have been laid in these directions to reduce the intermediate conversion stages and to ensure the reliability of hybrid input energy supply at the load side.

In pursuance of overcoming the redundancy involved in the conversion stages, a PV-wind sources based single stage hybrid power converter has been proposed that takes into consideration the concurrent conversion processes of wind sources and solar sources power together to the supply load demand simultaneously. In this work, primary focus is laid down on the design and development of this hybrid input based power converter. The converter aspects of operating principle and operational modes have been discussed to bring out the operational merit over the other existing hybrid system structures in standalone system. The comprehensive control strategies and appropriate PWM scheme for performing simultaneous conversion processes has been discussed. Further, the operational aspects of the proposed converter is verified through simulation case studies. In addition, a laboratory prototype power converter is developed and operational aspects are validated through experimental case studies. Lastly, with regard to the simulation and experimental results, it can be stated that the proposed hybrid power converter offering the single stage circuitry is suitable for PV-wind sources based standalone DC system.

Contents

List of Figures

List of Tables

Chapter 1

INTRODUCTION

1.1 Background

In today's time, there are still some unelectrified places in both the developing and developed nations. Many distant communities are physically and geographically located far away from the main grid, making it impossible for them to access electricity (Finance et al., 2016). As per the survey (Arriaga et al., 2014), it is estimated that approximately 1.2 billion people still rely on conventional techniques to keep their houses powered and remain in the dark. The lack of power has substantially hindered the growth of such areas. In order to combat this prevailing issue, power delivery in both a qualitative and quantitative way has been prioritized by all nations, international energy agencies, and non-governmental organizations (NGOs) to encourage economically excluded communities with access to the essential services. This prevailing problem of power scarcity can be solved by installing an off-grid DC (Direct Current) systems that are specifically developed under these circumstances. Utilizing a DC off-grid system has the primary benefit of being completely powered by renewable energy. This is regarded as golden opportunity to start developing and thereby deploying renewable energy solutions in the areas where the grid cannot reach. Because most necessities, like lights and phone chargers, require DC, renewable energy technologies, such as solar PV and wind turbines, can be incorporated for catering this DC loads. These devices require recharging their storage batteries that also require the usage of DC power. The DC off-grid solutions will therefore be appropriate for isolated areas where obtaining grid access is challenging.

In the recent years, DC microgrid systems have gained immense popularity. Many coun-

tries are conducting research in this area to alter the method by which buildings are electrified. This DC grid based system is viewed as a potential alternative to the conventional AC electricity network due to its numerous benefits. Therefore, there is a common viewpoint in using DC electricity for providing electrification in localities of isolated areas as well as in the buildings of metropolitan areas.

The concept of DC electrification is existing in ancient times as well since it used to exist in practice before the arrival of AC based electrification as there was the need for electricity at the time was DC. The usage of AC energy was impacted by the development of the more modern appliances such as air conditioning, AC (Alternating Current) motors, and long-distance power transmission (Anand and Fernandes, 2010), (Rodriguez-Diaz et al., 2015). Now, the number of home appliances that are able to function with the DC is continuously increasing, and new ones are being developed all the time. Most electrical equipment in use today, such as laptops, computers, televisions, and so on, require DC to operate. The adaptors that come with these appliances allow the appliances to take in alternating current and convert it to a low voltage direct current. However, if the electricity is DC, this conversion can be avoided. DC is employed in the majority of the appliances that are used in day-to-day life, such as light bulbs that have been in use for a long period. Due to the technological advancements, now LED lights are in use, which work by converting AC to DC with a sufficient working voltage. The power loss involved with this AC to DC conversion is one of the major drawbacks which is making energy availability at the consumer side very less. Due to these drawbacks, the DC electrical network is being considered as a possible alternative to the conventional AC grid in many countries (Rodriguez-Diaz et al., 2015).

1.2 Characteristics of DC Microgrid

A DC microgrid is a self-contained network of power sources, energy storage devices, and loads that are often interfaced to a larger grid. This type of network is also known as a distributed control microgrid. Similar to a conventional power grid, a microgrid incorporates power generation, distribution, and control systems for voltage management (Kurohane et al., 2011), (Kumar et al., 2012). The near proximity of power generation and end users is the primary distinguishing feature of a microgrid in comparison to the conventional grid. Owing to the recent advancements in various renewable energy sources, there has been a

significant upsurge in interest in microgrids in recent years. One way of contemplating the microgrid is like a conventional power grids that has been compressed down to a smaller scale. Traditional utility grids, which are often measured in megawatts (MW), are typically far larger than their more compact counterparts, known as microgrids. Microsources such as solar arrays, wind turbines, and other forms of renewable energy may be combined to form microgrids. These microgrids are then able to supply electricity to the demand that they were designed to serve. Over the past several years, as technology related to renewable energy has evolved, an increasing number of renewable energy sources have been employed in microgrids. The bulk of the load is comprised of microprocessor-based control and power electronics devices, which are becoming an increasingly large proportion of the equipment that is becoming increasingly sensitive to fluctuations in power quality in comparison to the past.

1.2.1 Merits and Demerits of DC based electrification

Merits of DC distribution

Compared to AC electricity, DC electrification has many advantages (Zhang et al., 2012). Among the notable features that distinguish DC in the distribution field, are a few of the following (Oliver and Line, 2012):

- Unlike AC distribution, DC distribution does not require synchronization.
- It can be drawn either directly or indirectly from the grid and renewable energy sources.
- There is no requirement for phase-balancing
- There are no harmonic issues.
- In comparison to the AC distribution, the investment in conductors, cables, etc. is relatively less.

The significance of DC microgrids is not just restricted to rural areas where it is difficult to extend grid connection, but it is also being taken into account to power office buildings, data centers, etc (Zhang et al., 2012). Also, when coordinated with the grid, it can supply a steady and dependable amount of energy.

Demerits of DC distribution:

Despite many benefits of the DC distribution systems, it still has several shortcomings. The DC distribution's safety measures are the main issues. In this regard, there is a research ongoing in the safety aspects (Dragičević et al., 2015), (Kumar et al., 2017).
The safety concerns pertaining DC distribution:

- No current and voltage zero crossing .
- An arc occurring during switching.

1.3 Various Stand-alone DC Systems

The Stand-alone DC system is an alternative power network that includes distributed energy sources such as photovoltaic (PV) arrays, micro-wind turbines, fuel cells, and various types of energy storage devices (such as batteries, super capacitors, etc.)(Anand and Fernandes, 2010),Samrat et al. (2015). Because of the intermittent nature of these resources, it is necessary to utilise the appropriate power converters in order to extract their energy and channelise in useful form. As a result of this, several different architectures of the standalone DC systems have been proposed and developed, that tries to extract their energy depending on the availability of the resources.

1.3.1 Wind Energy Conversion System

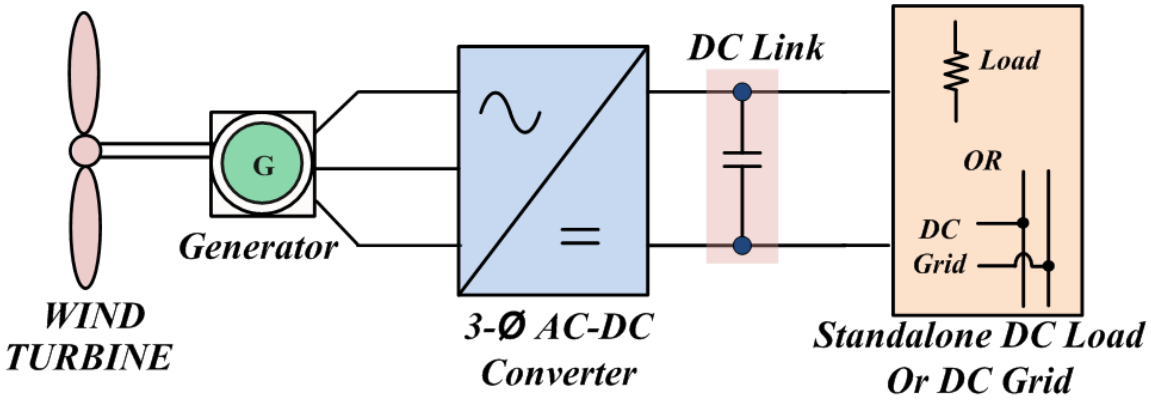

Figure 1.1: Wind Energy Conversion System for Standalone DC system

In a wind energy conversion system(WECS), the wind energy is transformed into mechanical energy so that it can be fed to an electrical generator to produce electricity. Figure 1.1

presents the configuration of a wind energy conversion based DC system. In this system, it is possible to employ variety of generators in wind turbines, including a permanent magnet synchronous generator (PMSG), a doubly-fed induction generator, an induction generator, a synchronous generator,etc. (Wu et al., 2011),(Amin and Mohammed, 2011),(Misra and Jain, 2018) and (Amin and Mohammed, 2011). As the generator receives the mechanical energy fed by the wind turbine thereby with the use of appropriate three-phase AC-DC converter (Iacchetti and Marques, 2015) , (Gundavarapu et al., 2017), the power generated by the generator will be delivered to either a standalone DC load or the DC grid. Depending on the load requirements, the control scheme can be on the employed converter to derive the necessary power out of the wind energy conversion system.

1.3.2 Solar PV array based conversion system

A system is regarded as a solar PV array based standalone system when it draws its major supply of power from the sun's rays alone. At any locations which is having ample amount of solar energy, a standalone solar electrical system can be the ideal source of electricity with regard to availability of solar energy. These systems can simply be consisting of PV modules and a load, or they might include batteries as well. However, as solar PV provides intermittent DC output, it is often required for using an appropriate DC-DC converter that needs to be interfaced with the PV array in order to extract PV power in usable form.

Figure 1.2 depicts the solar PV array based standalone DC system (Chiang et al., 2009), (Coelho et al., 2010), (Singh et al., 2017). As it can be perceived that PV array is connected to the DC-DC converter in order to supply power to the standalone DC load or DC Grid. Depending on the application requirements, an appropriate control strategy can be employed to supply the necessary power at the load port continuously. Therefore, depending on the DC grid system or standalone DC system, operational aspects of the system can have either maximum power extraction control or DC voltage regulation control.

1.3.3 Hybrid Structures

Because of the scarcity of fossil fuels and the global greenhouse effect, demand for renewable energy has risen significantly (Daniel and AmmasaiGounden, 2004). Solar and wind energy, among the different types of renewable energy sources, are the most promising for human use. The photovoltaic (PV) and wind power generation systems have grown fast as

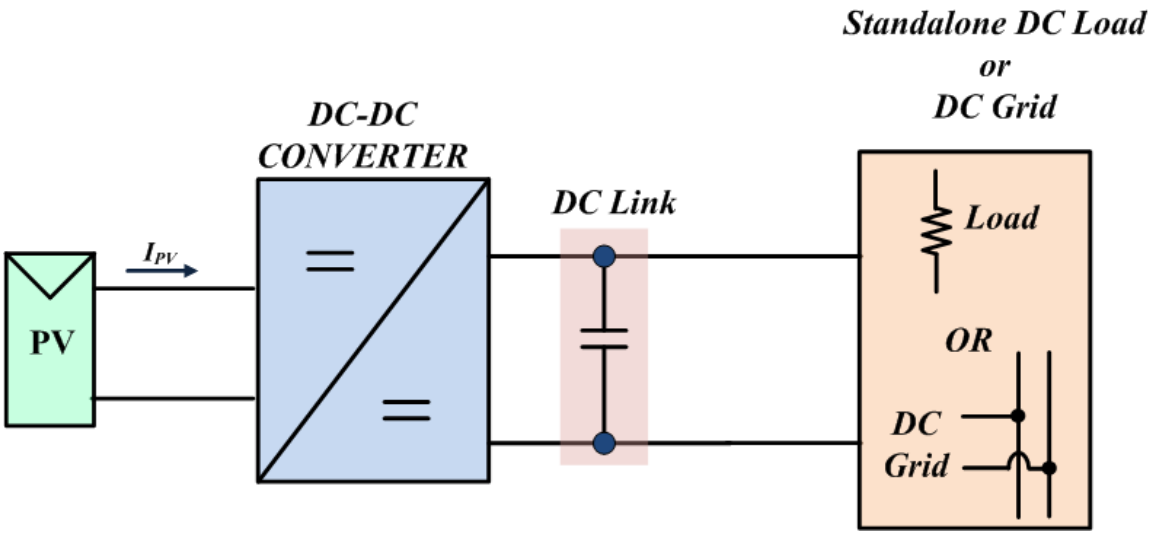

Figure 1.2: Solar PV Array based Standalone DC system

a result of the rapid growth of power electronics technology (Krishna and Kumar, 2015). With regard to the inherent nature of solar and wind energy, the PV source and the wind source are complementary in nature. Therefore, the hybrid PV-wind power system is more reliable than any single source in terms of supplying constant electricity. The important hybrid inputs-based configuration has been explored in this section (Figure 1.3 - Figure1.6).

Structure 1 :- In Figure 1.3, this structure is regarded as primitive approaches in hybrid based systems wherein individual converters or conversion stages are being employed with each sources as mentioned in (Chen et al., 2006), (Chiang et al., 2010). Furthermore, some researchers have used this structure to optimise the use of connected hybrid sources while using various control techniques as mentioned in (Rezkallah et al., 2017), (Rezkallah et al., 2022),(Sharma et al., 2019) ,(Sekhar and Kumaresan, 2021).

In this structure, the individual output of power converters from each sources are being tied to the DC link. This configuration is straightforward in terms of operation and associated control circuitry. However, the number of conversion stages becomes high with regard

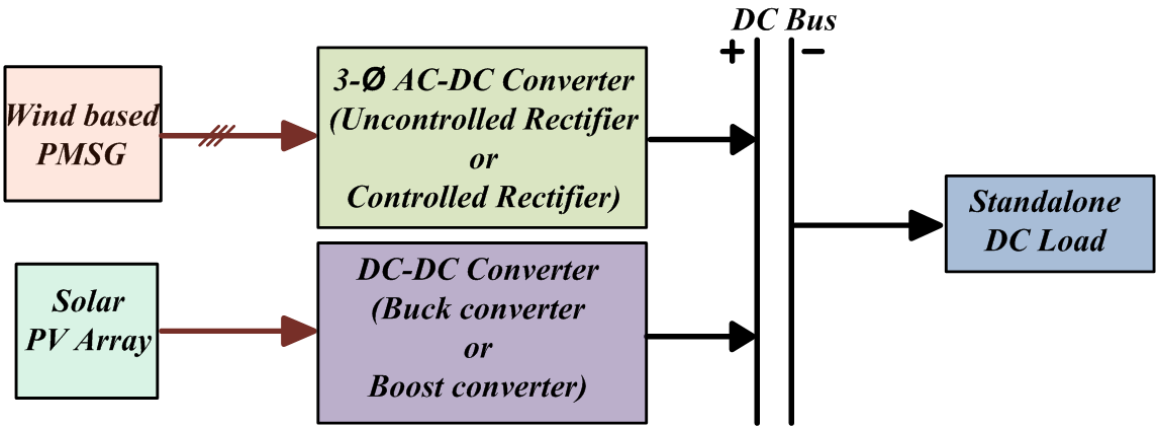

Figure 1.3: Configuration presented in Chiang et al. (2010)

to each sources. Therefore, this aspect makes the overall configuration less reliable. This is because if any intermediate stages involved with any sources gets faulty or disturbed, then the general layout will be affected in supplying power to the DC link side. Also, despite having abundant power availability at the source side, the power availability at the DC link or load side will be affected either due to faulty conversion stages or extra losses in the intermediary stages.

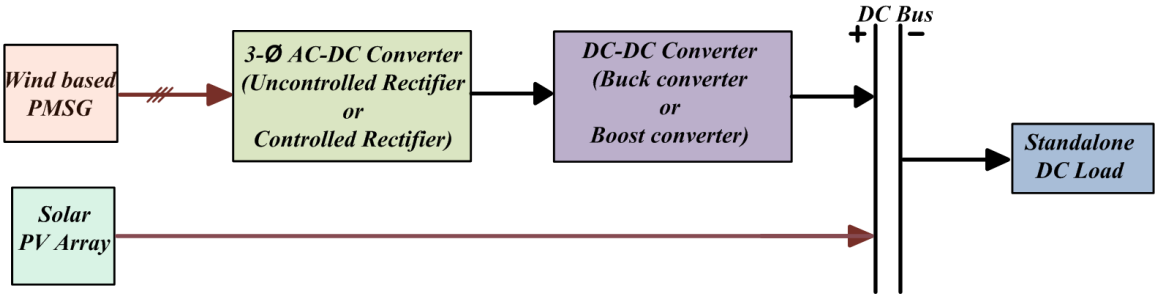

Figure 1.4: Configuration presented in Singaravel and Daniel (2015)

Structure 2 :- In Figure 1.4, authors in Singaravel and Daniel (2015), Priyadarshi et al. (2019) have attempted to reduce the conversion stages with respect to previously mentioned structure (***Structure 1***). Herein, the conversion stage from one of the sources is eliminated. Since output power from both hybrid sources needs to be transformed into DC before interfacing to the DC link, and as the solar PV array provides DC output only, therefore, this source is considered to be directly connected to the DC-link. In this structure, PV array output gets fixed to the DC link voltage which is being decided by the output of wind

based power converter.

This structure brings simplicity, eliminates conversion stages involved with one source and thereby, an overall number of conversion stages involved becomes less than the previously mentioned structure. However, certain aspects affect the reliability of the overall system. Though solar can provide more power, it may be possible that the PV output might get reduced compared to the potentially available voltage(MPP) due to some disturbances associated with wind conversion stages. Therefore, this structure does reduce conversion stages, but its reliability decreases during some instances of operations.

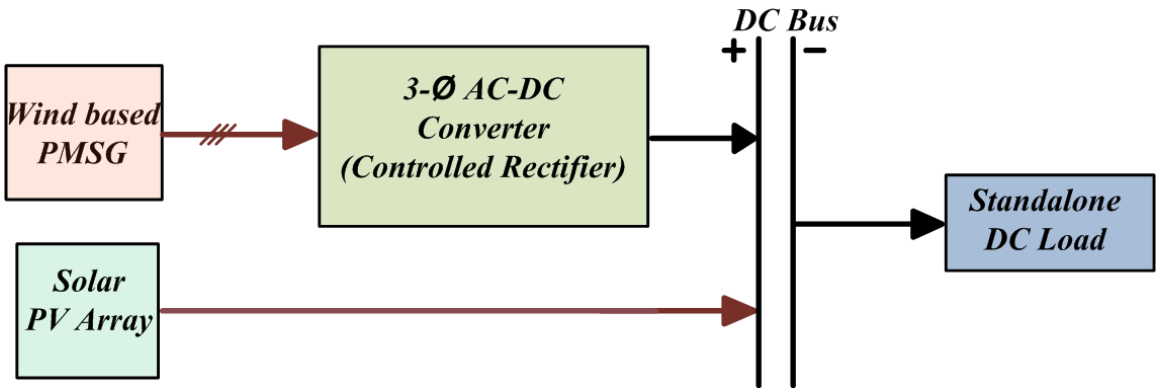

Figure 1.5: Configuration presented in Shanthi et al. (2017)

Structure 3 :- The Figure 1.5 represents another structure in the realm of hybrid systems. As proposed in the Wandhare and Agarwal (2014) Shanthi et al. (2017), Radwan and Mohamed (2019) this structure is similar with structure as outlined in the ***Structure 2*** [Singaravel and Daniel (2015)]. Both ***Structure 3*** and ***Structure 2*** have directly interfaced solar PV arrays to the DC link. However, herein wind-based power converter is a controlled 3-phase rectifier that decides the DC link voltage.

Thus, it can be stated that since the solar PV array is directly interfaced with the DC-link, there is a dependency on wind-based systems to extract peak power from the solar PV array. Additionally, misgating effects among the switches in the wind-based power converter may reduce the system's overall dependability. As a result, despite offering a simple configuration, this system can become less reliable.

Structure 4 :- Authors in Mangu et al. (2016), Ravada et al. (2021) have proposed the structure as presented in Figure 1.6. This structure consists of transformer that provides

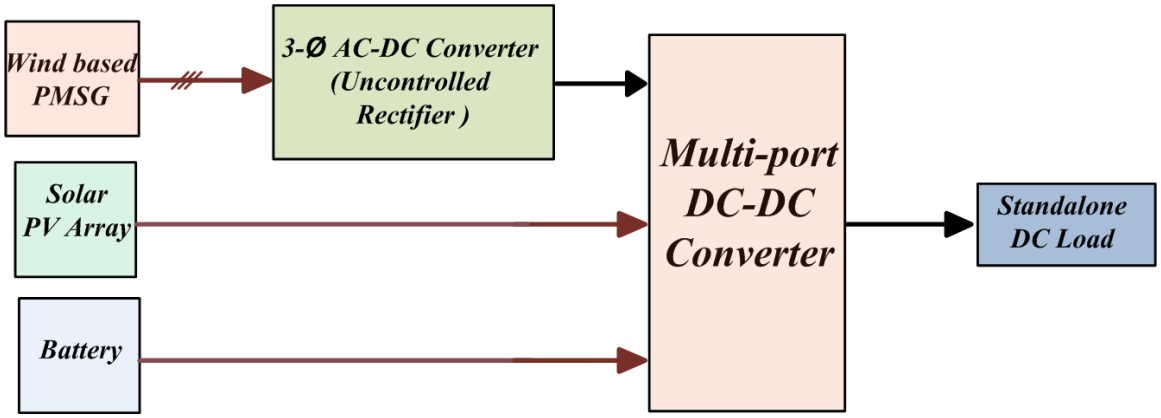

Figure 1.6: Configuration presented in Mangu et al. (2016)

galvanic isolation. Further, the structure is multi-port converters based that can integrates multiple sources. The structure is quite intricate in terms of architecture and thereby any misgating in the switches impacts the overall credibility of the system.

1.4 Review of PV-wind based Standalone AC systems

There are many architectures discussed pertaining to the PV-wind based standalone AC system.

- A standalone three phase AC system with a wind-driven induction generator, PV array, and inverter is proposed in (Daniel and AmmasaiGounden, 2004), (Arutchelvi and Daniel, 2006). This system is supplying a three-phase load of constant frequency balanced voltages. In this structure, the PV array is connected to the boost converter, the output of which is connected to the battery bank, and finally, the battery bank is directly connected to the inverter. This AC load is interconnected between the output of inverter and the wind source based induction generator. Further, using duty ratio regulation of the boost converter regulation of load voltage is accomplished in accordance with the availability of solar and wind energy. The wind unit, however, is running without any converter and thereby under no direct control. When the battery is switched ON, the generating system will deliver the steady voltages despite fluctuations in irradiation and wind speed.

- Another standalone AC load system is illustrated in (Prakash et al., 2016) with the generator terminals of wind unit directly interfaced to the three phase AC load. With

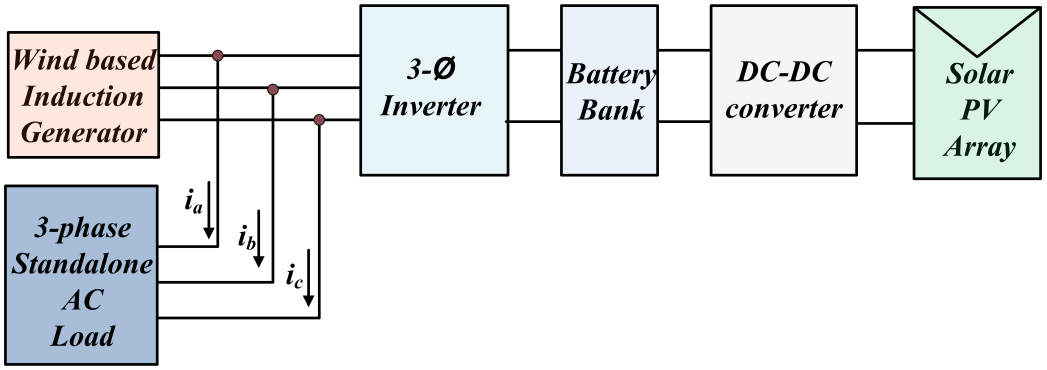

Figure 1.7: Configuration presented in (Daniel and AmmasaiGounden, 2004),(Arutchelvi and Daniel, 2006)

regard to the PV unit, power flow is occurring through the dual conversion stages of DC-DC conversion succeeded by an inversion stage with the output connected to the standalone AC load. This system uses a cascaded PI-SMC based regulator in boost converter, which is connected between the PV array and the three-phase voltage source inverter in order to administer the inverter DC link voltage as well as regulating the AC load voltage.

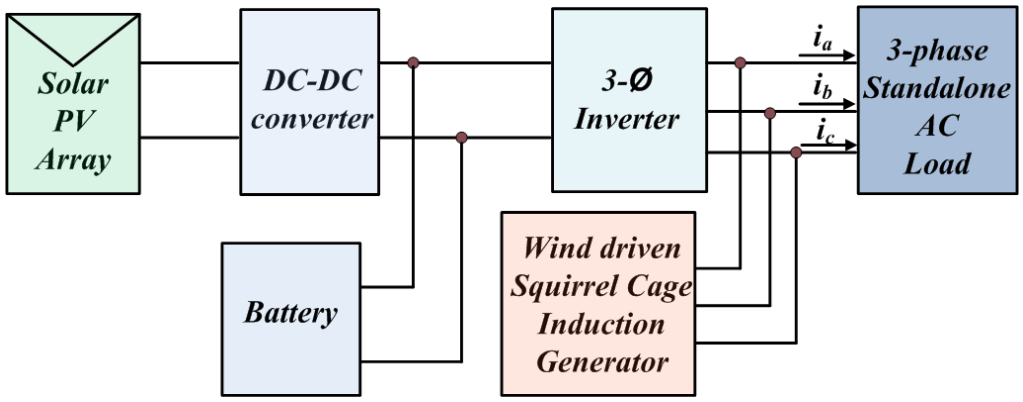

Figure 1.8: Configuration presented in (Prakash et al., 2016)

As it is observed from the above two configurations that there is only PV based power conversion unit employed and no wind based power conversion unit is used. This implies that there is no direct control over the wind based power extraction and thus the overall configurations are simple but appears less dependent in the context of wind based power extraction. Thereupon, there have been configurations with the individual conversion units with each sources are presented for supplying the standalone AC load.

- In this context, the configuration described in (Rezkallah et al., 2019) is a stand-alone hybrid wind and solar system with a fixed speed diesel generator and a storage battery for an isolated water treatment station(three phase standalone AC). This configuration utilizes the individual converters with each sources to meet the load requirements and overall power balance. Herein, solar PV array is interfaced to the DC-DC boost converter whose output terminals are connected to the parallel combination of dump load and battery energy storage system. Thereupon, the battery energy storage system is interfaced to the DC link. Also, wind unit is connected to the DC link via diode bridge rectifier and DC-DC boost converter unit. The DC link, outsourcing power from wind and solar sources will then power the 3-phase inverter which thereby supplies to the AC loads via transformer. Additionally, fixed speed diesel generator used as backup source is also supplying power to the AC load in concurrence with the power coming from PV-wind sources. In regulating the power flow from PV-wind sources, the power ratio variable step perturb and observe based maximum power point tracking algorithm is employed. Also, an in-phase and quadrature unit-based control algorithm is used for synchronizing the Diesel Generator with the point of common coupling (PCC). Further, an active power control based on proportional–integral controller with anti-windup is utilized for regulating the voltage and the frequency. Therefore, herein the system consists of individual converter unit along with the discrete controllers for fulfilling the load requirements.

- In continuation of using the similar approach, another system depicted in (Kant et al., 2017) is supplying to the three phase standalone AC system with the PV-Wind-Diesel based battery energy storage system. Herein, wind energy conversion system unit is interfaced to the battery bank (acting as DC link stage) via dual conversion stages of diode bridge rectifier and a boost converter. Thereupon, PV unit is connected to the battery bank with the use of boost converter. Now, the battery bank is connected

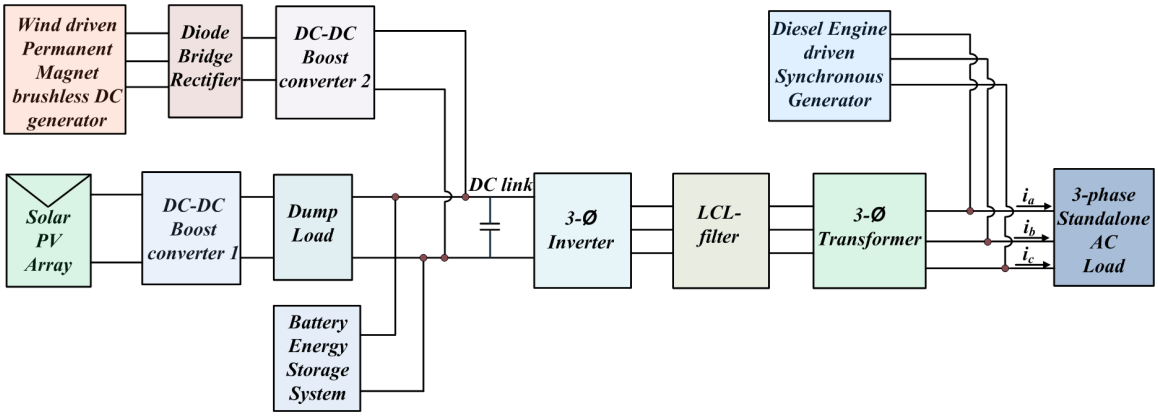

Figure 1.9: Configuration presented in Rezkallah et al. (2019)

to the 3-phase voltage source inverter which will supply the AC load. Also, diesel engine based synchronous reluctance generator is supplying power to the AC load alongside with the other PV-wind unit. For controlling the wind based power, perturb and observe maximum power tracking algorithm is employed to control the duty ratio signal of the boost converter which is connected between the diode bridge rectifier and the battery bank of the wind conversion unit. This maximum power tracking operation involves the usage of diode bridge rectifier output voltage and current as reference signals and thereby generating the duty ratio signal for the WECS based boost converter. And, in context of regulating the PV based power an incremental conductance based MPPT algorithm is used to extract peak power from the solar PV array which produces appropriate duty ratio signal for the boost converter employed PV array and the battery bank. As DG is the only ac source in the system, so the system and the load end frequency is related to the operation of the DG only. The control algorithm for the inverter is comprising of $I\cos(\phi)$ algorithm and hysteresis current control with the inverter interposed between the battery bank and the AC load. As the multiple renewable energy sources are used to meet the standalone AC load requirements adequately, the overall system is complex as PV-wind sources based power extraction is accomplished with the adoption of multiple conversion stage that requires different control units as well. Therefore, the hybrid sources based power extraction meeting the requirements of AC load in conjunction with the DG unit leads to the challenging operation in ensuring the synchronization among these dispersed units to meet the load requirements appropriately.

- Thereupon, in order to emphasis more control in addition to use the individual con-

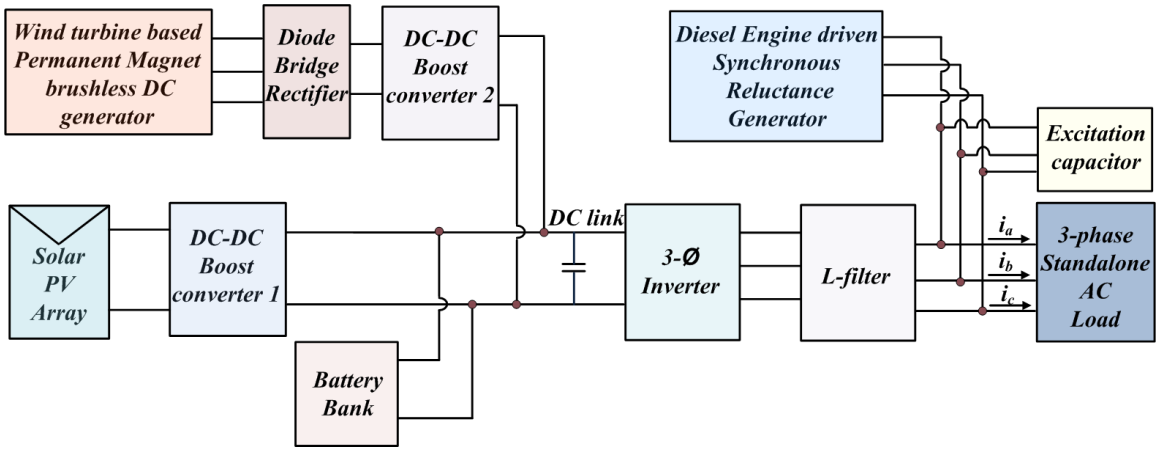

Figure 1.10: Configuration presented in (Kant et al., 2017)

version units for each sources for single-phase standalone AC load, another system is presented in (Merabet et al., 2016) that discusses about an energy management and control scheme for laboratory scale microgrids based on hybrid energy resources of solar panels, wind turbines, and batteries as shown in the Figure 1.11. This laboratory scaled microgrid is operated as a smart system by an energy management and control system. The PV system is controlled to run under maximum power point tracking (MPPT) under low energy generation and off MPPT during excess of energy to meet the load requirement. The proposed microgrid is a laboratory scale system which is functioning by an energy management and control system. Herein, the photovoltaic (PV) system is regulated to operate in maximum power point tracking (MPPT) mode during the scenario of low energy generation and to exit from MPPT mode during periods of high energy generation. The wind energy conversion system, also known as WECS, is managed by a feedback control law, which ensures accurate tracking of wind speed. This law is supplemented by a disturbance compensator, that eliminates the impact of unknown turbine torque. An energy management algorithm, based on the available power from the renewable sources, the load power demand and the state of the battery, is developed to operate the microgrid as an autonomous system. Finally, the load side voltage is supervised in order to conduct power transfer efficiently from the energy sources to the load.

- Further, another three-phase standalone AC system structure in (Pradhan et al., 2018) extracts energy using a composite sliding mode controller in the PV based DC-DC converter and wind based 3-phase AC-DC converter as demonstrated in Figure 1.12.

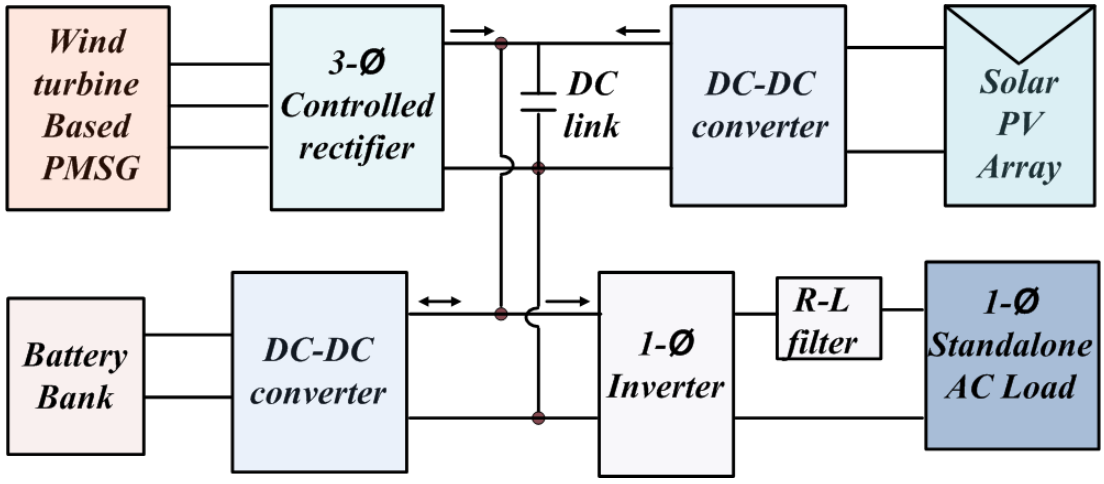

Figure 1.11: Configuration presented in (Merabet et al., 2016)

The outputs of both conversions are then connected to the battery-powered DC link, and this DC link is then connected to the AC load via an inverter. Herein, the composite sliding mode controller with disturbance rejection ability is implemented to harvest maximum wind power. While in order to extract peak power of solar unit, a perturb and observe maximum power point tracking strategy is utilised. And thereby to keep the voltage constant(AC load voltage) at the point of common coupling, a voltage control strategy is implemented.

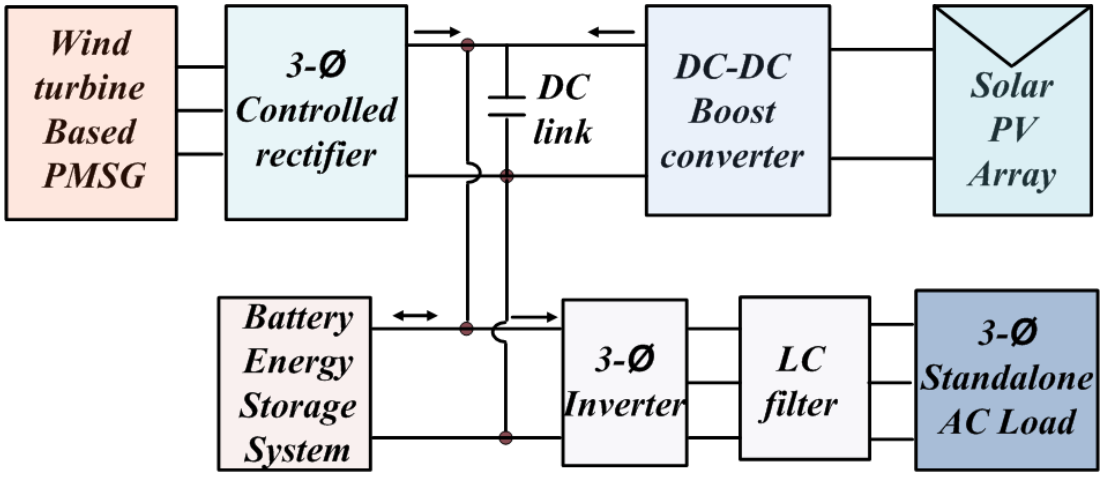

Figure 1.12: Configuration presented in (Pradhan et al., 2018)

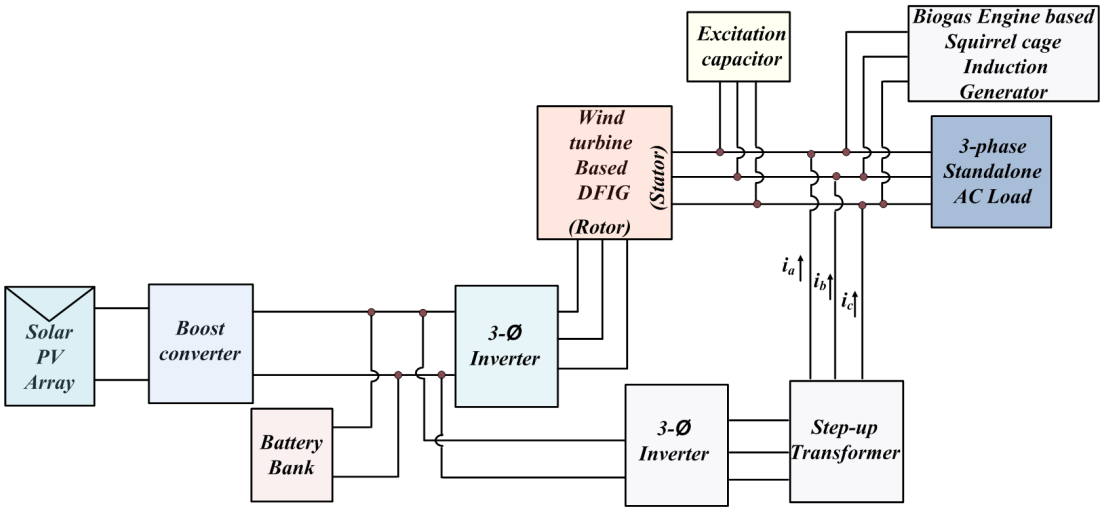

Figure 1.13: Configuration presented in (Sekhar and Kumaresan, 2022)

- Also, the architecture proposed in (Sekhar and Kumaresan, 2022) is for standalone three-phase AC system with PV-wind-biomass sources as shown in the Figure1.13. Herein, power extraction from each sources are carried out using individual conversion units that necessitates for individual closed loop control logic as well. This system includes a squirrel-cage induction generator (SCIG) powered by biogas, a wind-powered DFIG, a solar PV unit, and an energy storage battery system. In this system, the voltage and frequency are controlled by a single bi-directional SPWM inverter on the rotor side of the DFIG, which feeds the load, to keep them constant. Additionally, the load is powered by the PV batteries via another inverter and a hysteresis controller. To share the reactive power requirement of the system, addition of a capacitor bank and a DSTATCOM has been considered.

  As it is perceived in the aforementioned configurations with individual conversion units for PV-wind sources that there is a direct control needed for extracting power from the PV-wind sources and thereby the individual conversion units has to be employed with each sources. In some configurations, battery (with or without converter unit) is used as an intermediate unit for providing power to the inverter unit of standalone AC loads. The merit of using an individual converter offers simple control in the power extraction from the source, however, to operate all the conversion units together in accordance with the load requirements becomes complex. Also, the overall configurations becomes bulky and costly.

1.5 Review of single source based systems

The structures above are related to the power management and control for the PV-wind sources with the use of individual conversion units for each source. Thereby, these architectures will results in the multiple converter units and complex control. However, there are systems formed with either single source of wind (AC) or solar alone(DC) and with use of single stage conversion unit for power extraction.

- As discussed in system (Ahmed et al., 2005), the induction generator is delivering AC and DC load simultaneously as presented in Figure1.14. The DC load is supplied via output of uncontrolled rectifier powered by induction generator of the wind source and AC load is supplied with the aid of direct interconnection to the induction generator terminals. Herein, a dynamic performance characteristics of a three-phase induction generator which is directly coupled to a full-bridge diode rectifier together with a DC-link filter is presented for use in small-scale DC power applications. Also, a deadbeat current controller-based adaptive power factor (APF) is presented for a stand-alone induction generator system operating with variable speed and supplies both DC and AC loads.

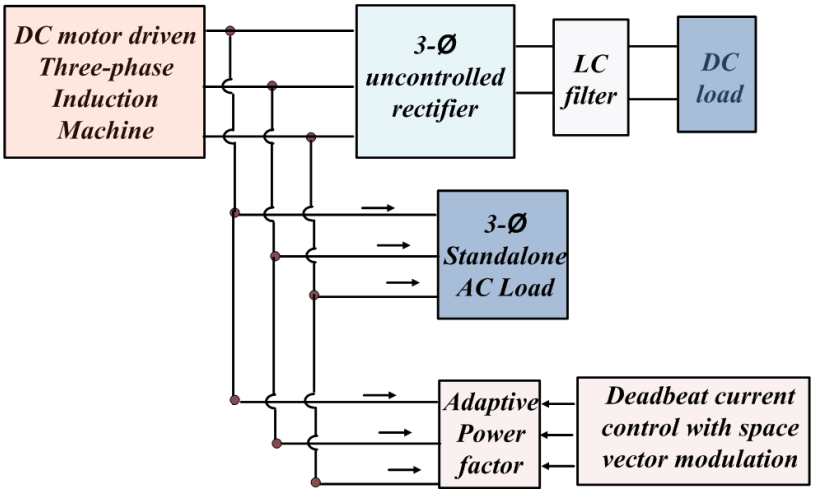

Figure 1.14: Configuration presented in Ahmed et al. (2005)

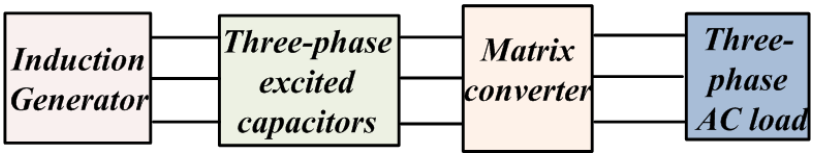

Figure 1.15: Configuration presented in Mahajan et al. (2017)

- In (Mahajan et al., 2017), a stand-alone AC system comprising of a capacitor-excited induction generator that provides power to AC loads through a Matrix Converter is presented. In this configuration as shown in Figure1.15, a system for supplying stand-alone alternating current (AC) loads that consists of a Capacitor Excited Induction Generator (CEIG) coupled with a Matrix Converter (MC) is presented. With the use of Space Vector Modulation (SVM) approach, the varying output voltage magnitude and frequency from CEIG is changed into a constant voltage magnitude and frequency at the load terminals. This single-stage MC is being considered as a solution for the standalone AC system as an alternative against traditional AC/DC/AC two stage power converters. The controller herein can operate the closed-loop system such that the AC load voltage is maintained at a constant level, regardless of the prime mover speed and the load.

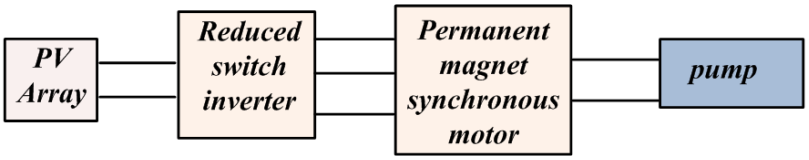

Figure 1.16: Configuration presented in (Prabhakaran et al., 2020)

- Also, a PV based standalone AC system with the usage of reduced switch inverter single stage conversion for PMSM drive in water pumping systems is discussed in the (Prabhakaran et al., 2020). The configuration herein as shown in Figure 1.16 is a standalone single stage photovoltaic (PV) fed reduced switch inverter (RSI) based permanent magnet synchronous motor (PMSM) drive for the water pumping application(standalone AC). By employing a reduced switch inverter, the system aims to lessen the switching losses as well as the overall cost. This system is made up of a PMSM drive that is powered by a PV source and supplied through an inverter using fewer switches. This inverter only utilizes of four switches, in contrast to the traditional voltage source inverter, which uses six switches. Control of the PMSM drive is

accomplished through the use of a field-oriented control system. Further, in order to produce a speed reference for the PMSM drive, the "perturb and observe" maximum power point tracking method is utilized.

As it is perceived herein in the aforementioned configurations with single conversion units either for Photovoltaic source alone or wind source alone based system. It is beneficial to employ single converter that makes the overall configuration more compact and cost effective. Also, the control scheme becomes simpler as there are no requirements of synchronising the multiple conversion units altogether for supplying the load requirements.

1.6 Review of single source or multiple sources based DC systems

In recent times, majority of the loads are being catered by the DC power only, which grants the necessity and applicability to the requirements of DC system (Dragičević et al., 2015). There are several systems that are either solar based DC system (González-Castaño et al., 2021)or wind power based DC system (Hazzab et al., 2023).

- The architecture depicted in (Nayanar et al., 2015) is for DC microgrid application, which is supplied from a wind energy conversion system employing a diode bridge rectifier and a buck converter as depicted in Figure1.17. Authors have presented a MPPT algorithm for DC microgrid applications which is supplied from a small-scale WECS for 120 V voltage level. This algorithm monitors the dc-grid current continuously and thereby changes the duty ratio signal of the buck converter for tracking the peak power operating point. This algorithm involves no need for the measurement of wind velocity or turbine rotor speed, i.e., with no mechanical sensors involved.

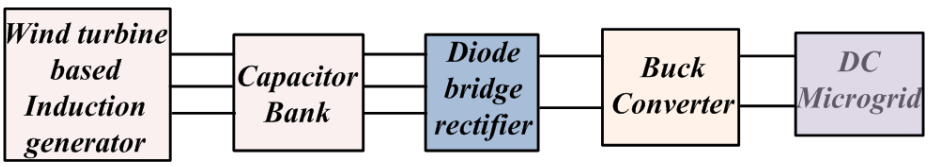

Figure 1.17: Configuration presented in (Nayanar et al., 2015)

- In the configuration presented in (Alagu et al., 2021) is an improved quadratic boost converter for PV based standalone DC system using perturb and observe MPPT control as shown in Figure 1.18. The converter delivers high voltage gain at lower duty ratio which results in less reverse recovery loss however it contains four semiconductor devices(one switch and three diodes), three inductors and three capacitors.

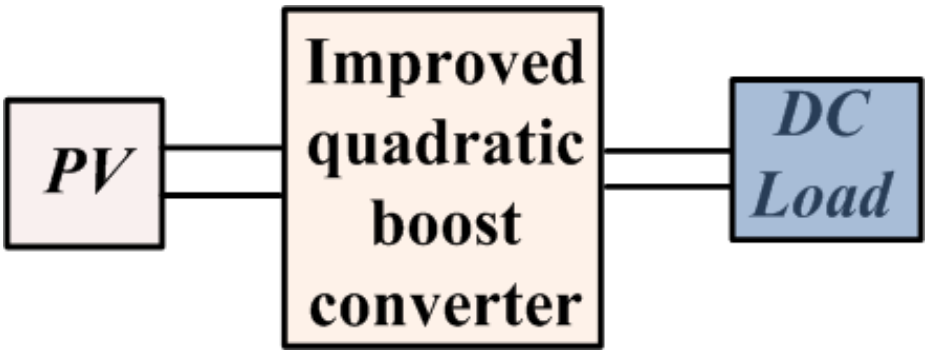

Figure 1.18: Configuration presented in (Alagu et al., 2021)

- The system discussed in the (Saafan et al., 2023) is a four-port converter using four semiconductor switches that includes three sources (three ports) which are photovoltaic source, fuel cell, and battery in order to supply a standalone DC load(fourth port) as shown in Figure1.19. This multi-port DC converter has bidirectional buck-boost capability. The control strategy used herein is to achieve the power control among the sources in addition to regulating the DC link voltage. Perturb and observe maximum power point tracking algorithm is employed for peak PV power extraction in this topology. Droop control strategy is employed for regulating the battery power.

- In (Misra and Jain, 2017), a comprehensive analysis for wind-DFIG based standalone DC system is presented. As Doubly fed induction generator (DFIG)-DC system consists of distorted stator voltages and currents as shown in Figure 1.20. Herein, scheme is developed that does not need sensing of stator side. This scheme is based on the fact that as the control variables, which is rotor circuit currents, and the controlled variable which is output dc link voltage, are both sensed, thus, the requirement of sensing the intermediate stator side variables can be avoided. Also, the mathematical analysis of the system is carried out, including dominant harmonics, for comprehension of the behavior of the system. By adjusting the flux reference in an appropriate manner in response to changing load conditions, the stator frequency is kept within a relatively close range to its specified value.

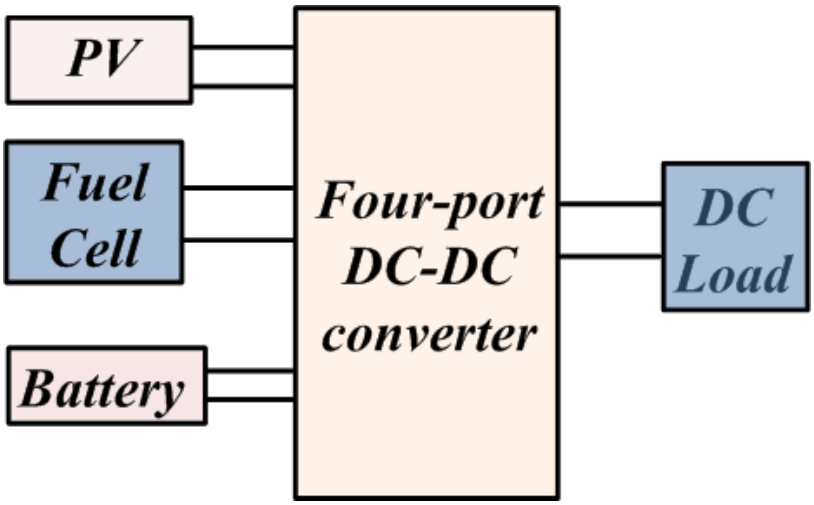

Figure 1.19: Configuration presented in Saafan et al. (2023)

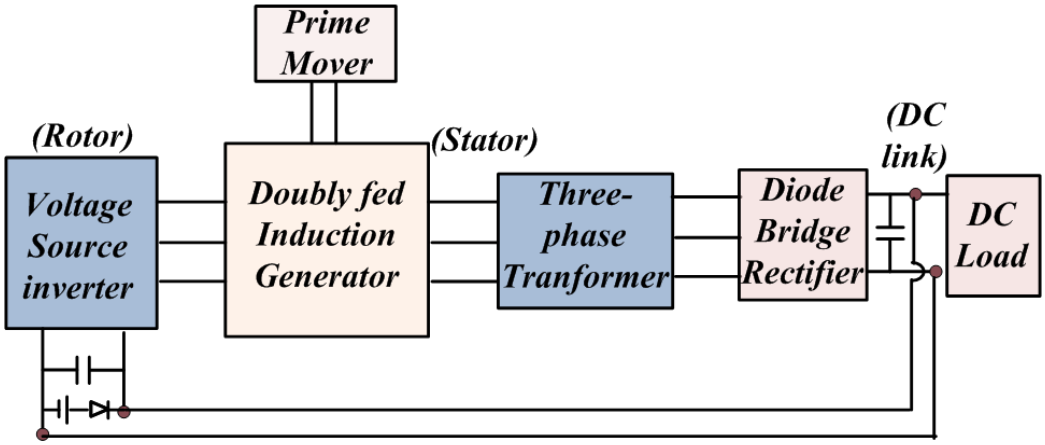

Figure 1.20: Configuration presented in (Misra and Jain, 2017)

- The architecture depicted in (Kumar et al., 2021) presents a universal converter for solar and wind sources with the wind unit being directly interfaced to the universal converter while solar unit is connected to the universal converter via a multiphase boost converter which is an additional conversion stage as shown in Figure 1.21. The proposed configuration consists of a universal converter with a boost converter and DC side to step up the voltage. This universal converter is proposed for hybrid water pumping system to mitigate multiple power conversion. A switch reluctance generator, whose output is fed to the universal converter, is a wind power system. A universal converter is coupled to a multiphase boost converter in the solar system.

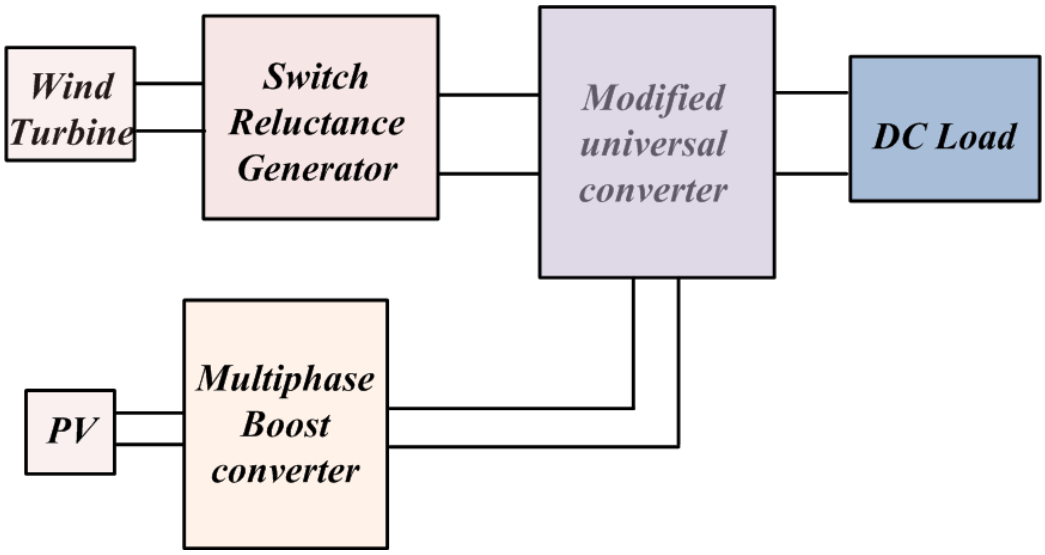

Figure 1.21: Configuration presented in (Kumar et al., 2021)

- Also, an energy management scheme is illustrated for standalone DC system fed by PV-fuel cell-battery sources in (Gugulothu et al., 2023). Herein, an illustration of a centralized energy management strategy (EMS) for a standalone DC microgrid made up of solar photovoltaic cells (PV), fuel cells, and a battery energy storage system (BESS)is provided as represented in Figure1.22. This energy management scheme is meant to cut down on the amount of hydrogen that is taken in while also increasing the BESS's durability and dependability. The PV system de-rating approach is utilized in this method to achieve the goal of avoiding too deep charging of the battery in low-demand operating conditions. The power supply from the fuel cell is adjusted with the use of a reverse sigmoidal function which is based on the state of charge (SoC) of the battery. This not only increases the efficiency of the hydrogen fuel, but it also helps to reduce the amount of deep discharge the battery experiences when subjected to severe loading circumstances. The load power, state of charge of the battery, and individual source power information are all supplied into the centralized EMS. As a consequence of this, the energy management strategy issues the necessary commands to the local controller of each individual source in order to regulate the output power of each source.

- Further, the system depicted in (Zia et al., 2022) is presenting a dual-stage energy management strategy that makes use of PV, wind, and tidal energy sources to power DC loads with the help of individual converters that are dedicated to each source

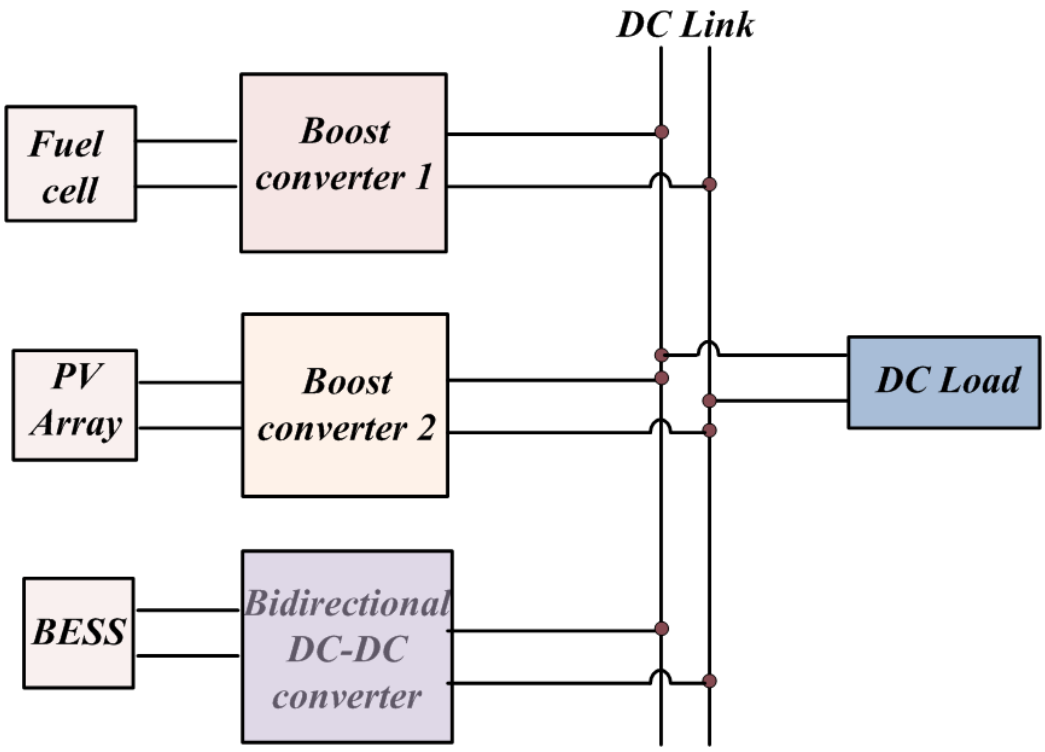

Figure 1.22: Configuration presented in (Gugulothu et al., 2023)

as represented in Figure1.23. In this, an islanded DC microgrid, which consists of renewable energy sources including solar, wind, and tidal combined with Li-ion battery storage, is considered as a case study for islands with tidal energy potential.An optimal energy management system is proposed for resource scheduling and usage in order to carry out the operation effectively. In order to minimize excessive real-time communication bandwidth utilization, the authors have proposed a two-stage supervisory energy management system for the effective operation of PV/Wind/Tidal microgrids. This was done in order to maximise the efficiency of the microgrid's power generation from renewable sources. The primary stage is responsible for scheduling the appropriate energy share from each energy source, which ultimately results in an increase in the operation's overall efficiency. In order to guarantee efficient utilisation, the aggregated planned generation and demand profiles are analysed in the secondary stage, which also includes an update to the decision strategies.

- The system in (Jacob and Farzaneh, 2022) illustrates an off-grid hybrid photovoltaic, wind, and battery microgrid that is appropriate for application in isolated residential

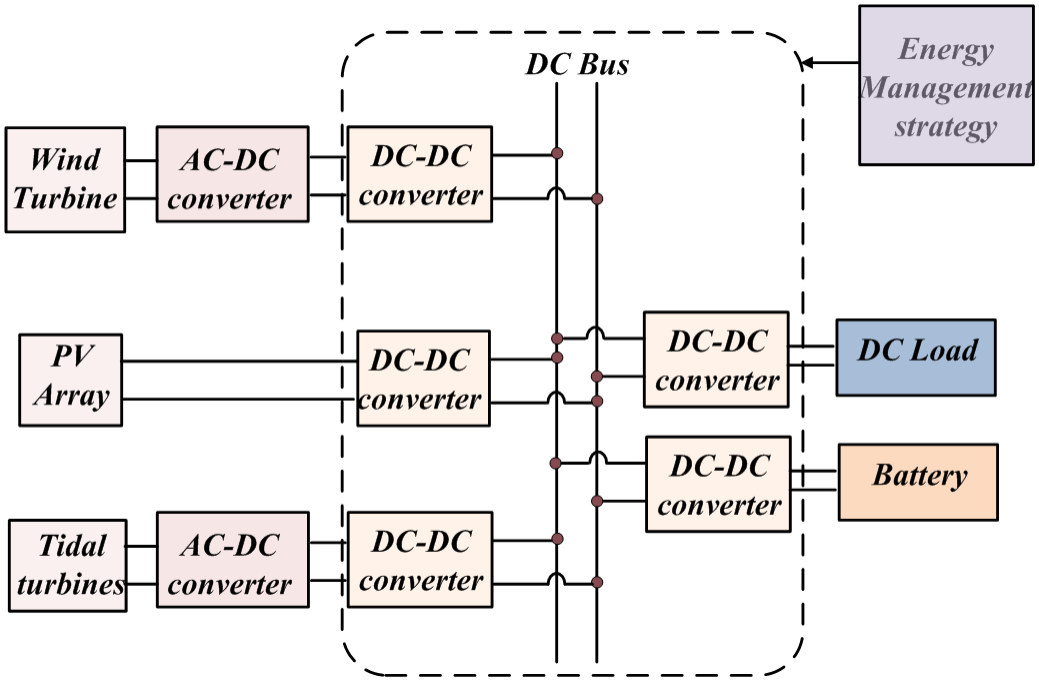

Figure 1.23: Configuration presented in (Zia et al., 2022)

regions. This microgrid uses individual converters for each source with an individual control as presented in Figure 1.24. Herein, dynamic modelling and simulation of an off-grid direct current (DC) microgrid consisting of the photovoltaic (PV) panel, wind turbine, battery, and a DC load are conducted along with the depiction of component-based power control strategies that ensure quality power output. In addition, the primary focus is on the real-time experimental validation of the dynamic simulation model, which is accomplished by designing and building the architecture of an indoor test system. The validation of the presented model is conducted by using a meteorological dataset from Fukuoka, Japan. Furthermore, a detailed scenario analysis for different weather conditions(sunny, windy, rainy, and cloudy) using real-time meteorological conditions are conducted and thereupon demonstrated the power balance between the presented microgrid sources and the load, showcasing it as self-sustaining hybrid renewable microgrid for residential areas in Japan with limited access to conventional power sources.

All of the configurations that have been discussed thus far for standalone DC systems have involved the usage of multi-conversion units, each of which requires its own control unit. In the recent years, there have been configurations that allow these

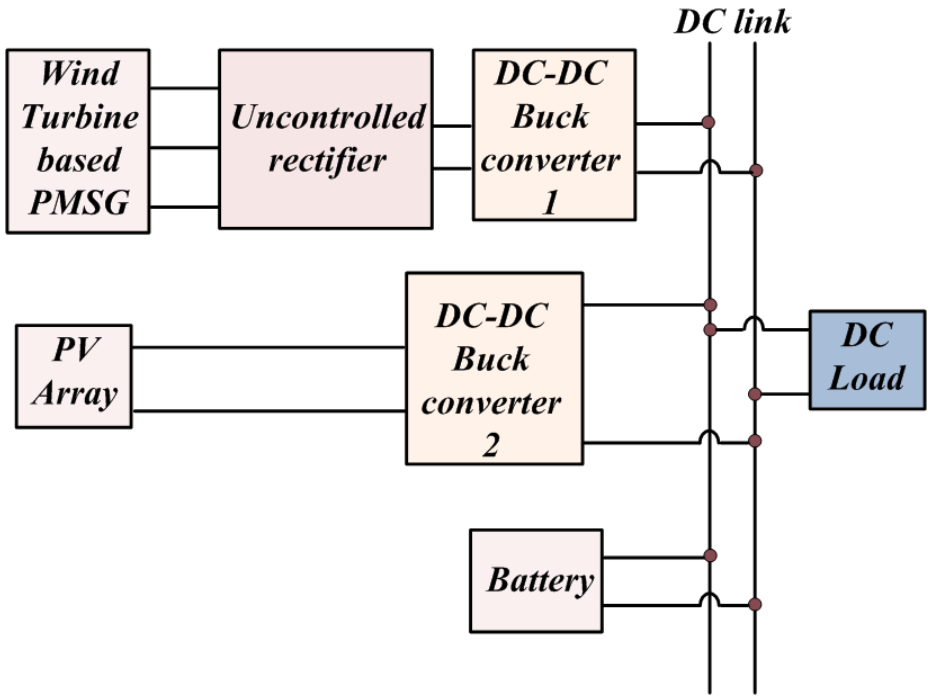

Figure 1.24: Configuration presented in (Jacob and Farzaneh, 2022)

sources to be integrated into multi-port-based architectures that perform DC-DC conversion.

- The system in (Prabhakaran and Agarwal, 2018) presents a single stage multi-port converter for PV-fuel cell based bipolar DC microgrid of low voltage level as depicted in Figure1.25. This four-port converter consists of two switches and three diodes in the single stage circuitry and the converter is able to regulate one of the pole voltage along with the maximum power extraction from the PV source as well. Also, the dynamic model of the converter is presented that remains unchanged for any duty ratio conditions that allows controller design to be simpler.

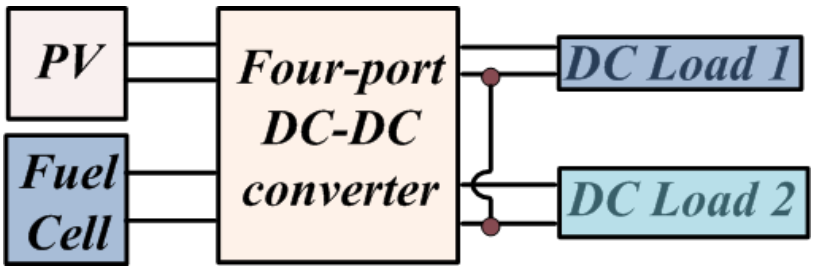

Figure 1.25: Configuration presented in (Prabhakaran and Agarwal, 2018)

- In the system discussed in the (Ravada et al., 2020) presents a topology comprising of PV-wind-hybrid energy storage units focused on the standalone DC system. Herein,as depicted in Figure 1.26, the wind source of this system involves an additional AC-DC conversion stage before interfacing it to the converter. PV unit and hybrid energy storage unit(batter and supercapacitor) are interfaced using bi-directional buck-boost DC-DC converter part of this multi-source converter and wind is interfaced to DC-link using DC-DC boost converter of multi-source converter via diode bridge rectifier. However, this topology cannot operate during the scenario of unavailability of PV source.

  .

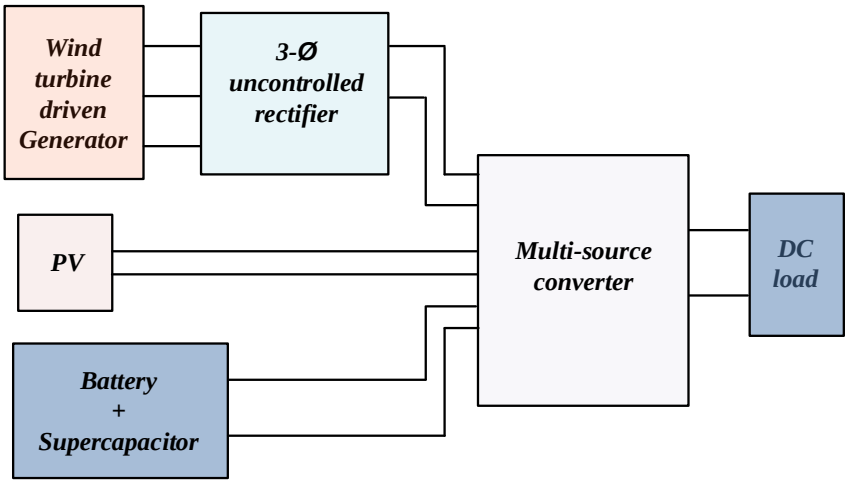

Figure 1.26: Configuration presented in (Ravada et al., 2020)

With regard to the aforementioned configurations for DC systems either with single source alone or with the combined sources(PV-wind) that caters to the DC load. It is imperative to utilize the single stage conversion circuitry with multiple sources that has the merit of more reliability, more compactness, less control complexity and an ability to integrate the multiple sources operation concurrently.

1.7 Motivation of the work

In today's continuous increment in load demand, there is a burden enhancement proportionally upon the conventional power distribution system which is primarily supported by

the utility grid. This traditional AC distribution system based approach will be catering DC load at the end of the power-chain. However, this system will undergo various power conversion points before providing DC output. Therefore, this approach is associated with power loss at various conversion points. Finally, with hike in power demand, the provision of power with higher reliability and better efficiency cannot be realized appropriately. In order to combat this challenging problem, distribution system involving harnessing solar and wind energy sources is the solution that will reduce aforementioned burdens (involved with the utility grid) but also can be well optimized. As it is known that solar and wind energy are complementary in nature with former is quite incessant on sunny days and while later one is associated with strong winds on cloudy days or at night time.

Also, as PV voltage is lesser in magnitude then in order to boost the PV input voltage, DC-DC boost converter is appropriate due to its voltage step up capability and slow dynamics compatibility. While wind energy extraction possess many configurations but PMSG-wind turbine system is suitable with its offerings of higher efficiency, energy yield and less complexity of control hardware with DC excitation current elimination. Further,3-phase AC-DC converter needs to be interfaced to convert AC output of wind-PMSG system into DC. Then, these two DC output obtained from individual sources can be integrated while connecting to the DC-link output of the hybrid input system and thereby to the DC load. However, two individual converters need to be used in order to process these two hybrid sources.

Therefore, in order to reduce the multi-stage conversion structures, a single stage hybrid power converter topology is proposed that can offer simultaneous aforementioned operation of AC-DC and DC-DC conversion being supplied by wind-PMSG and PV-array sources, respectively. The merit of this converter is the elimination of redundancy involved with usage of individual converters being integrated into one system for supplying DC load while using these two complementary sources and thereby improving the reliability of power supply.

1.8 Objectives

On the basis of the literature review of the PV-wind sources based standalone system, the following points are identified as the main objectives of the present research work.

1. Design and development of the power converter topology combining AC-DC and DC-

DC converters with input fed from the PV-wind sources for the standalone DC system.

2. Development of control strategy with appropriate modulation schemes for MPP techniques, voltage regulation of standalone DC system.

3. Experimental verification of the proposed system.

1.9 Contribution of the thesis

The present thesis work discusses about the single stage multi-port hybrid power converter for PV-wind sources based standalone DC system. The proposed converter is capable of operating with the concurrent energy harvesting from these hybrid sources. This single stage configuration comprises of concurrent PV based DC-DC conversion process and wind based 3-phase AC-DC conversion process. The contributions of the work are outlined as follows:

- The development of the proposed hybrid power converter combining the simultaneous operation of PV array DC-DC converter and wind-PMSG three-phase AC-DC converter is elaborated.
- The operational features of the proposed converter are presented, which exhibits the control of load voltage and thereby meeting load power as a result of the dynamic output capabilities of PV-wind sources.
- The detailed closed loop control architecture that administers the concurrent conversion operations together with the aid of generation of three-phase modulating signals and a duty ratio signal in accordance to the load voltage control is developed.
- A modified sinusoidal pulse width modulation (PWM) scheme is implemented in the proposed converter. This scheme demonstrates the unification of 3-phase modulating signals and duty ratio signal for the PWM pulses of the proposed converter, which makes it easier to perform concurrent power conversion processes.
- The performance of the proposed converter under a variety of scenarios is investigated using simulation and experimental case studies to validate the suitability of this converter.

1.10 Thesis organization

The present thesis is structured in following manner:
Chapter 1 : This chapter presents an introduction that comprises of a brief overview of the thesis, the motivation, the literature survey, followed by the research objectives and a concise description of the thesis organisational structure.

Chapter 2: In this chapter, the theoretical development of the proposed system is presented which discusses proposed single stage multi-port hybrid converter for PV-wind based standalone DC system. The principle of operation of the proposed converter with PV-wind sources is elaborated.

Chapter 3: In this chapter, the concept of control structure and the pulse width modulation scheme for the proposed converter is presented that discusses the concurrent power extraction aspects from the PV-wind sources pertaining to the standalone DC system.

Chapter 4: In this chapter, a detailed evaluation of the proposed hybrid power converter is carried out through the use of both simulation and experimental case studies.

Chapter 5: This chapter provides a summary of the significant contributions presented in the thesis, as well as some outline on the areas of future research.

Chapter 2

SYSTEM DESCRIPTION

2.1 Introduction

This chapter introduces the standalone DC system powered by the combined sources of wind-PMSG and PV sources. As it is discussed in the previous chapter that it is essential to have power conversion stages with lesser count to enhance the reliability of hybrid sources based standalone DC system, thereby this chapter details about the proposed single-stage hybrid power converter for the standalone DC system.

2.2 Wind turbine based Permanent Magnet Synchronous Generator system

The wind turbine and the permanent magnet synchronous generator (PMSG) are the primary elements of a wind energy conversion system. The wind turbine is responsible for harvesting the power that the wind provides for the system, and the PMSG is responsible for converting the mechanical power into electrical power.

2.2.1 Modeling of Permanent Magnet Synchronous Generator

In a wind energy conversion systems, permanent magnet synchronous generators (PMSGs) are crucial for converting mechanical energy into electrical energy. The machine control algorithms and the investigation of the steady-state and dynamic aspects of wind energy conversion systems both need a mathematical modelling of the PMSG. This section dis-

cusses the mathematical model of a PMSG in the *dq*-axes synchronously rotating reference frame.

In order to model the rotor circuit (Wu et al. (2011)), the field current in the rotor winding is being represented by a constant current source(I_f) in the *d*-axis circuit.In the permanent magnet synchronous generators,permanent magnets will be replacing the field winding and is modelled by an equivalent current source I_f with a fixed magnitude.

Stator voltage equations for the synchronous generator are given as :

$$v_{ds} = -R_s.i_{ds} - \omega_r.\lambda_{qs} + p\lambda_{ds} \tag{2.1}$$

$$v_{qs} = -R_s.i_{qs} - \omega_r.\lambda_{ds} + p\lambda_{qs} \tag{2.2}$$

The eq.(2.1) and eq.(2.2) are the *d*-axis and *q*-axis stator based voltage equations for the PMSG system. Here, λ_{ds}, λ_{qs} are the *d*-axis, *q*-axis stator based flux-linkages respectively that are given as :

$$\begin{aligned}\lambda_{ds} &= -L_{ls}.i_{ds} + L_{dm}.(I_f - i_{ds}) &(2.3)\\ &= -(L_{ls} + L_{dm}).i_{ds} + L_{dm}.I_f \\ &= -L_d.i_{ds} + \lambda_r &(2.4)\end{aligned}$$

$$\begin{aligned}\lambda_{qs} &= -(L_{ls} + L_{qm}).i_{qs} &(2.5)\\ &= -(L_q.i_{qs}) &(2.6)\end{aligned}$$

where λ_{ds}, λ_{qs} are the stator *d*-axis, *q*-axis based self-inductances respectively and, λ_r is the rotor flux given by $\lambda_r = L_{dm}.I_f$

L_d = direct-axis based stator inductance

L_q = quadrature-axis based stator inductance,are given as:

$$L_d = L_{ls} + L_{dm} \tag{2.7}$$

$$L_q = L_{ls} + L_{qm} \tag{2.8}$$

As rotor flux,λ_r is constant for the PMSG machine,it can be inferred that

$$\frac{d(\lambda_r)}{dt} = 0 \tag{2.9}$$

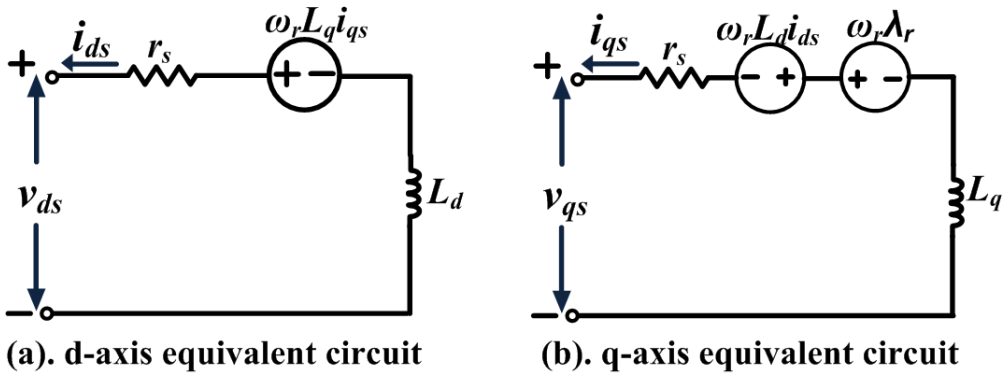

Figure 2.1: PMSG *dq*-axes equivalent circuit (a). d-axis equivalent circuit and (b).q-axis equivalent circuit

Substituting these constraints in the voltage equations (2.1) and (2.2) will give final equations as :

$$v_{ds} = -R_S.i_{ds} + \omega_r.\lambda_{qs} - L_d.pi_{ds} \tag{2.10}$$

$$v_{qs} = -R_S.i_{qs} - \omega_r.\lambda_{ds} + L_q.pi_{qs} \tag{2.11}$$

Then, the electromagnetic torque produced by PMSG system is :

$$\begin{aligned} T_e &= 1.5 * (P/2).[i_{qs}.(-L_d.i_{ds} + \lambda_f) - i_{ds}.(-L_q.i_{qs})] \\ &= 1.5 * (P/2).[(L_q - L_d).i_{qs}.i_{ds} + \lambda_f.i_{qs}] \end{aligned} \tag{2.12}$$

$$T_e = 1.5 * (P/2).[\lambda_r.i_{qs} - (L_d - L_q).i_{qs}.i_{ds}] \tag{2.13}$$

Further, the rotor speed ω_r of PMSG is given by :

$$\omega_r = \frac{P}{Js}(T_e - T_m) \tag{2.14}$$

$$\omega_r = \int \frac{P}{J}(T_e - T_m)dt \tag{2.15}$$

For the dynamic simulation of PMSG machine, the mathematical equations are rearranged

and represented as:

$$i_{ds} = \int (\frac{-v_{ds} - R_s.i_{ds} + \omega_r.L_q.i_{qs}}{L_d})dt \tag{2.16}$$

$$i_{qs} = \int (\frac{-v_{qs} - R_s.i_{qs} - \omega_r.L_d.i_{ds} + \omega_r.\lambda_r}{L_q})dt \tag{2.17}$$

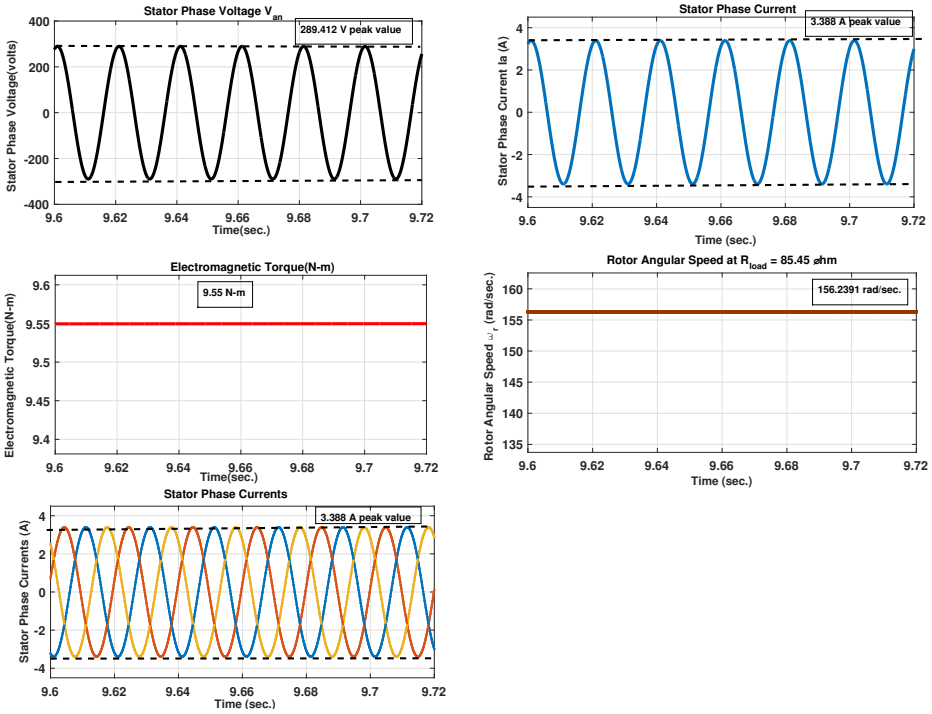

Figure 2.2: Steady State results of PMSG Model

Figure 2.1 shows the d-axis and q-axis equivalent circuit of PMSG. In this dynamic model , the dq-axes stator voltages v_{ds} and v_{qs}, the rotor flux linkage λ_r, and the mechanical torque T_m are the inputs to the synchronous generator model. The dq-axes stator currents i_{ds} and i_{qs}, the rotor mechanical speed ω_r, and the electromagnetic torque T_e are the outputs.

2.2.2 Validation of PMSG Model

This section presents the results of PMSG model with the modeling of machine carried out in the MATLAB/SIMULINK with the parameter details given in Table 2.1. These waveforms has been presented as validation of the PMSG modeling discussed in the previous section. In order to validate the model, the PMSG has been fed with mechanical torque input varying from 2 N-m to 9.55 N-m (rated value) in on open loop condition and output of the PMSG is given to the resistive load of 85.45 Ω.

PMSG DETAILS	
PARAMETERS	RATINGS
No. of poles	4
Flux linkage	0.9426 Wb
d-axis inductance	24.3 mH
q-axis inductance	24.3 mH
Moment of Inertia	$0.0145 kg - m^2$

Table 2.1: PMSG Ratings

- Figure 2.2 shows the steady state response of the PMSG model with the resistive load of 85.45 Ω with the mechanical torque input being equal to 9.55 N-m.

- Figure 2.3 shows the variation in the electromagnetic torque and rotor angular speed corresponding to the variation in the mechanical input torque. As it can be observed that with increase in the input torque, the electromagnetic torque and rotor angular speed increases.

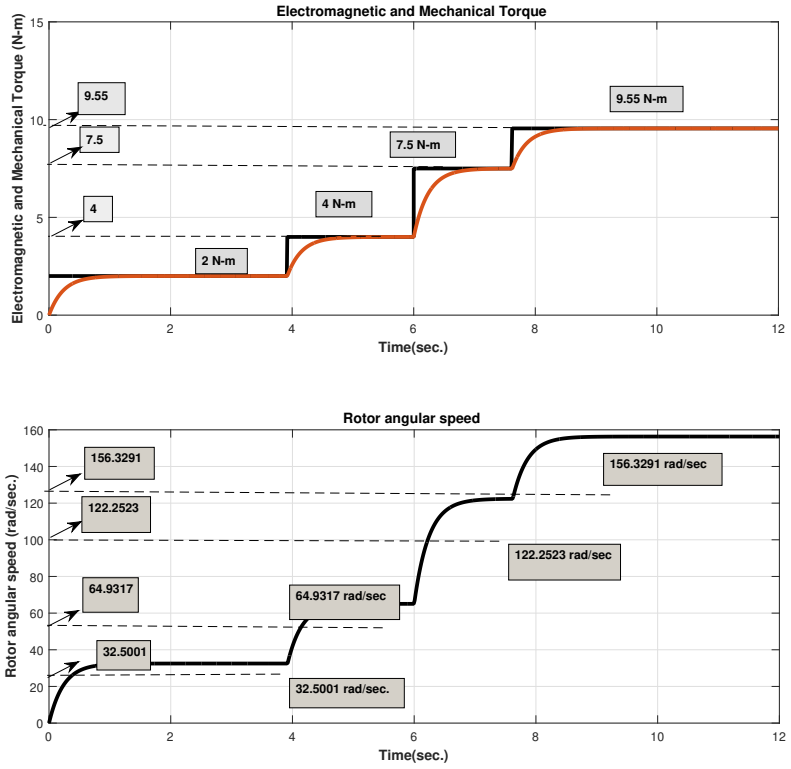

Figure 2.3: Electromagnetic Torque and Rotor angular speed waveforms at steady State

2.3 Solar Photovoltaic (SPV) array

2.3.1 Modeling of PV

The PV model considers the temperature (T) and irradiance (G) as input and generates the electrical parameters of an equivalent circuit model as an output. There are different types of equivalent circuit models: single diode model, two diode model, etc.

The electrical parameters utilized in the single-diode equivalent circuit :

- Photovoltaic current or Light Generated Current (I_{ph}),
- Reverse Saturation Current of diode (I_o),
- Diode Ideality factor (a),
- Series Resistance (R_s),

- Shunt Resistance (R_p)

These parameters will be determined for modeling a photovoltaic source. The current produced by PV source depends on amount of incident solar radiation falling on PV Surface. Therefore, the equivalent model of a PV cell is represented by a current source I_{ph}. The diode is connected in anti-parallel because the current due to recombination flows in opposite direction to the light generated current. The reverse saturation current (I_o) and diode ideality factor (a) are the parameters to be determined for finding diode current.

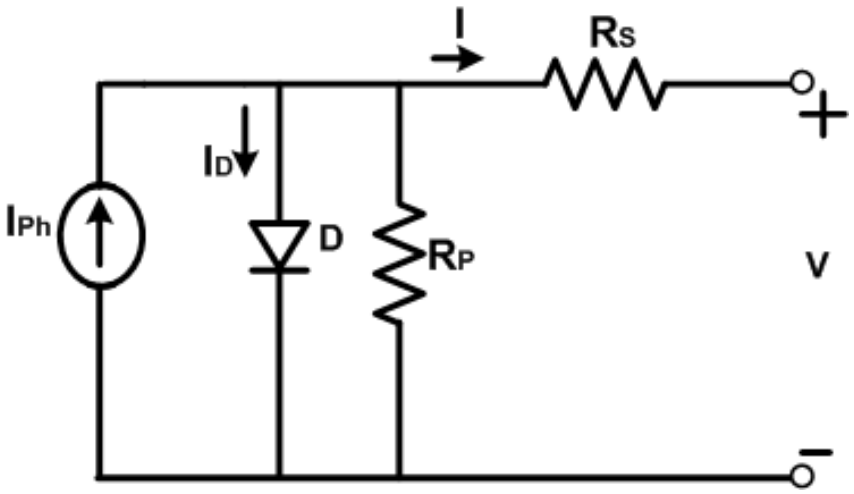

Figure 2.4: Single Diode Model

Series resistance (R_s) represents both the resistance of the metal connections and the resistance to the flow of electrons within the semiconductor. The current source is represented in parallel with the shunt resistance (R_p), which depicts the resistance provided to the current flow's leakage path in a PV cell (Solanki, 2015).

Figure 2.4 represents the single diode model. By using KCL in this model, the photovoltaic current is represented as

$$I_{ph} = I_D + I \tag{2.18}$$

Representing I_D in terms of diode saturation current (I_o) and then PV array current is represented as :

$$I = I_{ph} - I_o \left\{ \exp \frac{(q(V + IR_s)}{akTN_s}) - 1 \right\} - \frac{V + IR_s}{R_p} \tag{2.19}$$

PV PANEL RATINGS	
PARAMETERS	RATINGS
Peak Power	74 W
Voltage (V_{mp})	17 V
Current (I_{mp})	4.4 A
Open Circuit Voltage	21.8 V
Short Circuit Current	4.9 A

Table 2.2: Data Sheet of TATA BP Solar - TBP1275

where I_{ph} = photovoltaic current(A) ,
I_D = Diode current (A)
I = PV array current(A)
I_o = Diode saturation current(A)
T = Cell operating temperature(K)
R_s and R_p are series and parallel resistances(Ω)

N_s = Number of cells connected in series
N_p = Number of cell strings that are connected in parallel
q = electron charge = 1.60217646 $\times 10^{-19}$ C and
k = Boltzmann constant = 1.3806503$\times 10^{-23}$ J/K

2.3.2 Validation of PV model

By solving eq.2.19 for I and V , the characteristics of PV module are obtained. The PV module's current voltage (I-V) characteristics are shown in Figure 2.5. The PV Power(P) is obtained as a product of PV voltage (V) and PV current (I) and characteristics power-voltage(PV) obtained is as shown in Figure 2.5. There are three important points marked in the I-V curve. They are denoted as open circuit point (OCP), short circuit point (SCP) and maximum power point (MPP).

- At OCP, I = 0, V = V_{oc}.
- At SCP, V = 0, I = I_{sc}.
- At MPP,I = I_{mp},V = V_{mp}.
  It implies that at this point, the PV module's maximum power can be obtained. For a

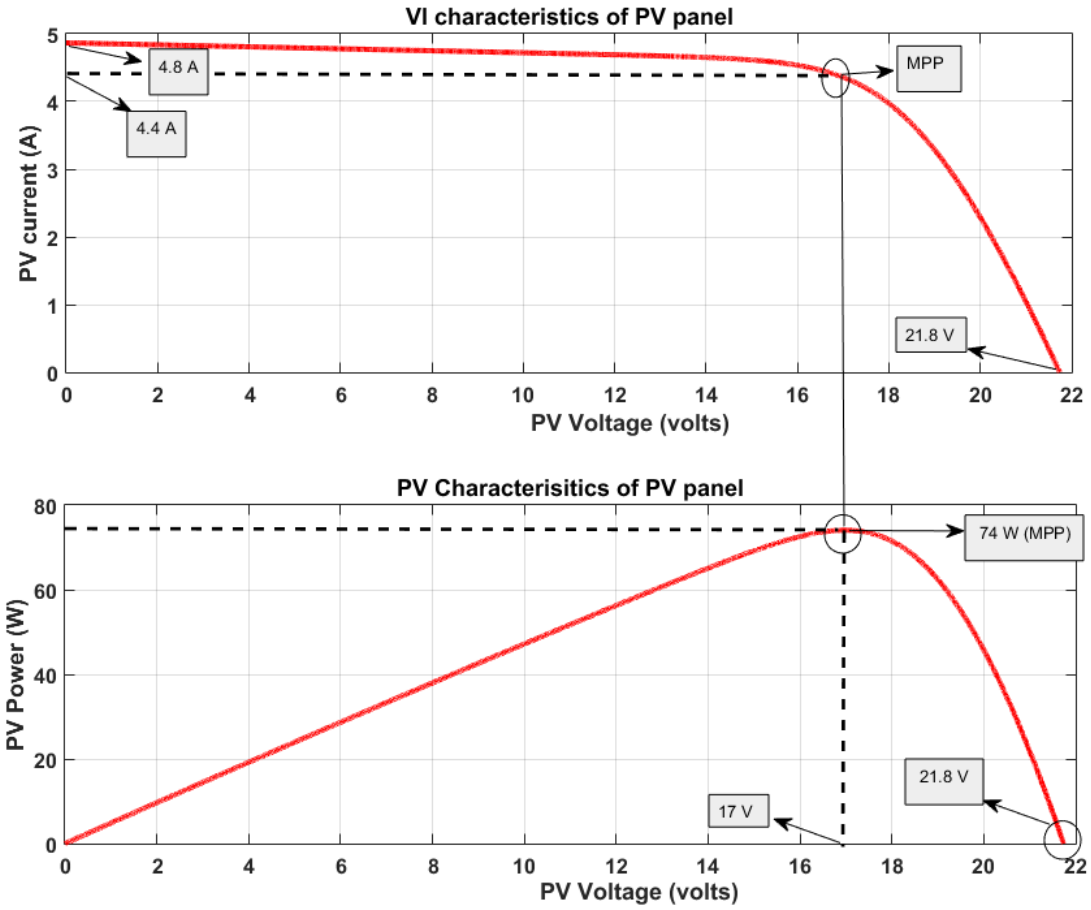

Figure 2.5: PV and VI Characteristics at G=1000 W/m^2

PV module there exists a maximum power point where peak power extraction from the panel can be accomplished.

- Figure 2.5 depicts the PV and VI characteristics corresponding to the irradiation of 1000 W/m^2. It is clear from the figure that power at MPP is 74 W while V_{mpp} is 17 V and I_{mpp} is 4.4 A. The values marked in the Figure 2.5 at MPP condition maps to the values that are given in the datasheet parameters of the PV panel as shown in the Table 2.2.

- Figure 2.6 shows the PV and VI characteristics corresponding to the different irradiation levels. It can be clearly seen that as the irradiation changes the short circuit current decreases drastically which will decrease the power output from the PV

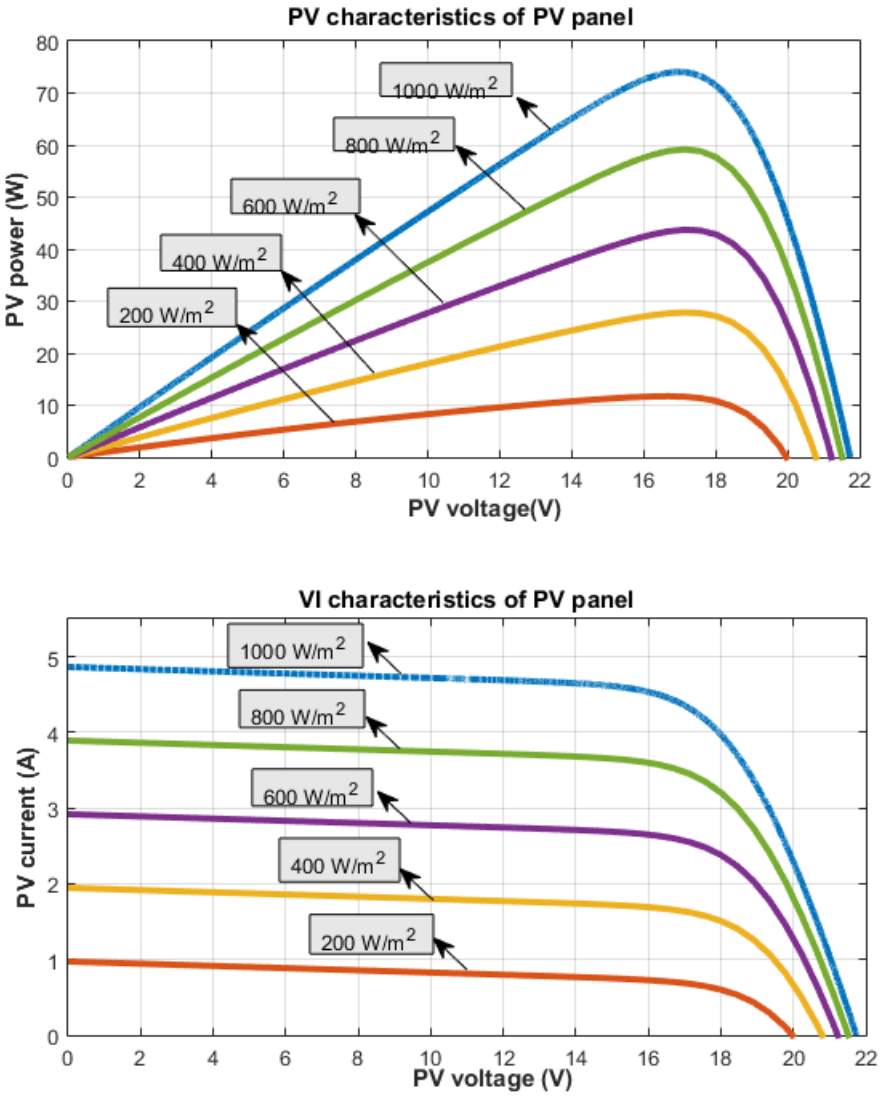

Figure 2.6: PV and VI Characteristics at other irradiation levels

panel. This conclusion can be further strengthened by observing the PV characteristics. Figure 2.7 depicts the PV array characteristics being used in carrying out the investigation studies

2.4 Configuration of Proposed Hybrid Power Converter

The configuration of the proposed hybrid power converter is depicted in the Figure 2.8. The converter is powered by the hybrid sources of solar photovoltaic array and wind source

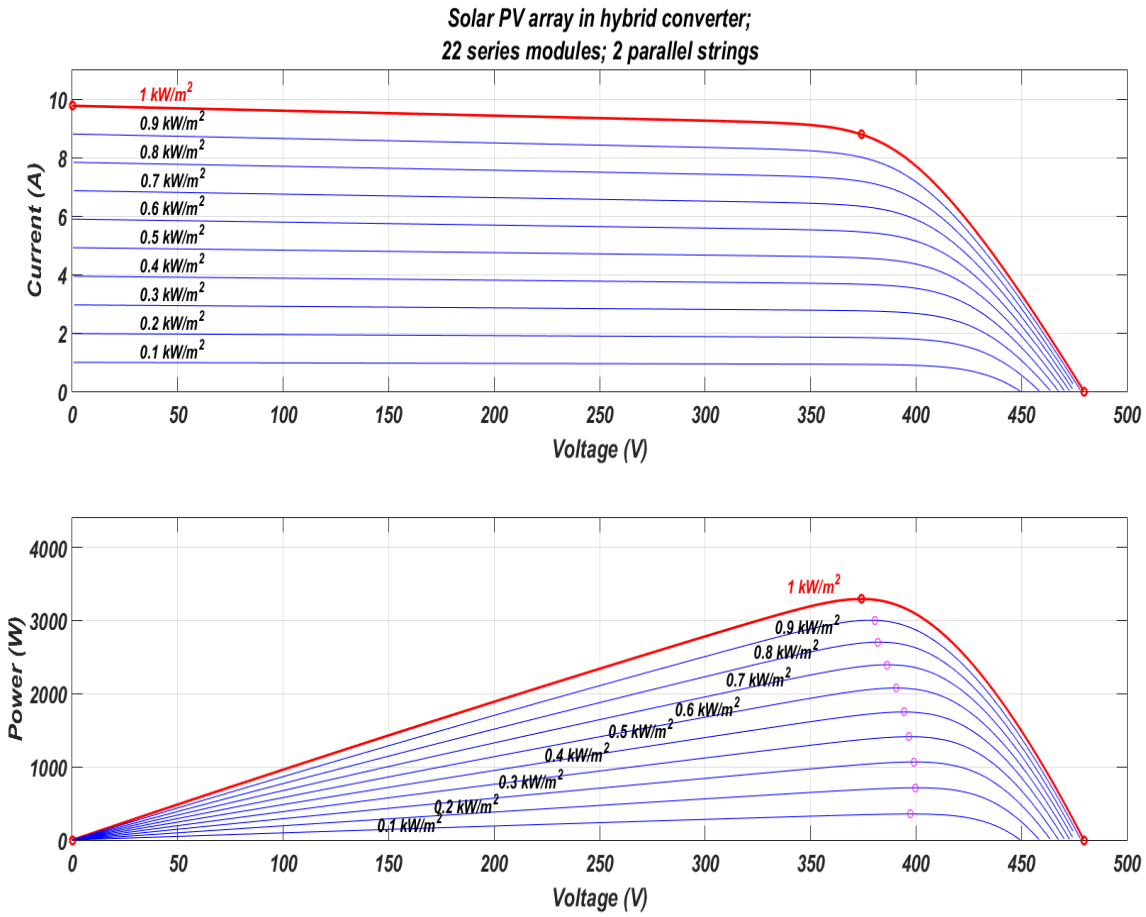

Figure 2.7: PV array characteristics

based permanent magnet synchronous generator. It is perceived that the proposed power converter consists of six controllable switches[S_{w1} - S_{w6}]. Herein, each PMSG phase terminals are connected to the mid-point of the leg. While a solar PV array is linked between the two nodes formed by the intersection point of top switches and bottom switches, respectively, and an inductor is interfaced between the PV array's positive terminal and the node formed by the intersection points of upper switches(marked as "s"). In addition, the output of the bridge network that was constructed with the switches S_{w1} - S_{w6} is connected in series with the diode, and as a result, the diode is connected to both the load capacitor and the load. Thus, the converter is constructed using six switches S_{w1} - S_{w6}, two diodes D_1 and D_2, two capacitors C_{PV} and C_{DC}, as well as four inductors L_{boost} (serially connected to PV) and L_a, L_b, L_c (in phase with the three terminals of PMSG). The diode D_1 is merely included for the purpose of protecting the PV array.

The proposed converter is capable of performing simultaneous AC-DC and DC-DC conversions, thereby facilitating the integration of hybrid PV-wind sources into this architecture with single stage power conversion capability. In addition to that, this converter can operate effectively across a wider range of irradiation levels, wind velocity, and load levels.

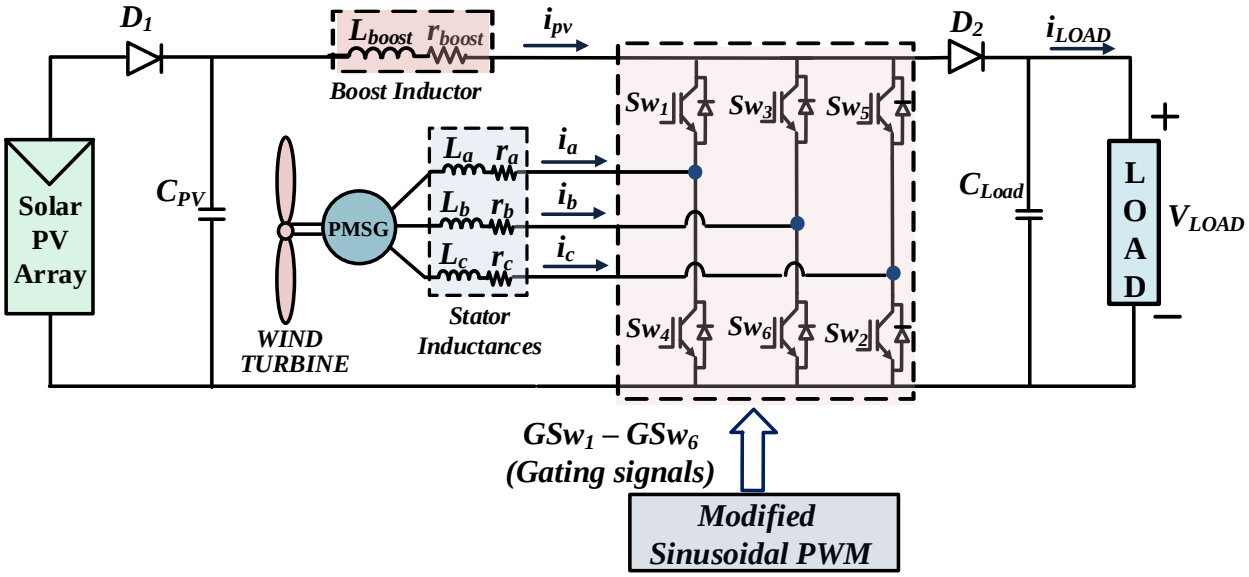

Figure 2.8: Proposed Single stage Hybrid Power Converter

2.4.1 Development of proposed hybrid power converter

Owing to the unpredictability of renewable energy sources, it is essential to deploy the power converter in order to transfer the energy into a form that can be utilised by the consumer or load. Because solar photovoltaic array produces DC output due to its intrinsic characteristic, it has to be interfaced to an appropriate DC-DC converter in order to extract solar energy in a form that is usable (regulated DC), as illustrated in Figure 2.9(a). In addition, wind source is both intermittent and variable in nature; thereby, a wind-based source will typically consist of a permanent magnet synchronous generator that is coupled to an AC-DC converter to convert the wind energy into a form which can be usable (regulated DC), as illustrated in Figure2.9(b).

Since wind and solar are complementary in nature in terms of availability, thereby they are being integrated to form one unified system and henceforth the hybrid inputs based standalone DC system is considered as more reliable system. As already mentioned in

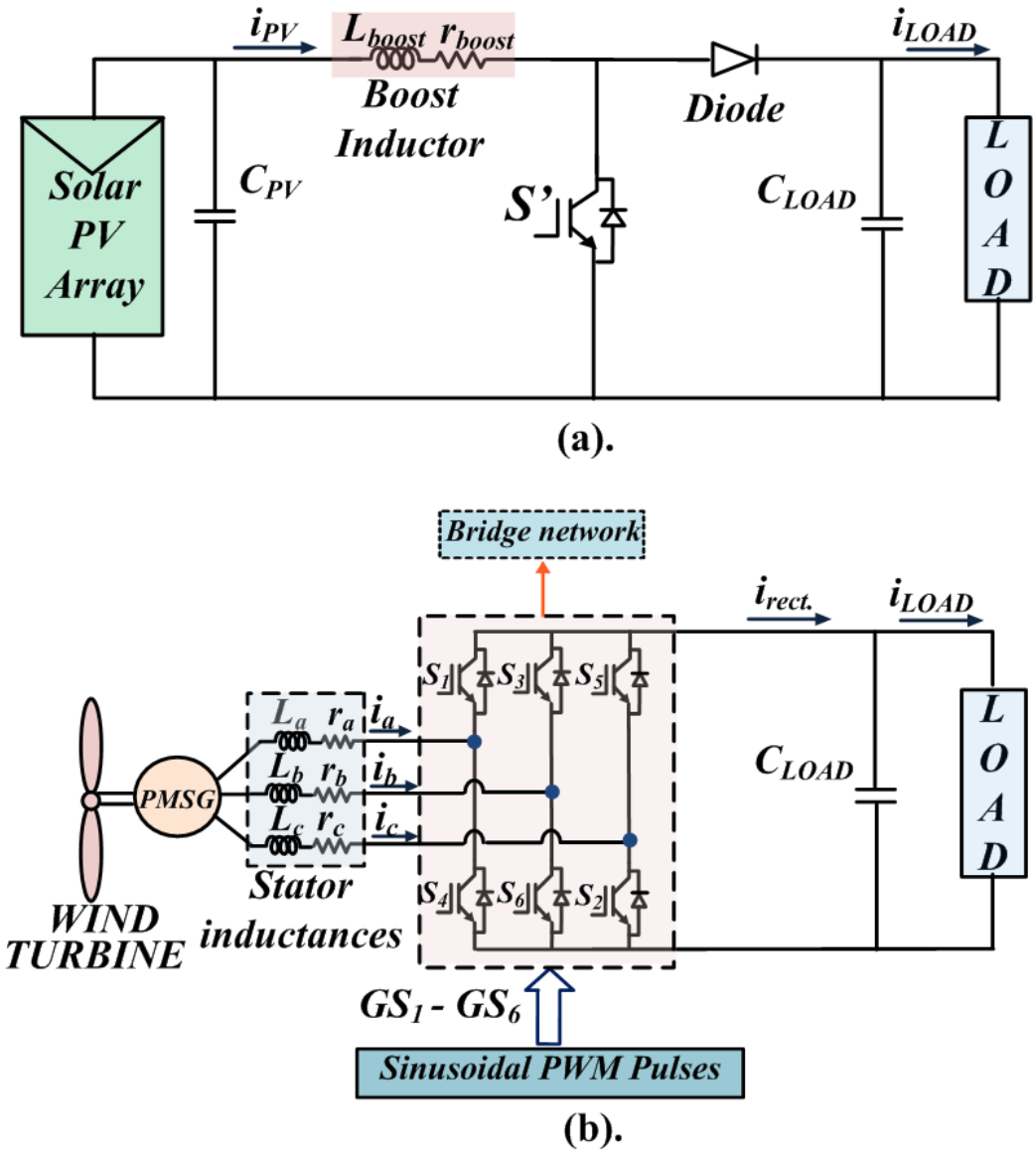

Figure 2.9: (a). Solar PV based Boost Converter, and (b).Wind-PMSG based 3-phase controlled rectifier

section 1.3.3 that reliability is an important aspect in standalone DC system. Also, under-utilization of any conversion stages should be avoided. Therefore, the proposed hybrid power converter complies with both the important aspects pertaining to the standalone DC system with hybrid inputs.

Concerning the fact that solar and wind energy sources are complementary in terms of their availability, they are combined to form one unified system. Consequently, the

hybrid inputs-based standalone DC system is perceived as having a better reliability. As it is discussed in the section 1.3.3, reliability is vital for a standalone DC system. Also, avoiding the under-utilization of any conversion units is another important consideration. As a result, the proposed hybrid power converter has been developed that satisfies both the requirements of the standalone DC system utilizing the hybrid inputs.

The construction of a proposed hybrid power converter can also be interpreted as the merging of a solar-based boost converter topology with a PMSG-based AC-DC converter structure. This was accomplished by replacing switch S' of the boost converter (Figure 2.9(a)) with the bridge network of S_1 to S_6 of the AC-DC converter (Figure 2.9(b)). Figure 2.10 illustrates the switch configurations that were utilised in the process of merging the structures described above.

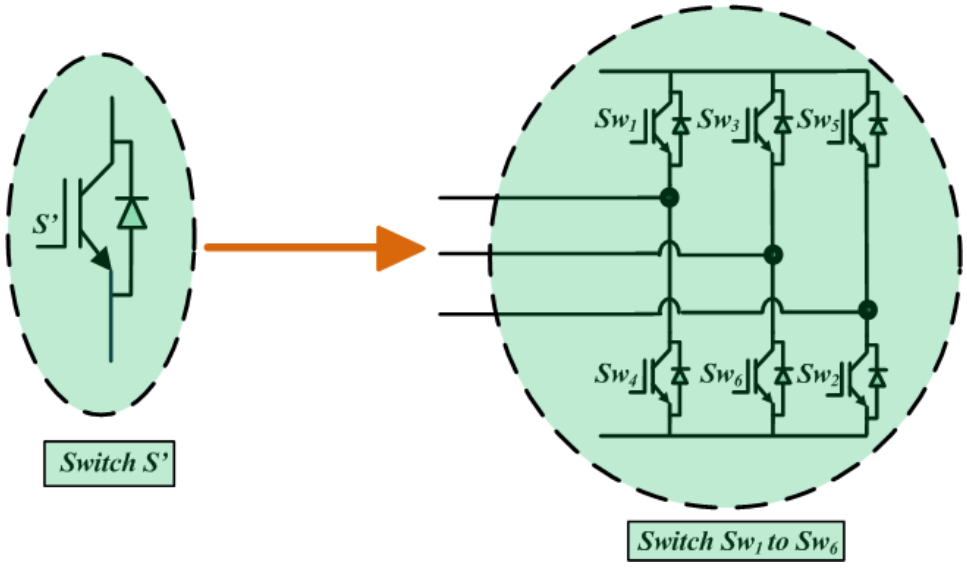

Figure 2.10: Switch Configuration of proposed hybrid power converter

It is necessary to take into consideration of the zero mode state of AC-DC conversion in order to achieve the simultaneous DC-DC conversion and AC-DC conversion from solar and wind-based systems, respectively in the proposed power converter configuration. It is important to take into account that the zero mode state of AC-DC conversion indicates that either all of the top switches are "turned ON" or all of the bottom switches are "turned ON". Within this switching state of proposed converter, a shoot-through mode state is inserted which ensures the concurrent operation of both the DC-DC conversion and the AC-DC conversion. Additionally, the shoot-through operation mode implies that there is no active transfer of power from both the sources side to the load side. As a result, this mode is being

utilised so that the photovoltaic energy can be stored in the inductor L_{boost}.

The overall architecture of the proposed converter, which comprises merging a PV boost converter and a wind-based PMSG AC-DC converter, is depicted in the Figure 2.11. The proposed hybrid converter makes use of both wind and solar power, and is operating with simultaneous AC-DC conversion and DC-DC conversion respectively.

The proposed converter has the additional advantages of having a simple configuration, increased reliability, and the elimination of redundant conversion stages in the event of any source unavailability. In addition to that, a PWM gating strategy based on a modified sinusoidal pulse width modulation approach has been incorporated to facilitate the converter operation.

In order to satisfactorily carry out the necessary shoot-through operation, it is necessary to make use of the zero states of the conventional voltage source rectifier appropriately in order to enable DC-DC conversion. Because the zero states of a voltage source rectifier (VSR) are used to store energy for AC side inductors coming from a wind source, a portion of this zero state is utilised to execute the shoot-through operation necessary for energy storage in a boost inductor supplied(near solar PV array side). During this interval, the load-side voltage will be supplied by the capacitor on the load side. Henceforth, a single-stage converter topology has been designed to accommodate both the simultaneous DC-DC conversion as well as the three phase AC-DC conversion process.

The proposed hybrid power converter topology that has been presented gives the following advantages over the existing systems with PV-wind sources[discussed in section 1.3.3]:

1. In comparison to other cascaded-based topologies for the hybrid inputs-based system, this topology has only one stage of conversion. While other topologies for the hybrid inputs-based system have cascaded stages.

2. Simultaneous power flow from the PV-wind sources is accomplished by integrating a DC-DC conversion and a three-phase AC-DC conversion in the single-stage architecture of the proposed hybrid power converter.

3. The requirements for the number of gate drive circuits are minimal. It is possible to accomplish a simultaneous conversion procedure by making use of the same set of gate drives that are utilised in the traditional AC-DC converter.

4. Conventional control methods can be utilised with the proposed power converter in

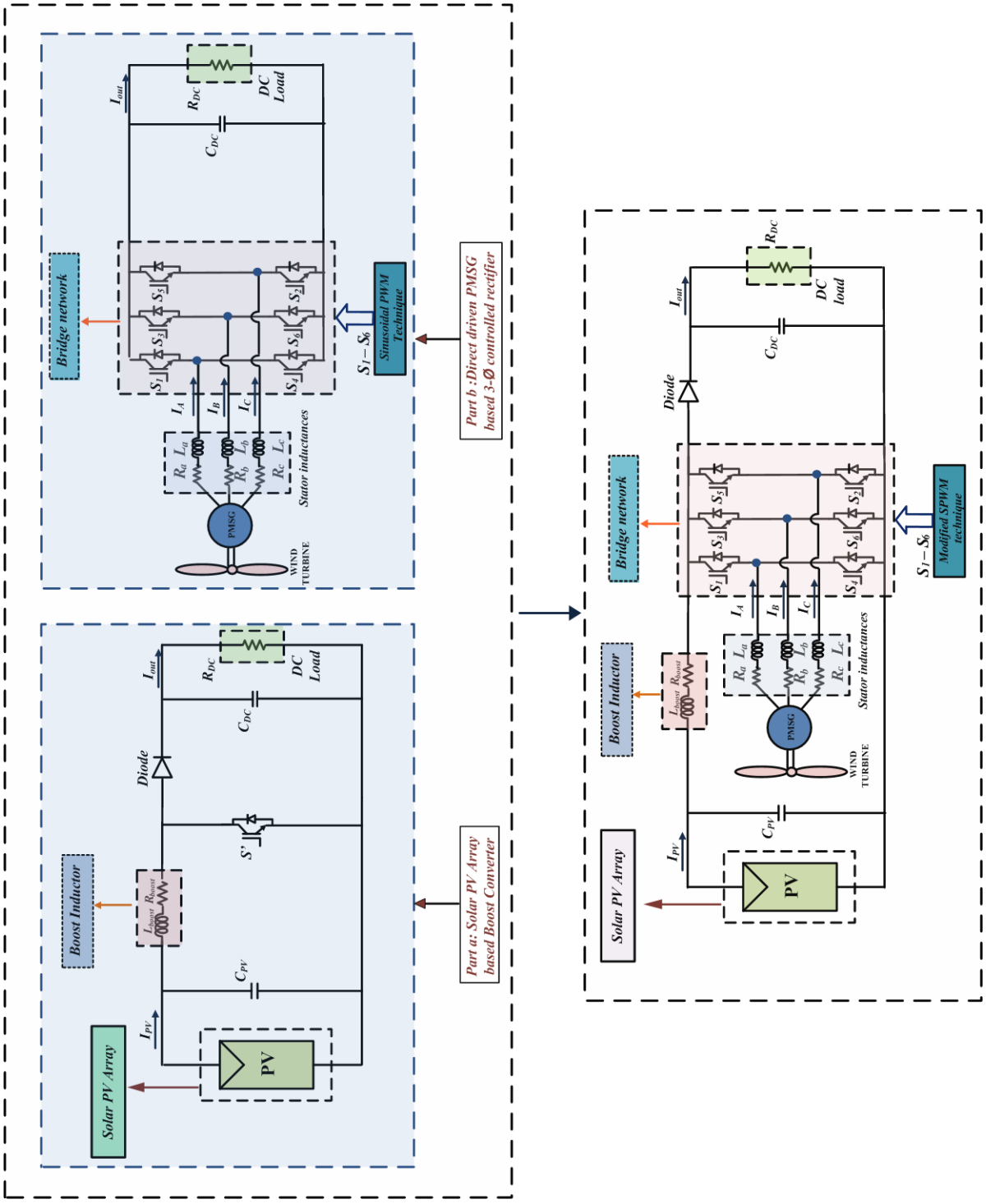

Figure 2.11: Construction of proposed hybrid power converter

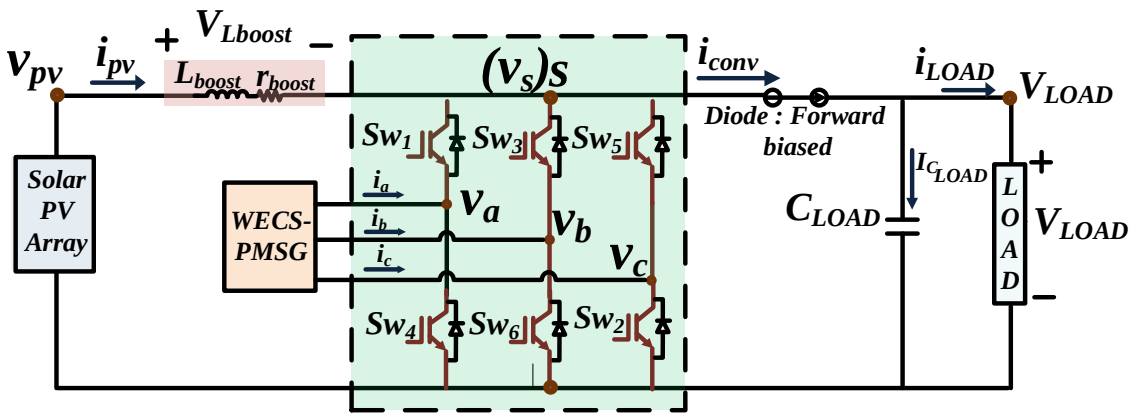

Figure 2.12: Illustration of concurrent power conversion in proposed circuit

order to accomplish simultaneous DC-DC conversion as well as three-phase AC-DC conversion.

5. In general, the availability of solar and wind resources are complimentary; hence, whenever anyone source is absent, the power converter that is linked with that source will be underutilised and this is because solar and wind resources are generally available in complementary manner. As a result, the overall arrangement will contain power converters that are redundant, which will result in the complete system being underutilised. Henceforth, this hybrid power converter helps in removing the redundant power conversion that is associated with the hybrid inputs-based systems.

6. Unlike conventional voltage source rectifier based hybrid systems, herein shoot-through state is part of the operation and therefore misgating effects are minimized.

2.5 Operating Principle of the proposed converter

With regard to the Figure 2.12, it is observed that the voltage at the node "s", v_s will exhibit certain relationships of PV-wind sources with the load when the diode D_2 is in the state of conduction. These relations are stated as follows :

$$v_s = V_{LOAD} \tag{2.20}$$

$$v_s = v_{pv} - v_{Lboost} \tag{2.21}$$

$$v_s = GS_{w1}.v_a + GS_{w3}.v_b + GS_{w5}.v_c \tag{2.22}$$

where GS_{w1}, GS_{w3} and GS_{w5} are the switching function for the corresponding switches S_{w1}, S_{w3} and S_{w5} respectively.
According to the relationships shown in (2.20), (2.21) and (2.22), it can be inferred that the load voltage is dependent on the voltage levels of both the sources as :

$$v_s = V_{LOAD} = [v_{pv} - v_{Lboost}] = [GS_{w1}.v_a + GS_{w3}.v_b + GS_{w5}.v_c] \tag{2.23}$$

In addition, the power demand on the load side is met by the hybrid PV-wind sources functioning together as:

$$Ideally,\ \ P_{PMSG} + P_{PV} = P_{LOAD} \tag{2.24}$$

With regard to the relations (2.23) and (2.24), it can be asserted that the proposed hybrid converter integrated to the PV-wind sources is capable of meeting the load requirements of the standalone DC system , regardless of the source or load variations. In this context, suppose if there is any instance of change in PV irradiation level then the PV voltage level will change which will disturb the PV power level thereby affecting the overall power balance. However, as both the hybrid sources are linked together in the proposed converter (node "s") for supplying demand of an standalone DC load , therefore the wind source will shift its operating voltage and the operating power to ensure the load voltage at constant level in addition of fulfilment of overall power balance. This implies that if there is any load level variations or any sources level variations then the voltage levels and the power levels of these sources will be varied concurrently in accordance to maintain the constant load voltage and overall power balance as stated in (2.23) and (2.24) with the hybrid sources capable of undergoing maximum power operating point to non-maximum power operating point.

2.6 Operational Modes of proposed hybrid power converter

The proposed hybrid power converter always operates in three different modes: dual source power mode, single source power mode and zero mode. These modes ensures the simultaneous AC-DC and DC-DC conversions, for wind-PMSG and PV sources respectively. In contrast to the conventional three-phase AC-DC rectifier, which only includes the power mode and the zero mode, the proposed converter includes the dual source power mode,

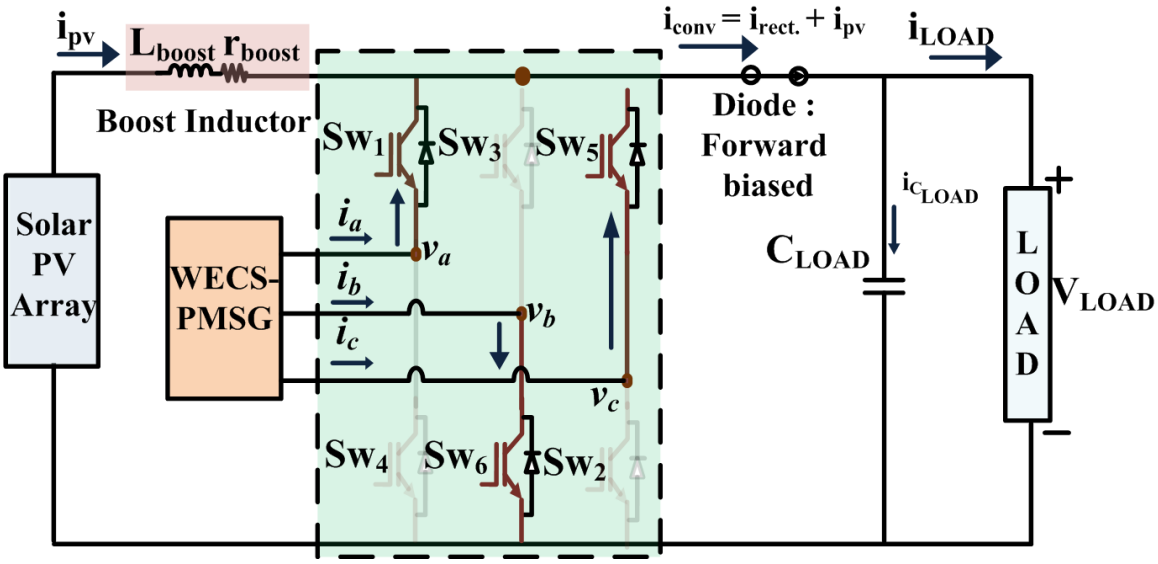

Figure 2.13: Dual source Power Mode of the proposed converter

single source power mode and zero mode. These modes are described in detail as:

1. ***Dual Source Power mode*** :-

   - This mode of operation is denoted by the combined PV-wind sources power being supplied to the load side. Figure 2.13 depicts this interval with switches S_{w1}, S_{w6}, and S_{w5} turned 'ON' with equivalent circuits corresponding to both the sources operations shown in Figure 2.14(a) and Figure2.14(b).
   - During this interval, the switch node voltage (v_s) is fixed to the load output voltage of the proposed hybrid converter, as shown in Figure 2.14(a). This mode of operation is a result of the load-side diode D_2 conduction during this interval. This diode(D_2) current is comprised of rectifier current($i_{rect.}$) and PV current(i_{pv}) from the PMSG and PV source, respectively as detailed in Figure2.13.
   - The power interval mode of operation of this hybrid converter may alternatively be considered as the concurrent occurrence of the switch-OFF mode of operation of a PV-based boost converter(Figure2.14(a))and the active power transfer mode of operation of a wind-PMSG three-phase controlled rectifier (Figure 2.14(b)). The duration of this PV-PMSG power interval is determined by the modulation index and duty ratio signal.

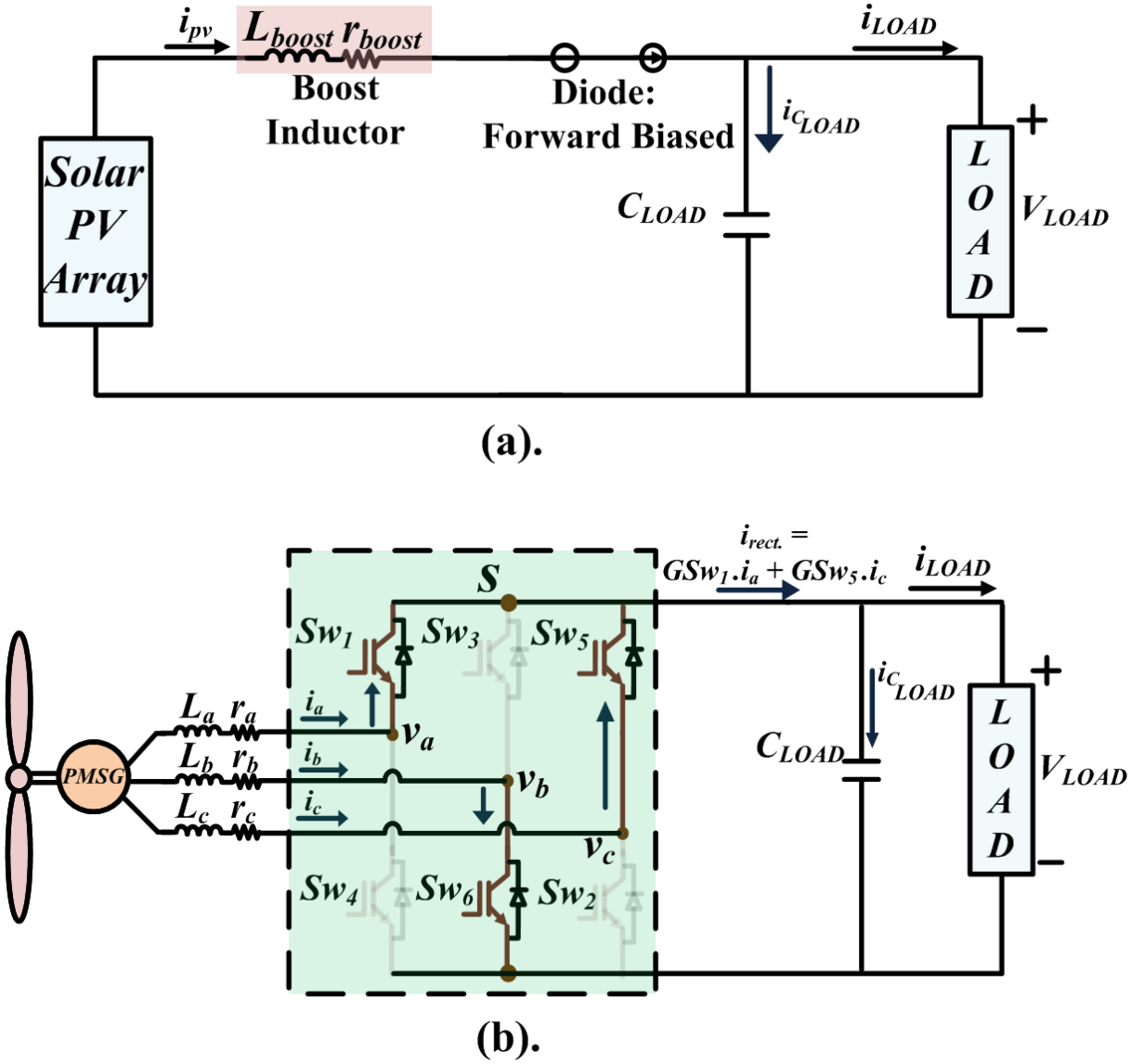

Figure 2.14: Dual source Power Mode of the proposed converter with equivalent circuits (a) PV based boost conversion and (b) Wind based 3-phase AC-DC conversion

■ The flow of power from the hybrid sources to the load side occurring in the dual source power mode of operation is represented in the form of mathematical equations which are represented as :

- Converter bridge current (i_{conv}) is represented as :

$$i_{conv} = GS_{w1}.i_a + GS_{w6}.i_b + GS_{w5}.i_c + i_{boost} \tag{2.25}$$

- Converter output capacitor current is represented as :

$$i_{C_{LOAD}} = i_{conv} - i_{LOAD} \tag{2.26}$$

$$i_{C_{LOAD}} = [GS_{w1}.i_a + GS_{w6}.i_b + GS_{w5}.i_c + i_{boost}] - i_{LOAD} \tag{2.27}$$

- Converter switch node voltage is represented as :

$$v_s = v_{LOAD} \tag{2.28}$$

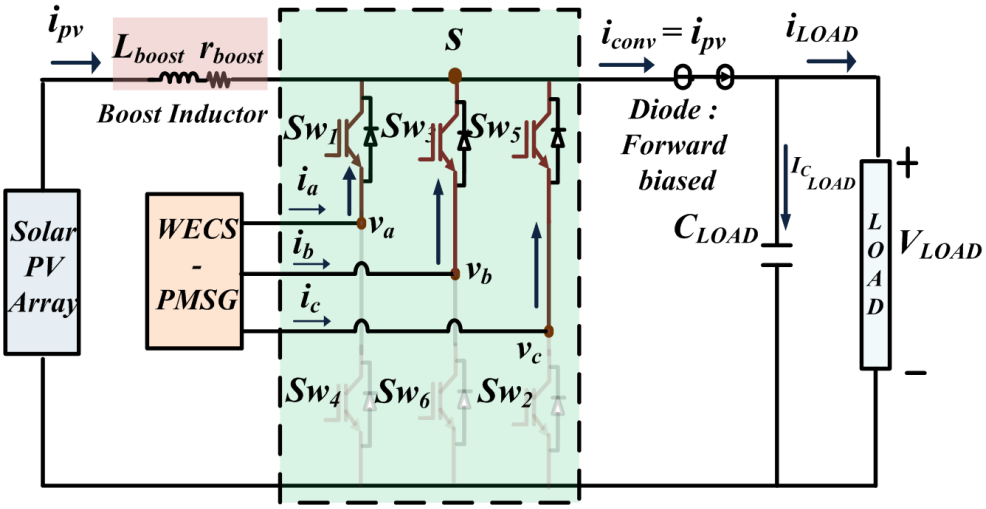

Figure 2.15: Single source power Mode of the proposed converter

2. ***Single source power mode***:-

- In this mode, only PV source supply power towards load side. However, there is no power flow happening from the PMSG towards the load side resulting in rectifier current($i_{rect.}$) to be zero. Therefore, the diode current is comprised of PV current(i_{pv}) only.
- This mode of operation is dictated with either all the top or all bottom switches of the converter being turned 'ON'. As depicted in Figure 2.15, the conducting switches in this interval are S_{w1}, S_{w3}, and S_{w5}.
- Additionally, the equivalent circuit for this mode of operation for hybrid sources is shown in Figure 2.16(a) and Figure 2.16(b), which demonstrates that the

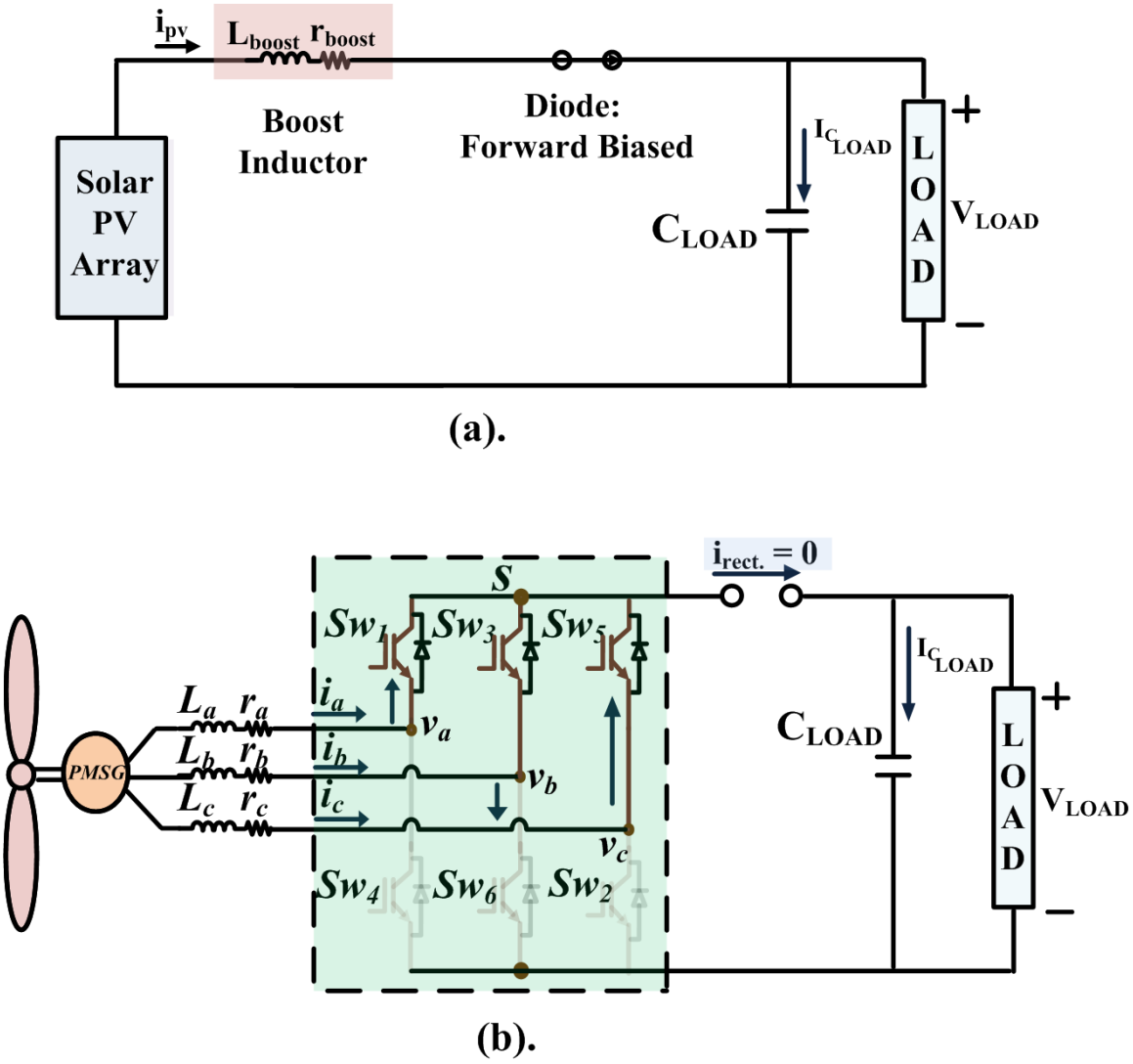

Figure 2.16: Single source power mode of the proposed converter with equivalent circuits (a) PV based boost conversion and (b) Wind based 3-phase AC-DC conversion

PMSG currents are free-wheeling among these conducting switches while the PV current is flowing in the direction of the load side, concluding that only the PV array is supplying power to the load side.

- Thereupon, the mathematical representations of power flow from the sources towards load side occurring in the single source power mode of operation is represented as:

- Converter bridge current (i_{conv}) is represented as :

$$i_{conv} = i_{boost} \tag{2.29}$$

- Converter output capacitor current is represented as :

$$i_{C_{LOAD}} = i_{boost} - i_{LOAD} \tag{2.30}$$

- Converter switch node voltage is represented as :

$$v_s = v_{LOAD} \tag{2.31}$$

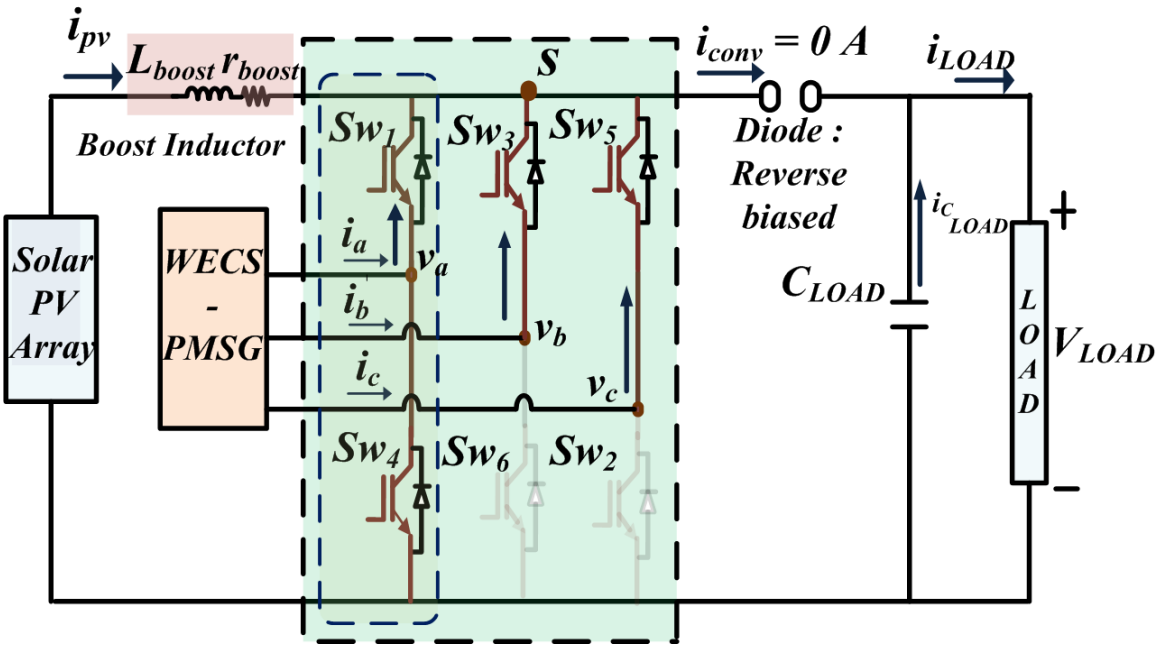

Figure 2.17: Zero Mode of the proposed converter

3. ***Zero mode***:-

- With regard to the proposed converter, this mode of operation is regarded as zero mode interval because both the source are disconnected from the load and therefore there is no power flow from sources towards the load side. Thus, diode(D_2) current is zero.
- In this interval also, the PMSG currents are in the free-wheeling mode only

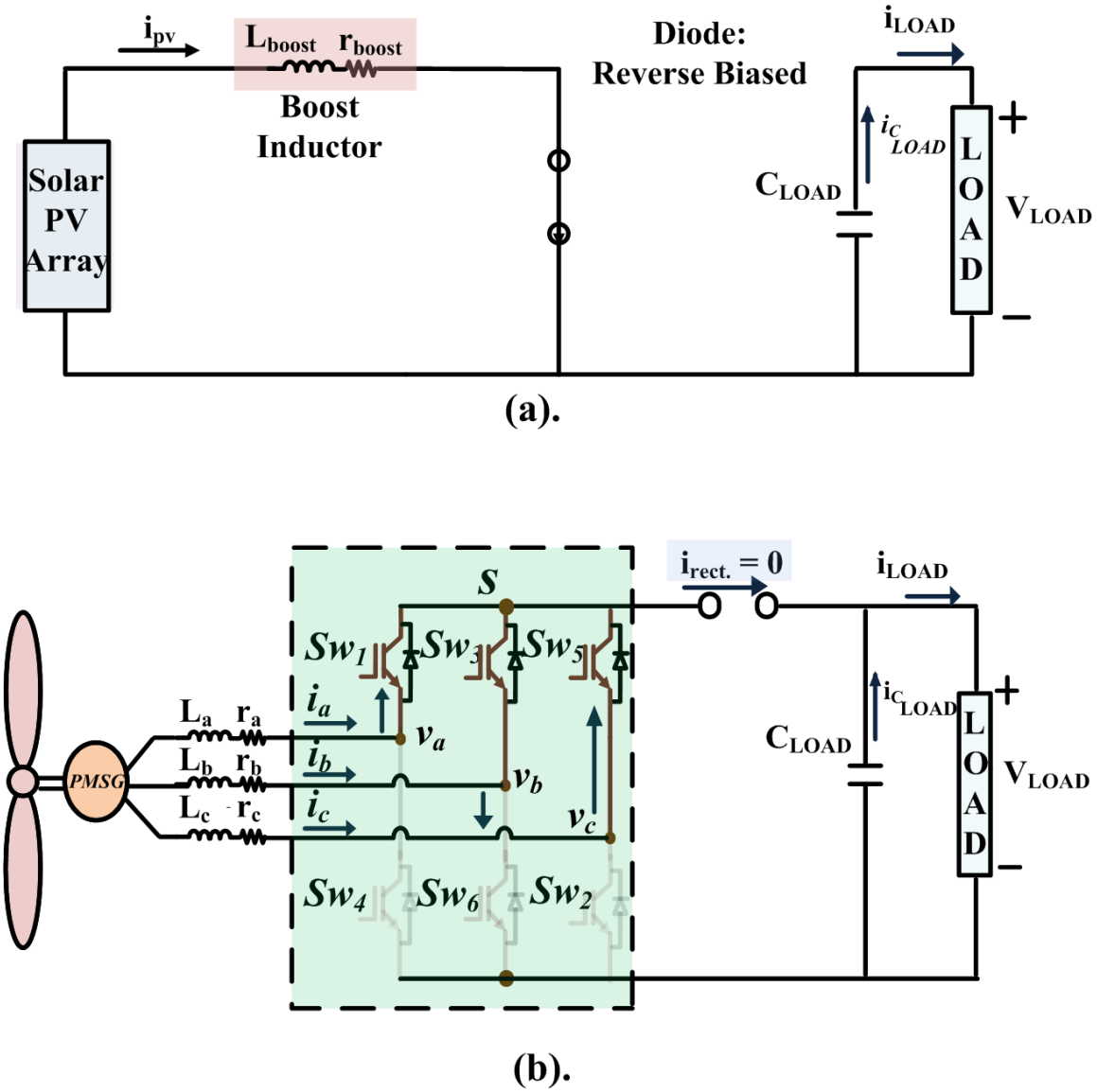

Figure 2.18: Zero mode of the proposed converter with equivalent circuits (a) PV based boost conversion and (b) Wind based 3-phase AC-DC conversion

implying $i_{rect.} = 0$. The PV source is disconnected from the load as PV current is undergoing shoot-through operation due to simultaneous turning "ON" of both the switches in a leg. It is to be noted that shoot-through can occur only when either all the top switches are turned "ON" or all bottom switches are turned "ON".

■ Figure 2.17 depicts the proposed converter operation in zero mode wherein

leg 'A' switches are undergoing the shoot-through operation. Additionally, the equivalent circuits corresponding to the concurrent conversion modes with the hybrid sources are shown in Figure 2.18(a) and Figure2.18(b). Herein, the switches conducting in this mode are S_{w1},S_{w4}, S_{w3}, and S_{w5}. In this period, PV current is running through the shorted leg(Leg- A, marked in Figure 2.17), which charges the inductor L_{boost} and PMSG phase currents are undergoing free-wheeling operation.

- Further, the power flow from the sources towards load side in this zero mode of operation is represented in the form of equation as:
  - Converter's bridge current (i_{conv}) is represented as :

$$i_{conv} = 0 \tag{2.32}$$

  - Converter's load capacitor current is represented as :

$$i_{C_{LOAD}} = i_{LOAD} \tag{2.33}$$

  - Converter switch node voltage is represented as :

$$v_s = 0 \tag{2.34}$$

Table 2.3: Steady-state representations of proposed hybrid power converter in different operational modes

Modes	**Dual source power mode**	**Single source power mode**	**Zero mode**
Converter current(or diode D_2 current)	$i_{conv.} = GS_{w1}.i_a + GS_{w5}.i_c + i_{pv}$	$i_{conv.} = i_{pv}$	$i_{conv.} = 0$
Load capacitor current	$i_{C_{LOAD}} = i_{conv.} - i_{LOAD}$	$i_{C_{LOAD}} = i_{LOAD}$	$i_{C_{LOAD}} = i_{LOAD}$
Converter switch node voltage	$v_s = v_{LOAD}$	$v_s = v_{LOAD}$	$v_s = 0$

The mathematical representation of the power flow for each of the operating modes of the proposed hybrid power converter is presented collectively in Table 2.3. Further, with regard

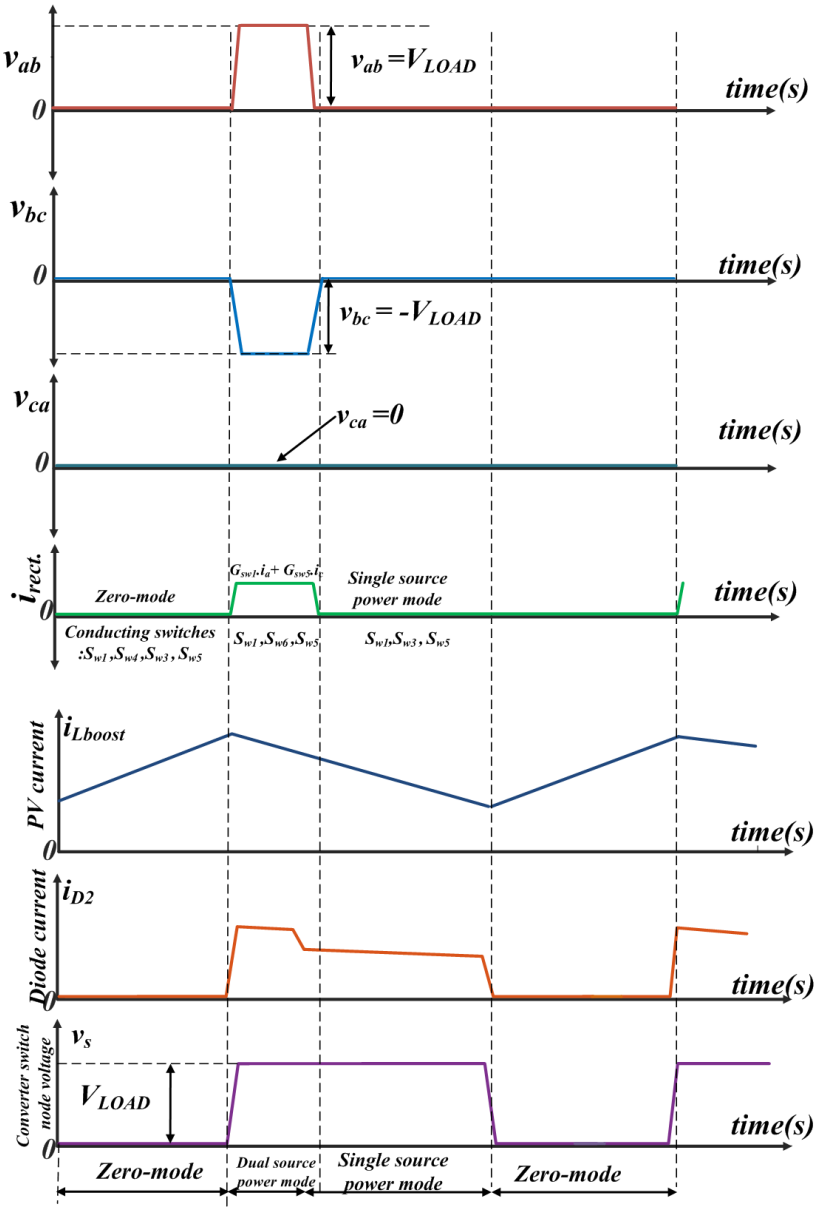

Figure 2.19: Steady state key waveforms of all operational modes during switching period

to Figure 2.19, the steady state key operating waveforms for all these modes are depicted and are illustrated as:

1. As illustrated, with regard to "zero mode of operation", the rectifier current is zero (phase current are free-wheeling) which also infers that PMSG line voltages v_{ab},v_{bc},v_{ca} are zero as shown in Figure2.17 which implies that there is no power transfer between the PMSG and the load. The PV current is rising (undergoing shoot-through oper-

ation) which indicates the charging of L_{boost}. As a result, the current through diode D_2 is zero, and the converter switch node voltage is also zero, that implies there is no power flow from both the sources towards the load.

2. Then, in the "dual source power mode", both the PV current and rectifier current ($i_{rect.} = GS_{w1}.i_a + GS_{w5}.i_c$) are flowing towards the load side and thus the diode D_2 current builds up with this combined current of PV and PMSG sources while converter switch node voltage equals the load voltage. The rectifier current consists of PMSG currents flowing to the load side as a result of conducting switches(S_{w1}, S_{w6}, and S_{w5}) and thereby the PMSG line voltages $v_{ab} = v_{LOAD}$, $v_{bc} = -v_{LOAD}$, $v_{ca} = 0$ as shown in the Figure2.13.

3. Further, at "single source power mode", converter switch node voltage is equal to load voltage and the diode D_2 current is flowing due to PV source current, implying that only PV source is supplying power to the load. The PMSG line voltages v_{ab}, v_{bc}, v_{ca} are zero in this mode as depicted in the Figure 2.15 with $i_{rect.} = 0$ (PMSG phase currents are free-wheeling). As there is no PMSG power transfer towards the load side(i.e,$i_{rect.} = 0$) during "single source power mode", it is to be noted that the magnitude of diode D_2 current is greater during dual source power mode" than during "single source power mode" which indicates that both the sources together are supplying power to the load during "double source power mode".

2.7 Summary

This chapter discusses the architecture of the proposed hybrid converter. It highlights the construction of the power converter and associated merits concerning the existing hybrid structures. Further, it states the principle of operation and elaborates on the various mode of operation. Modes of operations with their equivalent circuits have been outlined.

Chapter 3

Proposed converter Control Structure and PWM Scheme

3.1 Introduction

The proposed hybrid power converter consists of the hybrid sources viz, wind and solar as inputs. Thus, the control scheme is devised to have the concurrent operation of wind-based PMSG 3-phase AC-DC conversion and solar PV array based DC-DC boost conversion. As it is known that the control structure for 3-phase AC-DC conversion (Wu et al., 2011), (de Freitas et al., 2016) is pertaining to the modulation index (m), which regards to generation of three phase modulating signals (reference signals) denoted as m_a, m_b and m_c for phases A, B and C respectively. In contrast, for the DC-DC conversion (Coelho et al., 2010), the control aspect herein is to generate the Duty ratio signal (D_{sh}) for performing the photovoltaic DC-DC conversion in the proposed single stage multi-port hybrid power converter.

The primary objective of this control structure in the present system is to maintain the load voltage regulation under varying sources or varying load conditions. Henceforth, the control structure for simultaneous AC-DC and DC-DC conversions will primarily emphasise on load voltage regulation while simultaneously extracting power from the hybrid sources. The detailed explanation pertaining to individual conversions of PMSG based AC-DC conversion and solar PV based DC-DC conversion is explained in further sections.

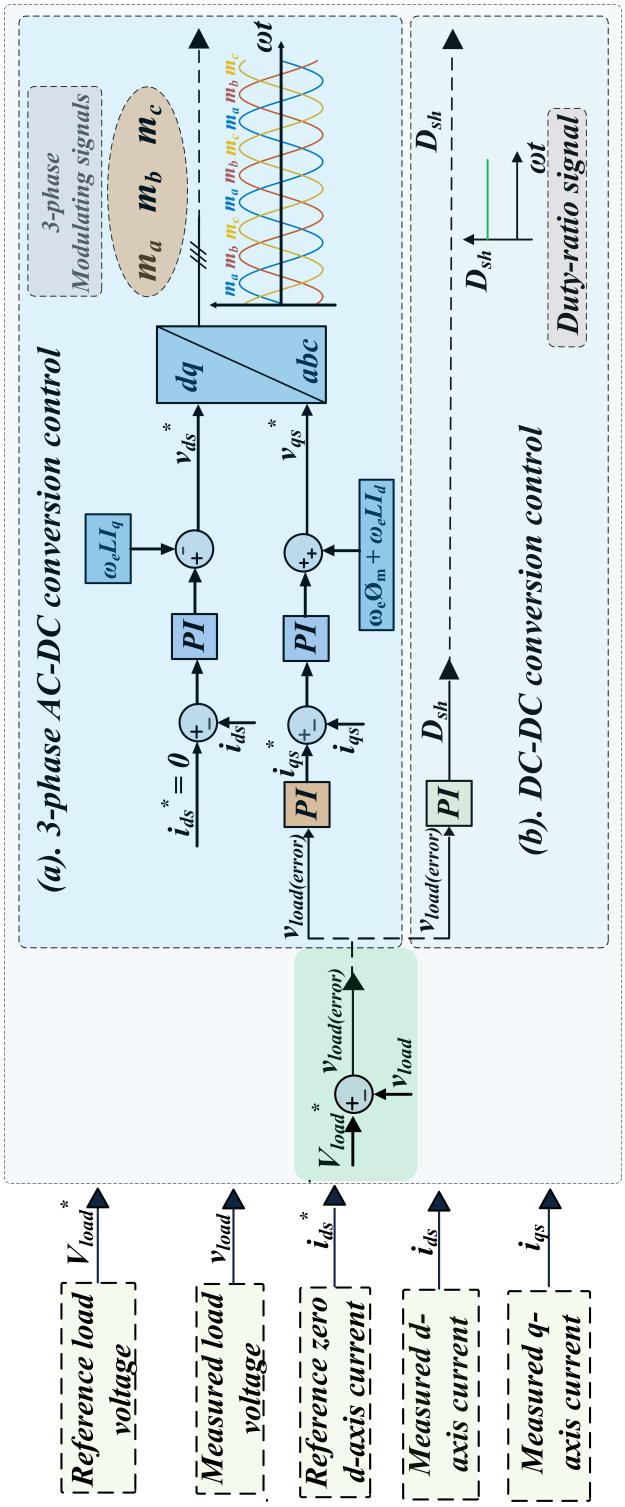

Figure 3.1: Control strategy for the Proposed single stage multiport hybrid power converter

3.2 Control logic framework

The hybrid sources tend to impose the different voltage levels at the load side in the proposed configuration if they are allowed to operate in the unregulated manner. Thus, in order to ensure that both the sources together act as a single source unit and thereby tend to provide the same voltage level at the load port, it is necessary to impose a common control constraint for conducting both the sources operation. Now, as per the relation in eq.(2.23), it can be stated that the constant value of load voltage will tend to regulate the voltage levels of both the sources and thereby the self-regulation will occur in the current levels from both the sources accordingly. This will form the logical framework of control architecture for the proposed converter.

The integration of hybrid sources in this single-stage architecture is to ensure that these sources together always fulfil the load requirement of constant load voltage and necessary load power. This implies that the sources will be undergoing necessary regulation in their operating points to meet the requisite of this standalone DC system. Therefore, the fundamental objective in this integrated control is to ensure the constant load voltage in the proposed system, thereby, the load voltage error serves as an important interlink in the control logic for both the sources as shown in Figure 3.1. This is instrumental in bringing together the functionality of both the sources in order to make them operate together coherently and adaptively, thereon achieving the necessary requirements of standalone DC system.

With regard to the PV based DC-DC conversion control, the load voltage regulator will be utilised to generate the duty ratio control signal which is needed to implement the DC-DC conversion operation in the proposed converter and also to regulate the PV operating voltage and current in accordance with the load requirements.

Now, in the wind-PMSG based 3-phase AC-DC conversion control, the load voltage regulator is used as an outer loop to generate the reference value for the inner current control, i.e, q- axis current ($i_{qs,ref}$). Further, this obtained $i_{qs,ref}$ and $i_{ds,ref} = 0$ will then be used for actuating the inner loop control in this wind-PMSG control.

Thus, this integrated control based on the load voltage regulation should be able to regulate the dynamic output capabilities of hybrid sources in pursuit of achieving the overall power balance and regulating the load voltage to be constant at all operating conditions.

Potential operating scenarios of the proposed single-stage multiport hybrid power converter under various power conditions among the source ports and load port are illustrated

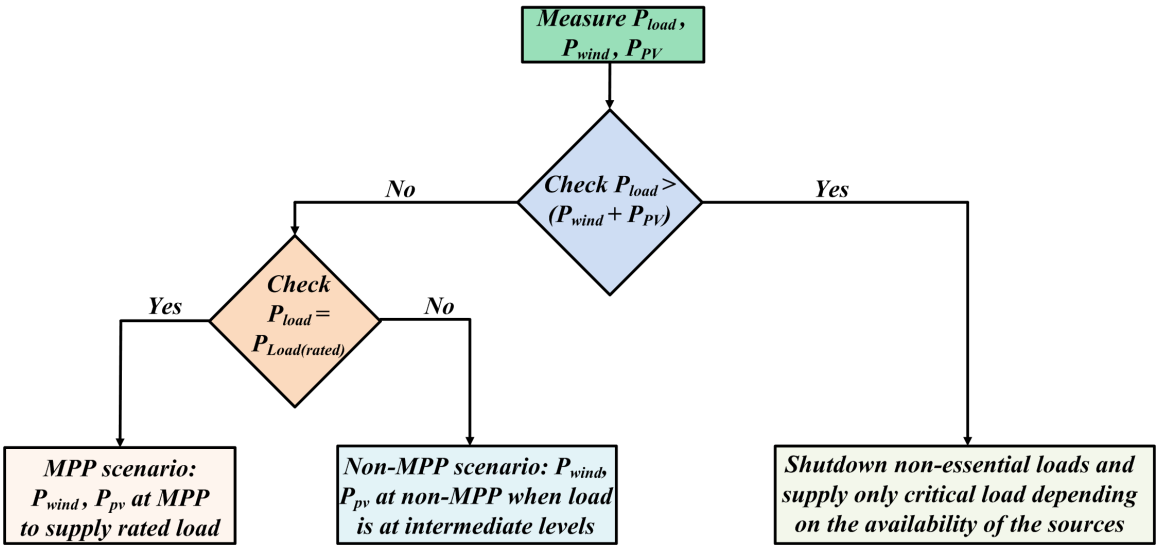

Figure 3.2: Power flow scenario of the proposed single-stage multiport hybrid power converter

in Figure 3.2 and are stated as follows:

1. *Scenario MPP* :-

   (a) When the load power requirement, P_{load} is at the high value such that it can be fulfilled by both the sources together(i.e.,P_{PV} + P_{PMSG} = P_{load}), then the load voltage regulations in the control architecture will tend to push these hybrid sources to function at their respective peak power levels.

   (b) Herein, no explicit MPP technique is involved in this control architecture however it is capable enough to achieve peak power operating point in both the sources together during the rated load level demand. Therefore, the voltage levels of hybrid sources are being regulated that will tend to actuate the necessary self-regulations in the current levels concurrently in both the sources as well and thereby MPP scenario can be attained in addition of fulfilment of constant load voltage and rated load demand.

2. *Scenario non-MPP* :-

   (a) When the load power requirement, P_{load} is not at its rated value but at some intermediate level such that it can be fulfilled by both the sources together then these hybrid sources will be functioning at some non-MPP power levels.

(b) In this scenario, the operating points of both sources will be varied in tandem in order to maintain a constant load voltage while simultaneously satisfying the load power.

3. *Scenario* $P_{load} > P_{PV} + P_{PMSG}$:-

(a) Herein, load shedding needs to be conducted.

(b) Only the critical load power demand is fulfilled by the both the sources together depending on the availability of the sources level.

3.3 Control Structure for simultaneous AC-DC conversion control and DC-DC conversion control

Figure 3.1 shows the control structure for the proposed converter that shows the AC/DC conversion control and DC/DC conversion control to maintain the load side voltage. It depicts the outline for generation of 3-phase modulating signals and duty ratio signal based on the closed loop control scheme for the proposed converter.

Figure 3.1(a) shows the control structure pertaining to the AC-DC conversion (Wu et al., 2011), (Mishra et al., 2019) for the proposed hybrid converter . It is observed that the AC-DC conversion closed control scheme is consisting of dual loop based structure (outer loop and inner loop). The outer loop is pertaining to the load voltage regulation based loop while inner loop consist of PMSG *dq*- axes based current loop. The control of load side DC voltage is achieved by employing PI controller that compares measured load voltage with respect to the reference load voltage. This load side voltage based outer loop will be generating the reference for the *q*-axis based PMSG current.

The output of the load voltage PI controller (AC-DC conversion control) is the reference for the *q*-axis stator current(i^*_{qs}) control. The reference for the *d*-axis stator current i^*_{ds} is zero to employ the zero *d*-axis current control scheme (ZDC). Thus, the *dq*--axes current reference signals, i^*_{ds} and i^*_{qs} are then sent to the generator controller block, which ensures controlling the *dq*-axes stator currents as per the required operating levels.

The permanent magnet synchronous generator herein is operated in a manner that establishes a linear relationship between the stator current and the electromagnetic torque,that requires the generator's *d*-axis stator current need to be set to zero (Wu et al., 2011), (Yaramasu et al., 2017). This method of control is known as zero *d*-axis current control (ZDC)

(Mishra et al., 2019). However, to employ zero d-axis current control, the three-phase stator current in the stationary reference frame is resolved into d-axis and q-axis components in the synchronous reference frame. With ZDC, the i_{ds} component of the d-axis is then imposed to be set to zero. As when i_{ds} becomes zero, then the stator current becomes equal to its q-axis component i_{qs}.

■ For $i_{ds} = 0$,

$$\left\{ \begin{array}{l} \vec{i_s} = i_{ds} + j i_{qs} \\ i_s = \sqrt{i_{ds}^2 + i_{qs}^2} = i_{qs} \end{array} \right\}$$

where $\vec{i_s}$ is the stator current space vector and i_s represents its magnitude in the stationary reference frame, which is also the peak value of the three-phase stator current.

■ The electromagnetic torque of the PMSG (Wu et al., 2011) is :

$$T_e = 1.5 * (P/2) * \lambda_r * i_s$$

where (P/2) is the pole pair and λ_r is the rotor flux linkage produced by permanent magnets of the PMSG .

Moreover, the primary goal is to regulate the load side voltage and this control is achieved by using PI controller that compares the measured DC voltage v_{load} with its reference value V_{load}^* as depicted in Figure 3.1(a). This implies that the irrespective of changes happening in the input or output conditions, load voltage should be maintained at constant value only.

The output of the PI controller serves as a reference for the q-axis stator current i_{qs}^*. This ensures that, regardless of changes in the system , the controller will give the necessary reference current signals to modify the electromagnetic torque value [while employing zero d-axis current control scheme].

The dq-axes current reference signals, i_{ds}^* and i_{qs}^* , are fed to the respective generators current controller, wherein actual currents are being forced to track to their respective reference values. Then, the output of both the current controllers will be merged with the decoupling terms in order to eliminate the dependency of d-axis based terms on q-axis and vice-versa. Finally, the obtained dq-axes signals v_{ds}^* and v_{qs}^* are being transformed to the 3-phase modulating signals m_a, m_b and m_c for A, B and C-phase, respectively as marked in

Figure 3.1(a).

Since the PMSG model in abc-frame cannot realise a zero steady state error for PI controller with time variant variables, three-phase stationary frame is transformed into the synchronously rotating dq-frame. The variables in *dq*-coordinates are DC quantities, and a PI controller can offer steady state error control with zero errors. Thus, the measured three-phase stator currents, i_a, i_b and i_c are transformed into the *dq*-axis currents, i_{ds} and i_{qs} (from stationary frame to rotor flux synchronous frame, using the abc-dq transformation). The transformation of the variables between the abc stationary frame to the *dq* synchronous frame or vice versa can be performed respectively by the equations (3.1) and (3.2).

$$\begin{bmatrix} \underline{i_a} \\ \underline{i_b} \\ \underline{i_c} \end{bmatrix} = \begin{bmatrix} \cos\theta_e & -\sin\theta_e \\ \cos(\theta_e - 2.\pi/3) & -\sin(\theta_e - 2.\pi/3) \\ \cos(\theta_e - 4.\pi/3) & -\sin(\theta_e - 4.\pi/3) \end{bmatrix} \begin{bmatrix} \underline{i_d} \\ \underline{i_q} \end{bmatrix} \tag{3.1}$$

$$\begin{bmatrix} \underline{i_d} \\ \underline{i_q} \end{bmatrix} = (2/3) \begin{bmatrix} \cos\theta_e & \cos(\theta_e - 2.\pi/3) & \cos(\theta_e - 4.\pi/3) \\ -\sin\theta_e & -\sin(\theta_e - 2.\pi/3) & -\sin(\theta_e - 4.\pi/3) \end{bmatrix} \begin{bmatrix} \underline{i_a} \\ \underline{i_b} \\ \underline{i_c} \end{bmatrix} \tag{3.2}$$

The parameter θ_e is the rotor position(electrical) related to rotor speed(electrical), ω_e as $\omega_e = d\theta_e/dt$.

Now, the control structure pertaining to DC to DC conversion (Xiao et al., 2007), (Villalva et al., 2010), (Dash and Nayak, 2015) for the proposed hybrid converter is as shown in Figure 3.1(b). The purpose of this control structure while employing DC to DC conversion in the proposed system is to maintain the DC voltage regulation of the load at different test conditions. As it can be observed that measured load voltage is being compared with the reference DC voltage and the error is being fed to the PI controller that will generate the duty ratio to impose shoot-through operation in the hybrid converter in order to allow DC to DC conversion operation. It it important to note that the value of reference load voltage being used for the load voltage regulator in the AC to DC conversion as well as in DC to DC conversion is same and is equal to 750 V. It is necessary to impose the common regulation constraint on both the sources control as otherwise both photovoltaic and wind sources will have a tendency to impose different voltage levels on the load side of the proposed hybrid power converter. Thus, in order to operate both sources as a single source unit and, as a result, tend to supply the same voltage level at the load port, it is necessary to impose

a common control constraint for the operation of both sources that also ensures dynamic operational capabilities of both the sources.

3.4 Dynamic Modeling of Proposed Converter

The proposed system consists of two sources which are operating coherently to supply power to the standalone DC load, it is necessary to model the proposed system from the perspective of both these sources which are simultaneously impacting the load voltage and load power.

3.4.1 Dynamic modeling for the AC source based AC-DC conversion

With regard to the PMSG side of the proposed hybrid power converter as shown in the Figure3.3, the dynamic equations in the abc-frame are presented as :

$$\left.\begin{aligned} \frac{\mathrm{di_a}}{dt} &= \frac{-r_a}{L_a}.(i_a) + \frac{1}{L_a}.(e_a - v_a) \\ \frac{\mathrm{di_b}}{dt} &= \frac{-r_b}{L_b}.(i_b) + \frac{1}{L_b}.(e_b - v_b) \\ \frac{\mathrm{di_c}}{dt} &= \frac{-r_c}{L_c}.(i_c) + \frac{1}{L_c}.(e_c - v_c) \end{aligned}\right\} \tag{3.3}$$

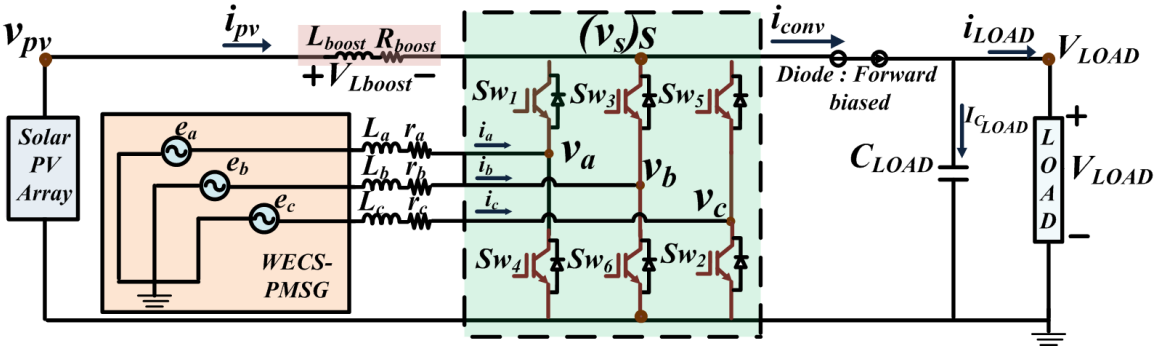

Figure 3.3: Schematic of proposed converter from AC and DC sources perspective

where e_a, e_b and e_c are the generator phase voltages, v_a, v_b and v_c are the bridge converter voltages which is regulated as per the required load voltage level, i_a, i_b and i_c are the phase currents, (L_a, r_a), (L_b, r_b) and (L_c, r_c) are the phase inductances between PMSG and the converter terminal.

Then, these dynamic equations are transformed into the synchronous reference frame and are depicted as :

$$\left.\begin{aligned} \frac{\mathrm{di_d}}{dt} &= \frac{-r_d}{L_d}.(i_d) + \omega.i_{L_q} + \frac{1}{L_d}.(e_d - v_d) \\ \frac{\mathrm{di_q}}{dt} &= \frac{-r_q}{L_q}.(i_q) - \omega.i_d + \frac{1}{L_d}.(e_q - v_q) \end{aligned}\right\} \tag{3.4}$$

Now, with the aid of using Laplace transformation, the dynamic equations in (3.4) are transformed into the s-domain as:

$$\left.\begin{aligned} i_d(s) &= \frac{1}{sL_d + r_d}.[e_d(s) - v_d(s) + \omega.L.i_q(s)] \\ i_q(s) &= \frac{1}{sL_q + r_q}.[e_q(s) - v_q(s) - \omega.L.i_d(s)] \end{aligned}\right\} \tag{3.5}$$

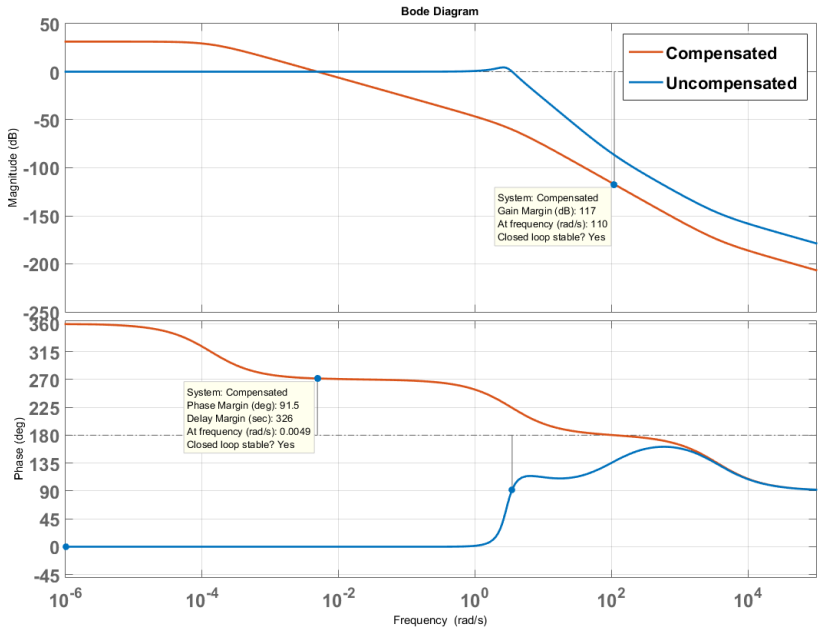

Figure 3.4: Bode plot for AC-DC conversion(both compensated and uncompensated system)

3.4.2 Dynamic modeling for the DC source based DC-DC conversion

By applying KVL between the PV source and switch node (s) of proposed converter as depicted in the Fig.3.3 as:

$$v_{pv} - v_s = r_{boost}.i_{pv} + L_{boost}.\frac{di_{pv}}{dt} \tag{3.6}$$

The PV current is represented as :

$$\frac{\mathrm{di_{pv}}}{dt} = \frac{1}{L_{boost}}.(v_{pv} - v_s) - \frac{r_{boost}}{L_{boost}}.(i_{pv}) \tag{3.7}$$

Now, transforming this equation in s-domain as :

$$i_{pv}(s) = \frac{1}{sL_{boost} + r_{boost}}.[v_{pv}(s) - v_s(s)] \tag{3.8}$$

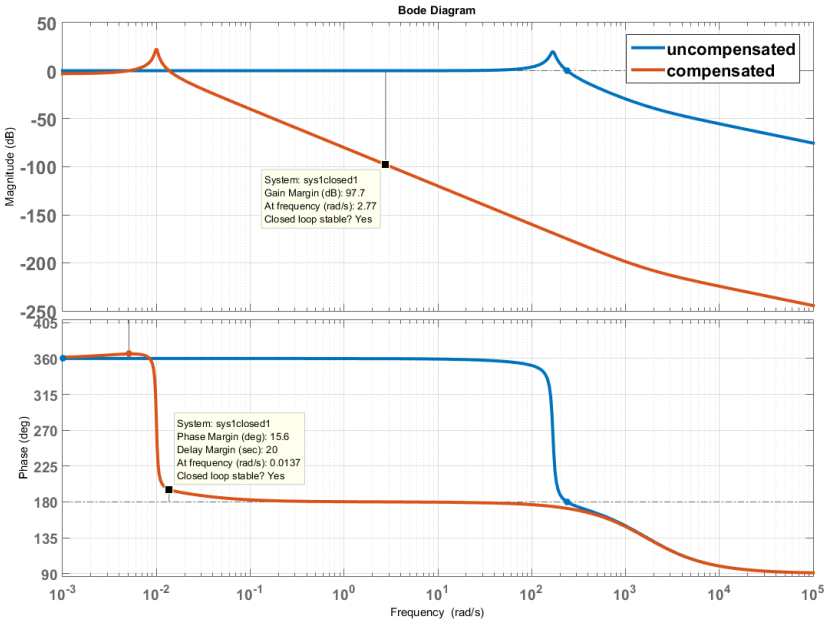

Figure 3.5: Bode plot for DC-DC conversion(both compensated and uncompensated system)

3.5 PWM architecture for the proposed converter

As per (Mohan et al., 2003), sinusoidal pulse-width modulation scheme is widely used in conventional voltage source rectifier and thereby this scheme is modified with the incorporation of shoot-through features for the proposed converter. Herein, as illustrated in Figure 3.6, the scheme utilizes high-frequency carrier signal (V_{tri}), three-phase modulating signals (m_a, m_b, m_c) and duty ratio signal (D_{sh}) for the generation of gating signals for the switches of the proposed converter. The process of generating the PWM signals are outlined as follows:

1. The generation of PWM gating signals initiates with the comparison of carrier signal with the 3-phase modulating signals as well as duty ratio signals to develop sinusoidal PWM(SPWM) pulses (of Figure3.6(i)) and the pulses for DC-DC conversion (of Figure3.6(ii)).

2. Then, the three-phase modulating signals are compared among themselves to generate the interlinking signals depicted in Figure 3.6(iii) to merge the sinusoidal PWM signals (of Figure 3.6(i)) and the DC-DC conversion pulse signals (of Figure 3.6(ii)).

3. Now, with the usage of DC-DC conversion pulse signals (of Figure 3.6(ii)) and the phase dominance signals (of Figure 3.6(iii)), the shoot-through based logical signals are generated as shown in Figure 3.6(iv).

4. Finally, as shown in Figure 3.6(v), a logical OR Gate is used for merging the sinusoidal-based pulse signals (of Figure 3.6(i)) with the shoot-through signals (of Figure 3.6(iv)) for the corresponding switches.

3.5.1 Generation of Sinusoidal PWM signals

This is the first stage of the PWM gating signals generation for the switches of the proposed converter. In this stage as shown in the Figure 3.7, the sinusoidal reference signals (m_a, m_b and m_c) are compared to the triangular carrier signal (v_{tri}) to generate the sinusoidal PWM pulses. Herein, the sinusoidal PWM pulses are denoted as :
S_{ap} and S_{an} for leg-A switches, $S_{ap} = 1$ for $V_{tri} > m_a$ while $S_{an} = 1$ for $V_{tri} < m_a$
S_{bp} and S_{bn} for leg-B switches, $S_{bp} = 1$ for $V_{tri} > m_b$ while $S_{bn} = 1$ for $V_{tri} < m_b$

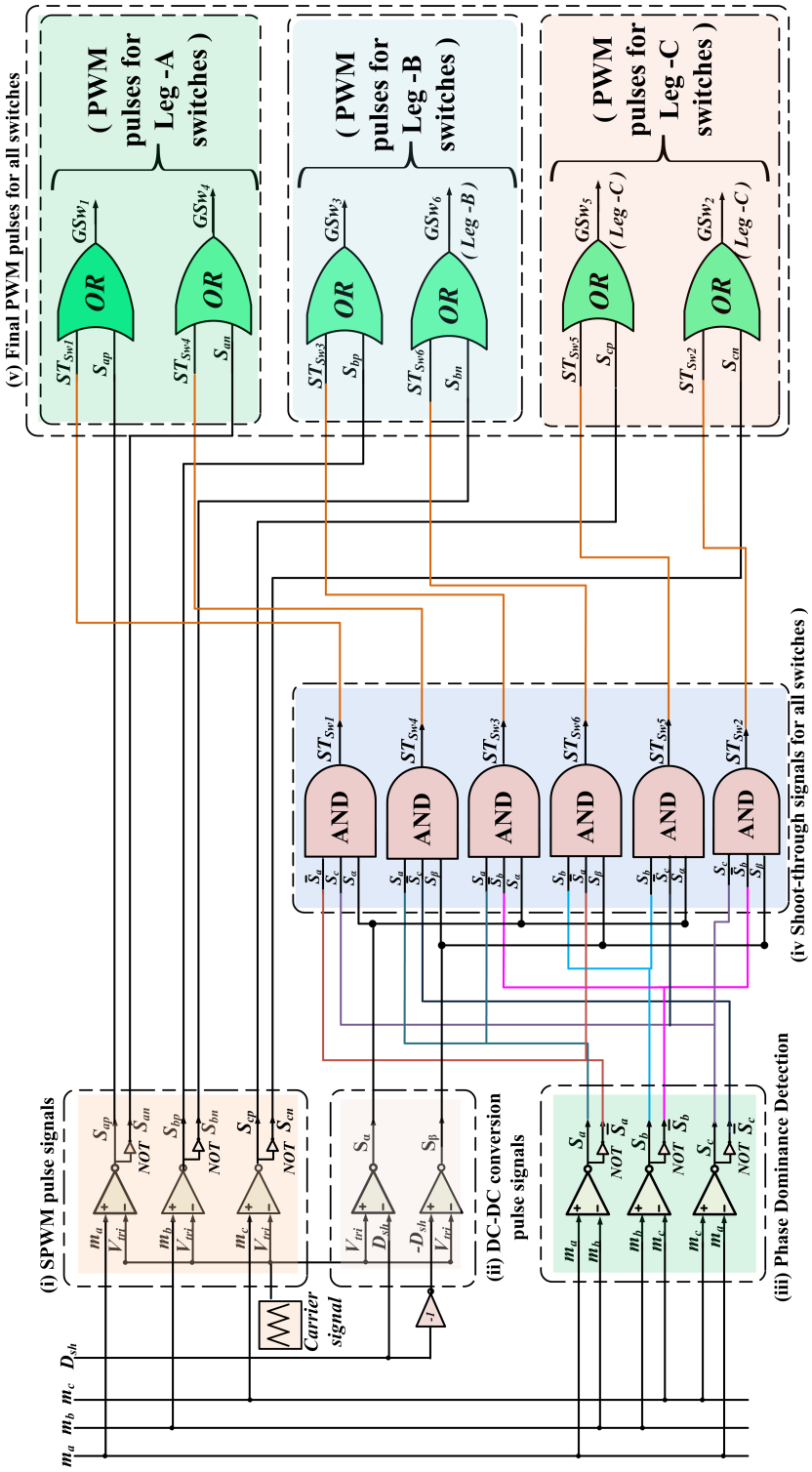

Figure 3.6: PWM logic for the proposed single stage multiport hybrid power converter

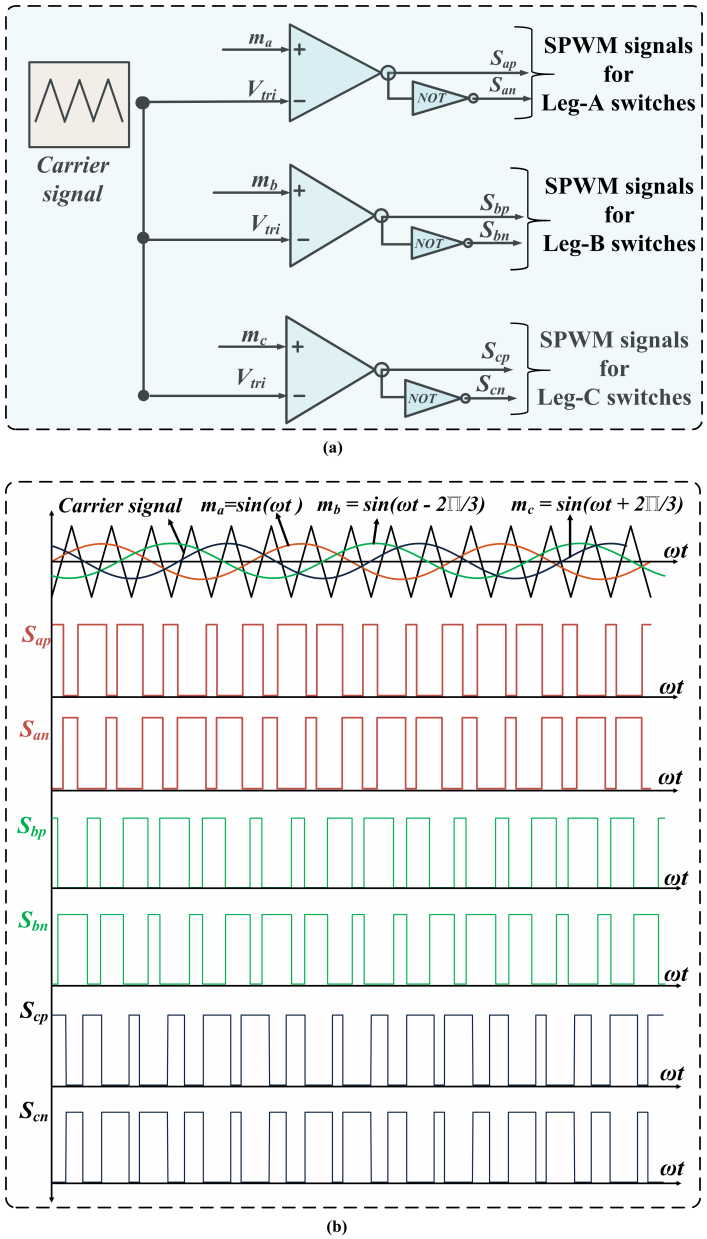

Figure 3.7: Sinusoidal PWM pulses (a). Generation of sinusoidal PWM signals and (b). Sinusoidal PWM pulses for all switches

S_{cp} and S_{cn} for leg-C switches, $S_{cp} = 1$ for $V_{tri} > m_c$ while $S_{cn} = 1$ for $V_{tri} < m_c$

These generated SPWM signals will be used further to realise the AC-DC conversion in the proposed hybrid power converter. It is important to note that these pulse signals consists of two modes of operation only namely power interval and zero interval mode which

are pertaining to the conventional three-phase AC-DC conversion.

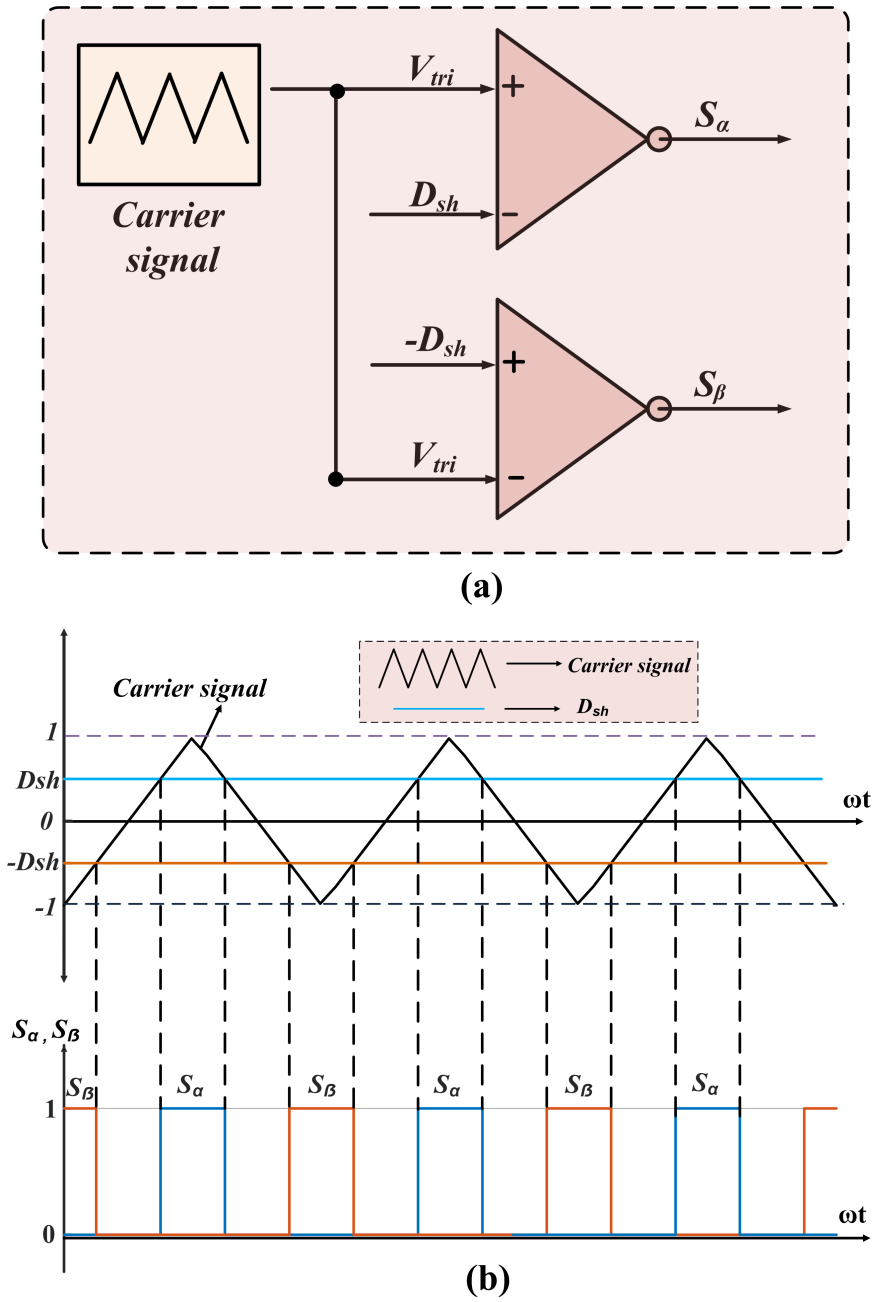

Figure 3.8: Comparison of shoot through duty ratio signals with triangle carrier signal:(a). Generation of DC-DC conversion pulse signals and (b). Logical output of DC-DC conversion ppulse signals

3.5.2 Pulse generation for DC-DC conversion signals

The carrier signal comparison with the duty ratio signal generates the logical signals for DC-DC conversion as shown in Figure 3.8. These logical signals denoted as "S_α" and "S_β" are linked to the development of shoot-through intervals around the carrier signal's positive and negative peaks, respectively.

S_α :-

1. S_α is a logical signal generated with the comparison of positive duty ratio signal with carrier signal. This implies that S_α is used for inserting the shoot-through signals during the positive phase of carrier cycle.

2. S_α will be high only when $V_{tri} > D_{sh}$.

S_β :-

1. S_β is a logical signal generated with comparison of negative of duty ratio signal with carrier signal. This implies that S_β is used for inserting the shoot-through signals during the negative phase of carrier cycle.

2. S_β will be high only when $-D_{sh} > V_{tri}$.

3.5.3 Phase Dominance Detection signals

Now, in order to implement the simultaneous operation of 3-phase AC-DC conversion and DC-DC conversion in the proposed converter, it is essential for the sinusoidal PWM signals to be integrated with the pulses for DC-DC conversion at an appropriate instances. This unification of both conversion pulses are carried out with the aid of interlinking signals denoted as phase dominance signals.

The phase dominance signals are generated with the comparison of the modulating signals among each other. This comparison of the modulating signals among themselves mark the dominant instances of one phases over another phases(most dominant and least dominant). As observed from the Figure 3.9, logical signals generated with this comparison are represented as S_a and $\overline{S_a}$ for phase-A, S_b and $\overline{S_b}$ for phase-B, S_c and $\overline{S_c}$ for phase-C.

1. The signal S_a represents the instances when phase-A modulating signal is greater than the B phase modulating signal.

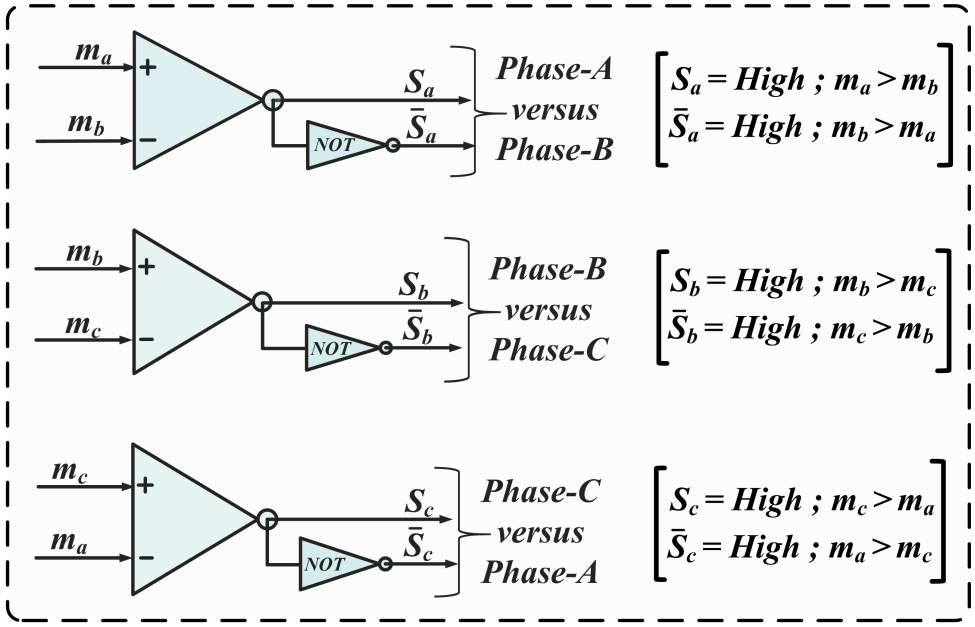

(a)

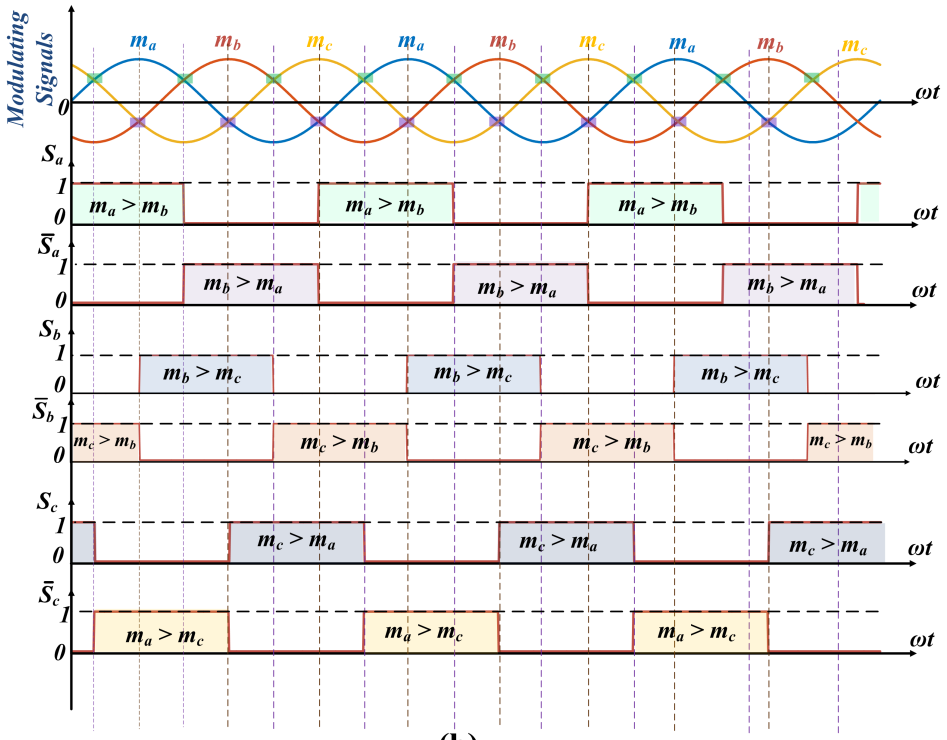

(b)

Figure 3.9: (a). Composition of Phase Dominance Detection Signals and (b). Logical output of phase dominance detection signals

2. The signal S_b represents the instances when phase-B modulating signal is greater than the C phase modulating signal.

3. The signal S_c represents the instances when phase-C modulating signal is greater than the A phase modulating signal.

While the complementary signals represents

1. The signal ("$\overline{S}_a$") represents the instances when phase-A modulating signal is lesser than the B phase modulating signal.

2. The signal ("$\overline{S}_b$") represents the instances when phase-B modulating signal is lesser than the C phase modulating signal.

3. The signal ("$\overline{S}_c$") represents the instances when phase-C modulating signal is lesser than the A phase modulating signal.

3.5.4 Composition of shoot through intervals

Figure 3.10 elaborates the process of unifying logically the DC-DC conversion pulse signals (S_α and S_β) with the phase dominance signals (S_a, $\overline{S_a}$, S_b, $\overline{S_b}$, S_c, $\overline{S_c}$).

1. ST_{Sw1} :- Shoot-through signal for switch S_{w1}.

    - Considering the signal ST_{Sw1}, it is observed that it is formed by combining the phase dominance signals with the DC-DC conversion pulse signals. In this process herein, phase dominance signals $\overline{S}_a$ and S_c are merged logically (using "AND" logic) with the DC-DC conversion signal pulse S_α.
    - S_α is responsible for shoot-through signals around the positive cycle of carrier wave. Therefore, this S_α is being considered for the top switch of leg A phase. It can also be interpreted that the shoot-through interval is inserted around the positive cycle carrier wave in the top switch. $\overline{S}_a$ represents the time duration when phase A voltage is less than phase B, while S_c depicts the time duration when phase C voltage is greater than phase A.
    - Thus, the $\overline{S}_a.S_c$ represents the overall or comprehensive-time duration when phase A voltage is lowest among the rest of the voltage signals. Therefore, when the phase-A voltage signal is least among other phases and when the

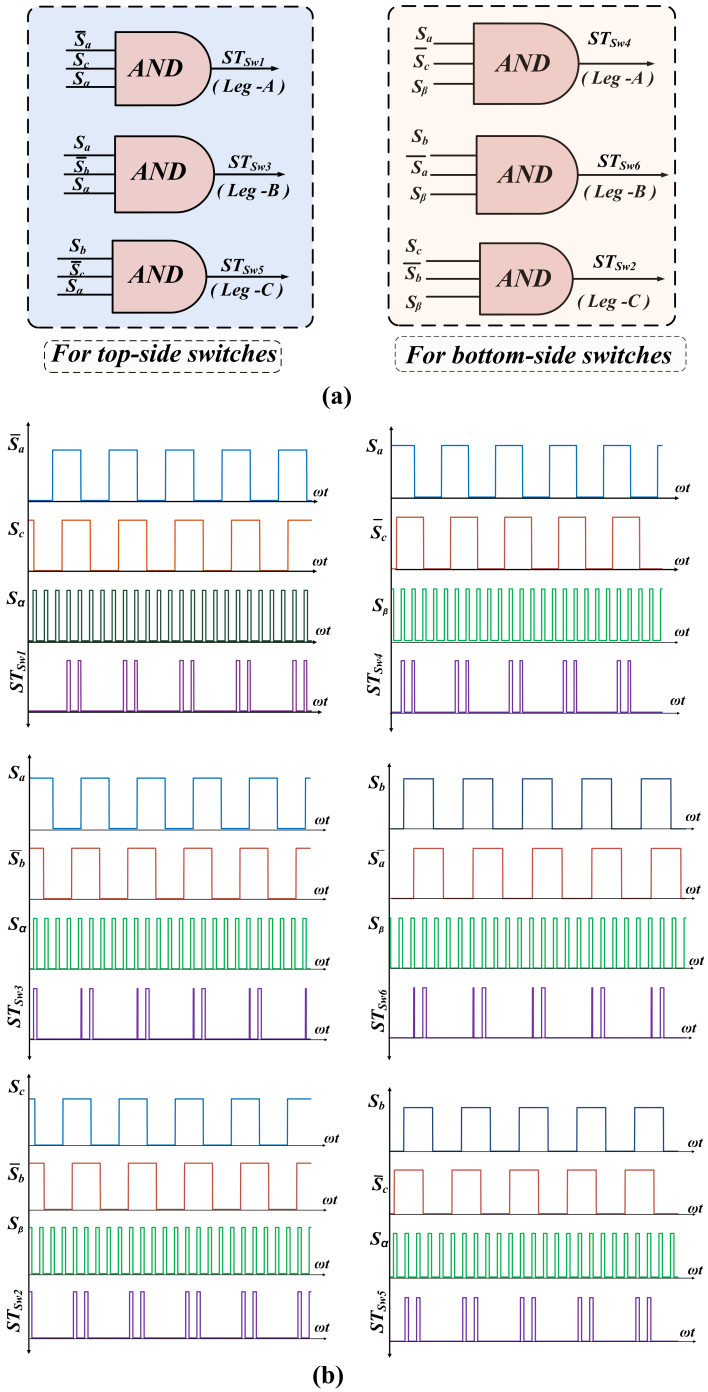

Figure 3.10: (a).Composition of shoot-through signals in PWM scheme and (b). Logical output of shoot-through signals for all switches

carrier signal is greater than the shoot-through duty ratio signal, only signal S_1 will be high. This is done to ensure that the shoot through interval is only

bounded within the zero interval region.

2. ST_{Sw3} :- Shoot-through signal for switch S_{w3}.

   - The signal ST_{Sw3}, as it can be observed that it is formed by combining the interlinking signals $\overline{S}_b$ and S_a with the DC-DC conversion based binary signal S_α. Herein, again, the binary signal S_α is being considered for the top switch of leg B phase and therefore the shoot-through interval is inserted around the positive cycle carrier wave in the top switch for leg B phase.
   - S_a represents the time duration when phase A voltage is greater than phase B, while $\overline{S}_b$ depicts the time duration when phase B voltage is greater than phase C. Thus, the $\overline{S}_b.S_a$ represents the overall or comprehensive-time duration when phase B voltage is lowest among the rest of the voltage signals. therefore, when phase-B voltage signal is least among other phases and when the carrier signal is greater than the shoot-through duty ratio signal, then signal S_3 will be high.

3. ST_{Sw5} :- Shoot-through signal for switch S_{w5}.

   - The signal ST_{Sw5}, is generated by combining the interlinking signals $\overline{S}_c$ and S_b with the DC-DC conversion based binary signal S_α. Herein, binary signal S_α is being considered for the top switch of leg C phase and therefore the shoot-through interval is inserted around the positive cycle carrier wave in the top switch for leg C phase. S_b represents the time duration when phase B voltage is greater than phase A, while $\overline{S}_b$ depicts the time duration when phase B voltage is greater than phase C.
   - Thus, the $\overline{S}_c.S_b$ represents the overall or comprehensive-time duration when phase B voltage is lowest among the rest of the voltage signals. Thereby, when phase-C voltage signal is least among other phases and when the carrier signal is greater than the shoot-through duty ratio signal, then signal S_5 will be high.

4. ST_{Sw4}:- Shoot-through signal for switch S_{w4}.

   - The signal ST_{Sw4}, is generated by combining the interlinking signals $\overline{S}_c$ and S_a with the DC-DC conversion based binary signal S_β. Herein, binary signal S_β is being considered for the bottom switch of leg A phase and therefore the shoot-through interval is inserted around the negative cycle carrier wave in the top

switch for leg A phase. S_a represents the time duration when phase A voltage is greater than phase B, while $\overline{S}_c$ depicts the time duration when phase A voltage is greater than phase C.

- Thus, the $\overline{S}_c.S_a$ represents the overall or comprehensive-time duration when phase A voltage is greatest among the rest of the voltage signals. Therefore, when phase-A voltage signal is greatest among other phases and when the carrier signal is lower than the negative of the shoot-through duty ratio signal, then signal S_4 will be high.

5. ST_{Sw6} :- Shoot-through signal for switch S_{w6}.

   - The signal ST_{Sw6}, is generated by merging the interlinking signals $\overline{S}_a$ and S_b with the DC-DC conversion based binary signal S_β. Herein, binary signal S_β is being considered for the bottom switch of leg B phase and therefore the shoot-through interval is inserted around the negative cycle carrier wave in the bottom switch for leg B phase. S_b represents the time duration when phase B voltage is greater than phase A, while $\overline{S}_a$ depicts the time duration when phase B voltage is greater than phase A.
   - Thus, the $\overline{S}_a.S_b$ represents the overall or comprehensive-time duration when phase B voltage is greatest among the rest of the voltage signals. Therefore, when phase-B voltage signal is greatest among other phases and when the carrier signal is lower than the negative of the shoot-through duty ratio signal, then signal S_6 will be high.

6. ST_{Sw2} :- Shoot-through signal for switch S_{w2}.

   - The signal ST_{Sw2}, is generated by combining logically the interlinking signals $\overline{S}_b$ and S_c with the DC-DC conversion based binary signal S_β. Herein, binary signal S_β is being considered for the bottom switch of leg C phase and therefore the shoot-through interval is inserted around the negative cycle carrier wave in the bottom switch for leg C phase. S_c represents the time duration when phase C voltage is greater than phase A, while $\overline{S}_b$ depicts the time duration when phase C voltage is greater than phase B.
   - Thus, the $\overline{S}_b.S_c$ represents the overall or comprehensive-time duration when phase C voltage is greatest among the rest of the voltage signals. Therefore,

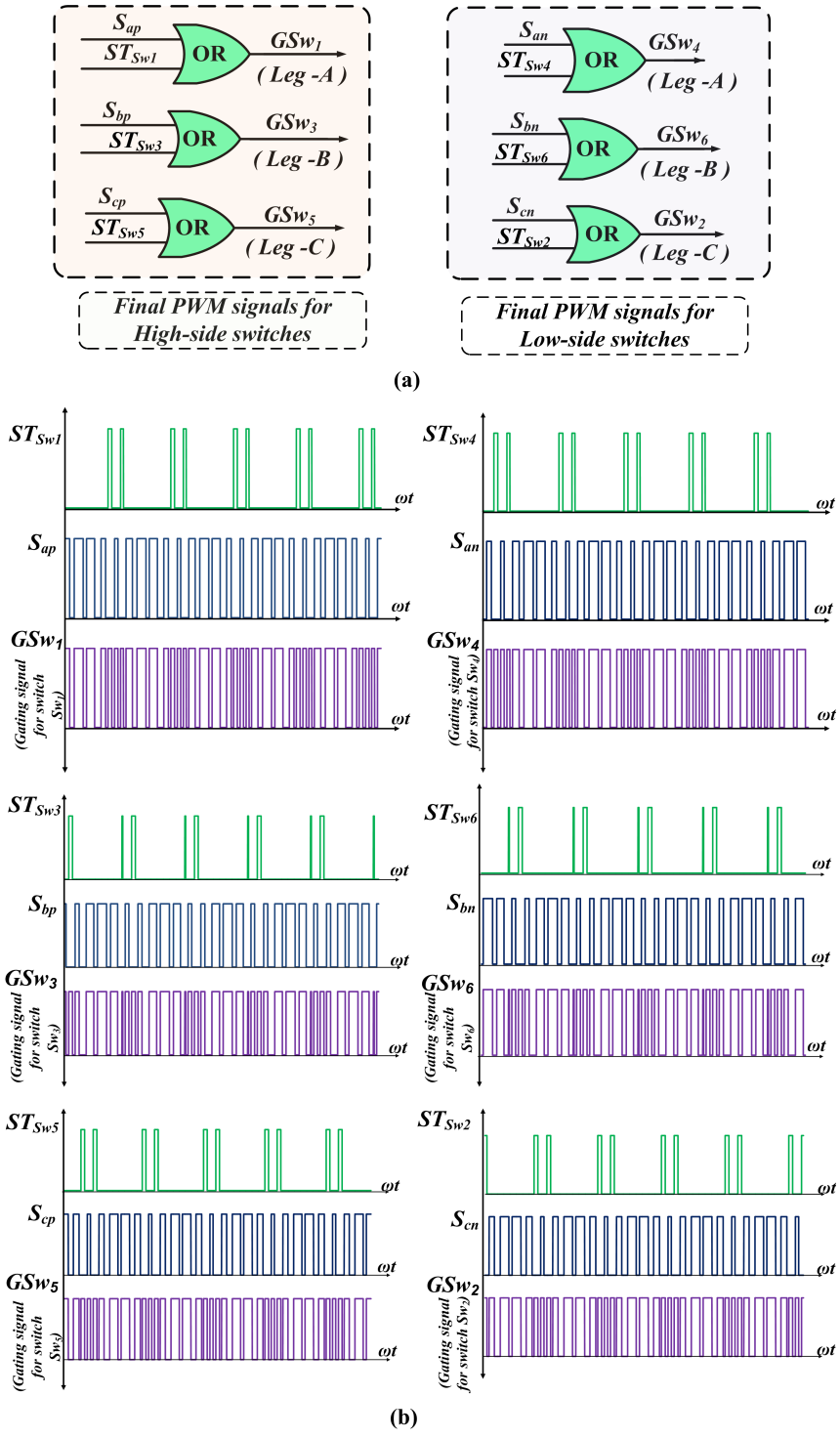

Figure 3.11: (a).PWM gating signals of the proposed converter and (b). Logical output of gating signals of all switches

when phase-C voltage signal is greatest among other phases and when the carrier signal is lower than the negative of the shoot-through duty ratio signal, then signal S_2 will be high.

3.5.5 Final PWM signals

The final stage of generation of the PWM signals of the proposed single stage multi-port hybrid power converter is depicted in the Figure3.11. It is essential to note that these PWM pulse signals are derived by integrating the corresponding sinusoidal pulse width modulation signals and logical shoot-through signals for each switch.

As priorly stated, the sinusoidal PWM signals for the switches S_{w1}, S_{w4}, S_{w3}, S_{w6}, S_{w5}, S_{w2} are represented as S_{ap}, S_{an}, S_{bp}, S_{bn}, S_{cp}, S_{cn} as depicted in Figure 3.7, respectively. Further, corresponding to each switch, the concerned shoot-through signals that have been derived in Figure 3.10 are represented as ST_{Sw1}, ST_{Sw4}, ST_{Sw3}, ST_{Sw6}, ST_{Sw5}, ST_{Sw2} . Now, the gating signals for the switches are obtained as :

- Gating signal for the switch S_{w1}:- $GS_{w1} = S_{ap} + ST_{Sw1}$
- Gating signal for the switch S_{w4}:- $GS_{w4} = S_{an} + ST_{Sw4}$
- Gating signal for the switch S_{w3}:- $GS_{w3} = S_{bp} + ST_{Sw3}$
- Gating signal for the switch S_{w6}:- $GS_{w6} = S_{bn} + ST_{Sw6}$
- Gating signal for the switch S_{w5}:- $GS_{w5} = S_{cp} + ST_{Sw5}$
- Gating signal for the switch S_{w2}:- $GS_{w2} = S_{cn} + ST_{Sw2}$

Therefore, it is affirmed to state that the overall PWM scheme is a modified sinusoidal PWM scheme with shoot-through signals that have been integrated in order to provide DC-DC conversion in addition to the AC-DC conversion in the proposed single stage multiport hybrid power converter.

3.6 Summary

This chapter discusses the control structure for implementing the load voltage regulation and meet necessary load demand of the proposed hybrid power converter. Control aspects of PMSG based 3-phase AC/DC conversion and PV array-based DC/DC conversion

have been elaborated with control logic framework pertaining to the load voltage control. Further, the three-phase modulating signals and the duty ratio signal obtained from the control structure have been merged logically in the PWM architecture described herein. This implemented modified sinusoidal PWM scheme have been elaborated to accomplish the simultaneous operation of 3-phase AC/DC conversion and DC/DC conversion while extracting power from the hybrid sources.

Chapter 4

Results and Discussion

4.1 Introduction

In this chapter, various operational scenarios are detailed to elaborate the performance validation of the proposed converter for the standalone DC system. In the present standalone DC system, a single-stage multi-port hybrid power converter with PV-wind sources is proposed. Since the proposed converter is capable of integrating these PV-wind sources into a single-stage configuration as shown in the Figure 2.8, it is necessary to examine its viability under various operational scenarios. This standalone DC system is required to have constant load voltage and meet necessary load power demand, which implies that both the sources need to be regulated to meet these load conditions. Therefore, the primary objective of the proposed system's operation is to regulate the load voltage in various operating conditions. Henceforth, the operational conditions appropriate for a standalone DC system that have been taken into account are :

- **Scenario 1**: Herein, a case study of constant source and variable load is discussed.
- **Scenario 2**: In this case study, investigation with variable source at constant load is elaborated. As the proposed system consists of two inputs(Wind based PMSG and Solar PV array), therefore a case study for variable input power has been discussed separately for PMSG rotor speed variations and then PV irradiation level variations.

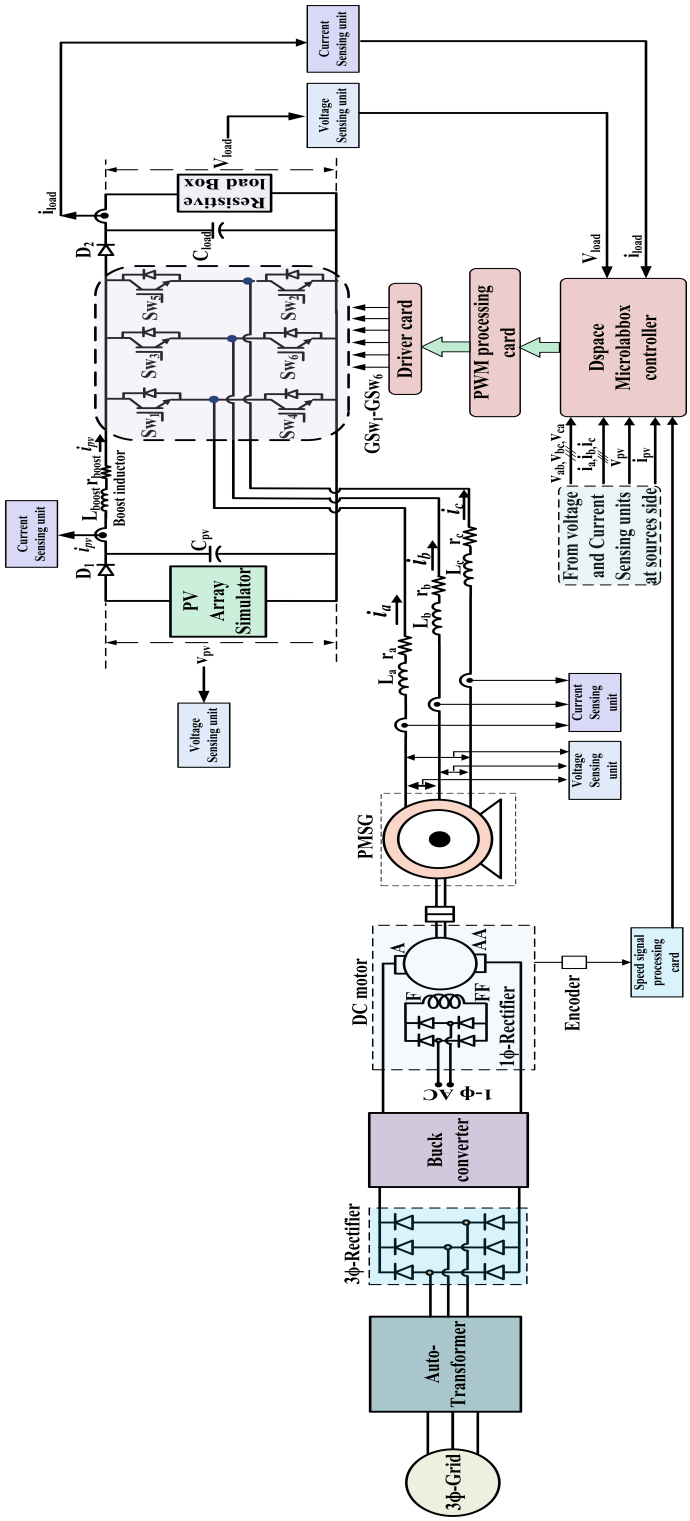

Figure 4.1: Experimental circuit diagram of the proposed system

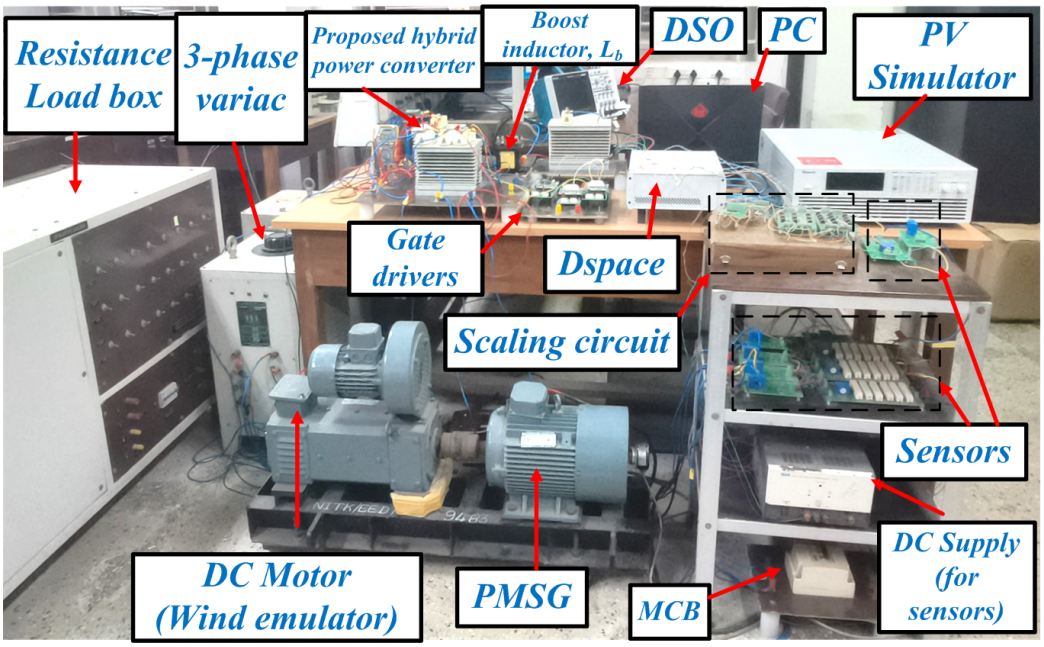

Figure 4.2: Experimental set-up of the proposed system

It is important to note that the reference value of load side voltage is 750 V, which is in accordance with the standard DC voltage levels (Li et al., 2022). This implies that irrespective of changes occurring at the source side or at the load side, the load side voltage has to be maintained constant at 750 V DC.

4.2 HARDWARE IMPLEMENTATION

A laboratory prototype is built to validate the proposed single stage multiport hybrid power converter for standalone DC system with PV-wind sources. The block diagram of laboratory prototype is presented in the Figure 4.1, which comprise power module and control unit. This prototype consists of power module and the control unit. Also, the design and development of PCBs for current, voltage and scaling circuit are also presented. While the Figure 4.2 depicts the experimental setup of the proposed system and Figure 4.3 depicts the photograph of the proposed converter built in the laboratory prototype of the proposed system.

The attributes of the proposed system being used both for simulation and experimental investigations are shown in Tables 4.1-4.3. In order to conduct the simulation investigation on different case studies, SIMSCAPE based models have been used from the MATLAB/SIMULINK library.

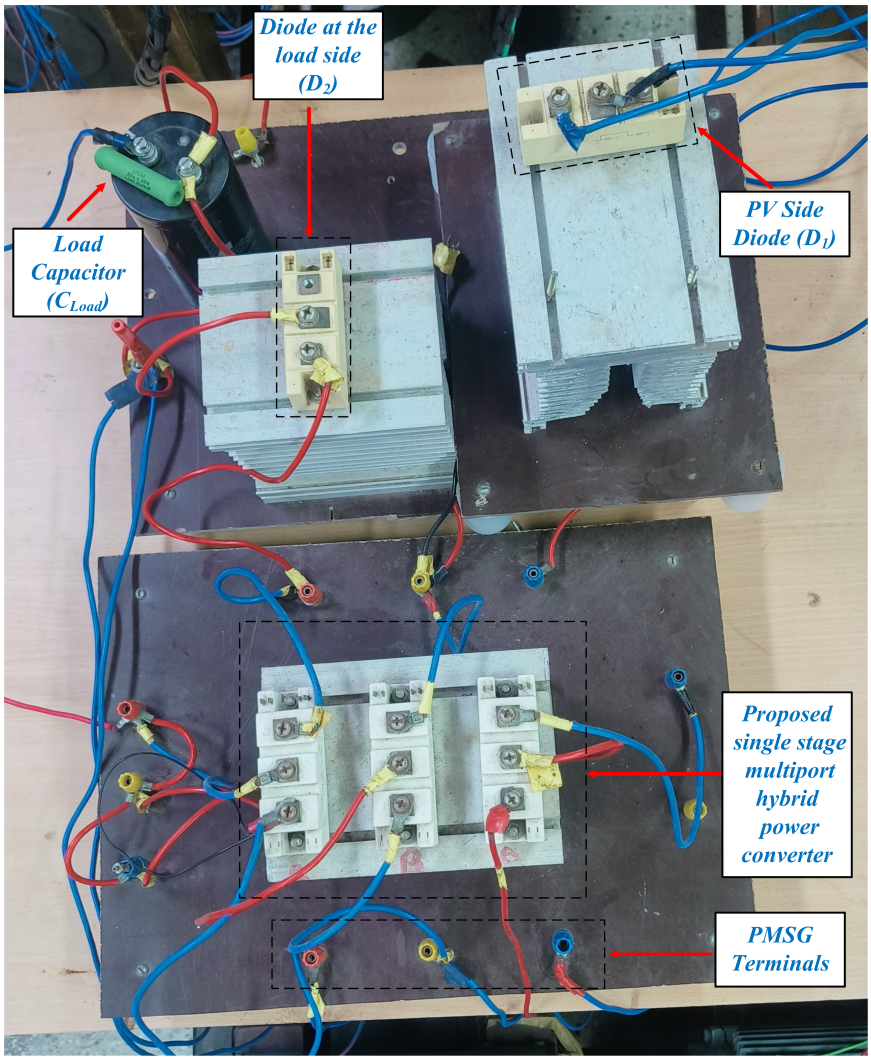

Figure 4.3: Converter photograph developed in the experimental set-up of the proposed system

Table 4.1: PV Source Parameters

Parameters	Ratings
Power at G =$1kW/m^2$	3291 W
V_{MPP} at G =$1kW/m^2$	374 V
I_{MPP} at G =$1kW/m^2$	8.8 A
Power at G =$500W/m^2$	1749 W
V_{MPP} at G =$500W/m^2$	394.2 V
I_{MPP} at G =$500W/m^2$	4.4368 A

Table 4.2: PMSG Source Parameters

Parameters	Ratings
Power	1500 W
Rotor speed	1500 rpm
No. of poles	4
Flux linkage	0.9426 Wb
d-axis,q-axis inductance	24.3 mH
Line voltage,phase current	360V,2.9A
Moment of Inertia	0.0145 kgm^2

Table 4.3: Power Converter Parameters

Parameters	Ratings
Rated load Power	4500 W
Load Voltage	750 V (DC)
Load Resistances	125 Ω to 750 Ω
Inductance in series with PV array	18.75 mH
Input capacitance at PV array	4.7 mF
Load capacitance	470 μF
Switching Frequency	2.5 kHz

The system consists of wind-PMSG source which is emulated with the use of PMSG-DC motor set-up and PV source characteristics are emulated with the use of PV simulator (CHROMA 62050H-600 S). Further, a laboratory prototype of the proposed hybrid power converter is developed with the usage of semikron-made IGBT switches (SKM50GB123D) and diodes (SKKD75F12). In addition, LEM made current sensors (LAH 25-NP) and voltage sensors (LV25-P/SP2) have been used.

- Power unit: The unit consists of the following module.
  1. Three phase rectifier module
  2. PMSG coupled with DC motor set
- Control unit: The unit consists of following control cards.
  1. Voltage and current sensing unit
  2. Scaling unit
  3. Dspace controller board

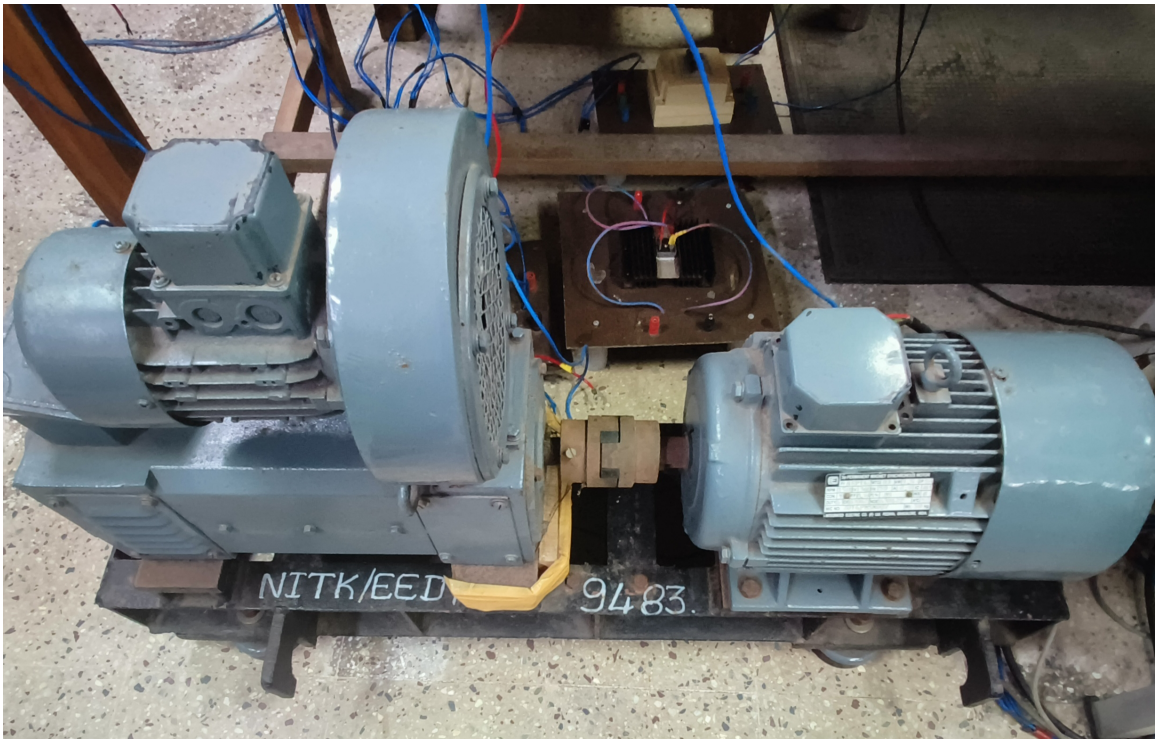

Figure 4.4: PMSG coupled with a DC Shunt Machine

4. PWM processing board
5. Driver unit.

4.2.1 Power circuit for PMSG drive

The permanent magnet synchronous generator (PMSG) used for this thesis is mechanically coupled with a DC shunt machine as shown in Figure 4.4. The parameters details of the PMSG is given in Table 4.2.

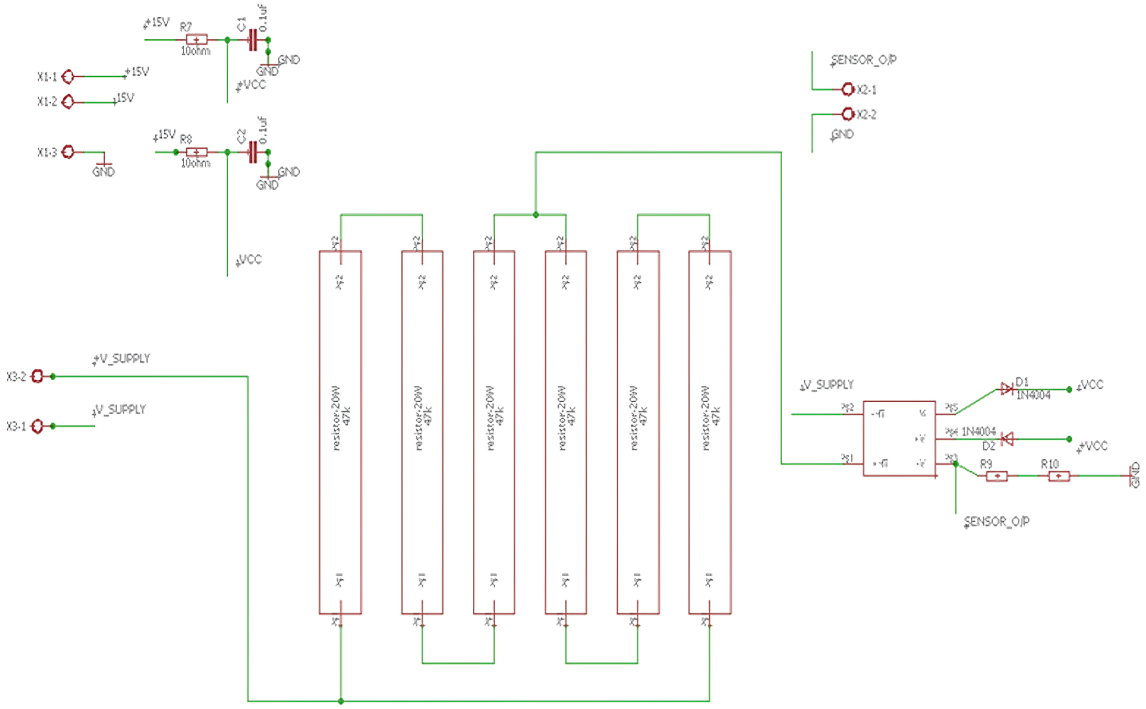

Figure 4.5: Schematic of voltage sensor LV-25P/SP2

4.2.2 Voltage sensor PCB

For sensing the voltage levels of PMSG (line voltage), PV and the load port, LEM made $LV25-P/SP2$ voltage sensors mounted on the PCB boards have been used. The conversion ratio for this voltage sensor is 2.5 : 1 and has the maximum primary current of 14 mA. Herein, the primary side resistor is chosen as 70.5 kΩ and thus the primary current to the sensor is 8.51 mA. The primary side resistor arrangement consists of two parallel arms. In each arm, three resistors of 47 kΩ are connected in series. The effective resistance value of the primary side is 70.5 kΩ. This arrangement is considered to avoid excess power dissipation in the resistor. The corresponding secondary current is 21.27 mA. To convert the output current to voltage a 150 Ω resistor is placed at the secondary side. Thereby, the voltage across secondary side resistor is calculated as 3.19 V. The schematic and the PCB layout of voltage sensor $LV-25P/SP2$ are shown in Figure 4.5 and Figure 4.6, respectively.

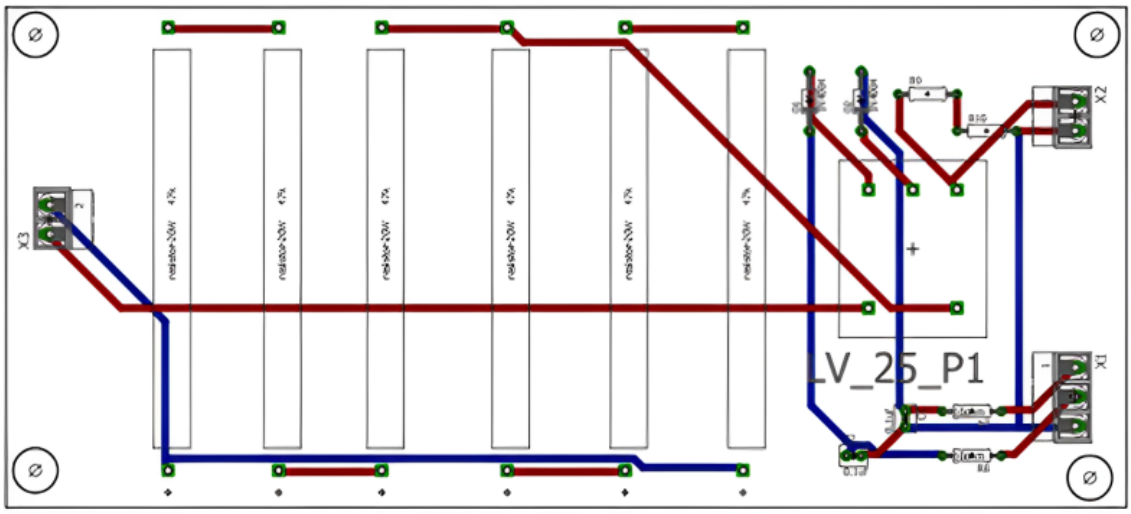

Figure 4.6: PCB layout of voltage sensor LV-25P/SP2

4.2.3 Current sensor PCB

In order to sense the current levels of PMSG phase currents, PV current and load side current, the LEM make current sensors LAH 25-NP are used that are mounted on the PCB boards. The conversion ratio for this current sensor is 3:1000. Herein, the current at the secondary side is 8.7 mA. This secondary current is converted to voltage by placing the resistor (200 Ω) whose value is chosen based on the data-sheet specifications. Thereby, the voltage across secondary side resistor is calculated as 1.74 V. The voltage across this resistor is measured and given to the scaling circuits. The schematic and the PCB layout of current sensor LAH 25-NP are shown in Figure 4.7 and Figure 4.8, respectively.

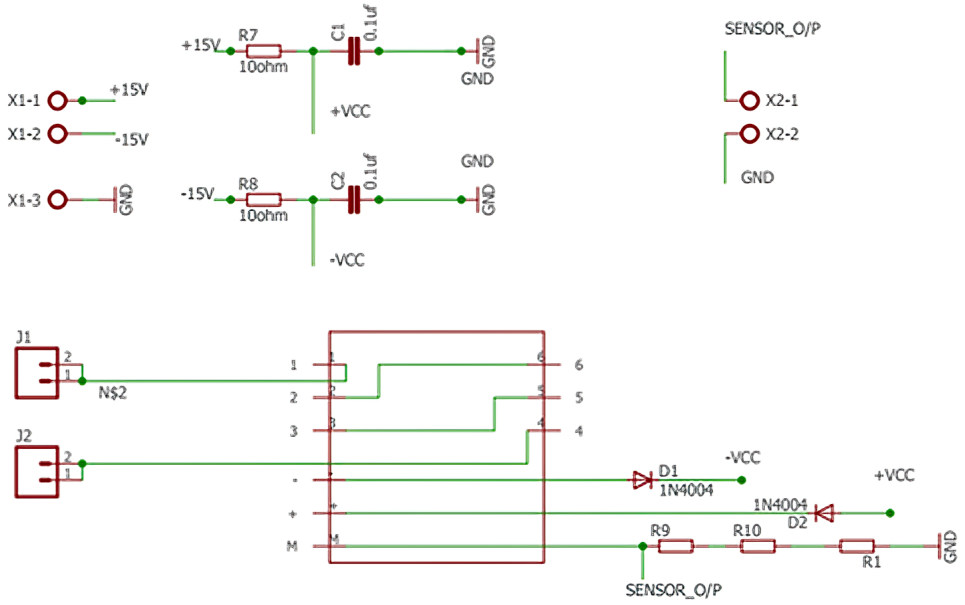

Figure 4.7: Schematic of current sensor LAH 25-NP

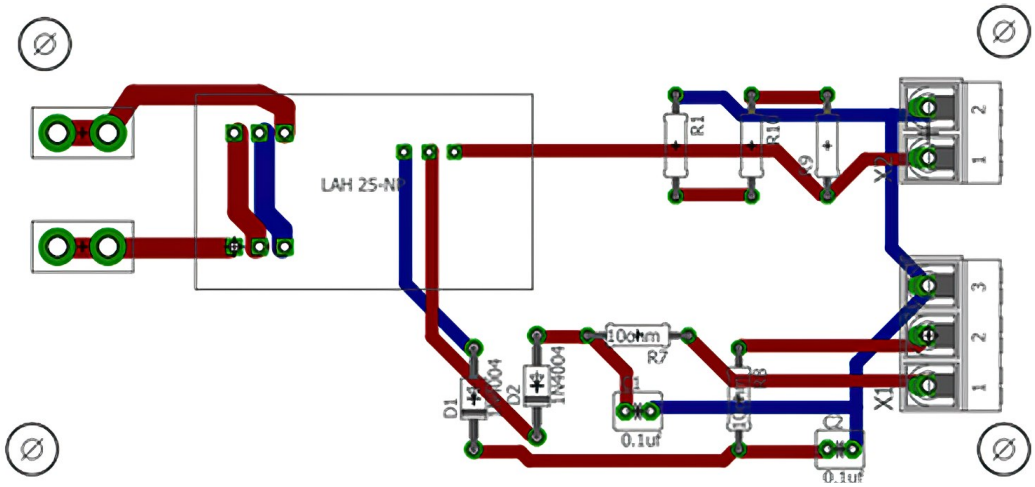

Figure 4.8: PCB layout of current sensor LAH 25-NP

4.2.4 Scaling circuit

The terminal voltages and currents of the PMSG, PV and the load port are scaled down to 5 V range using sensor circuit and scaling circuit and are thereby given as input to Dspace controller. The scaling circuit is used to amplify sensor output to 5 V range. The scaling circuit consists of active filter (op-amp) and passive filter (R and C). The gain of voltage and current scaling circuit are chosen as 1.567, 2.8 respectively because the output of voltage

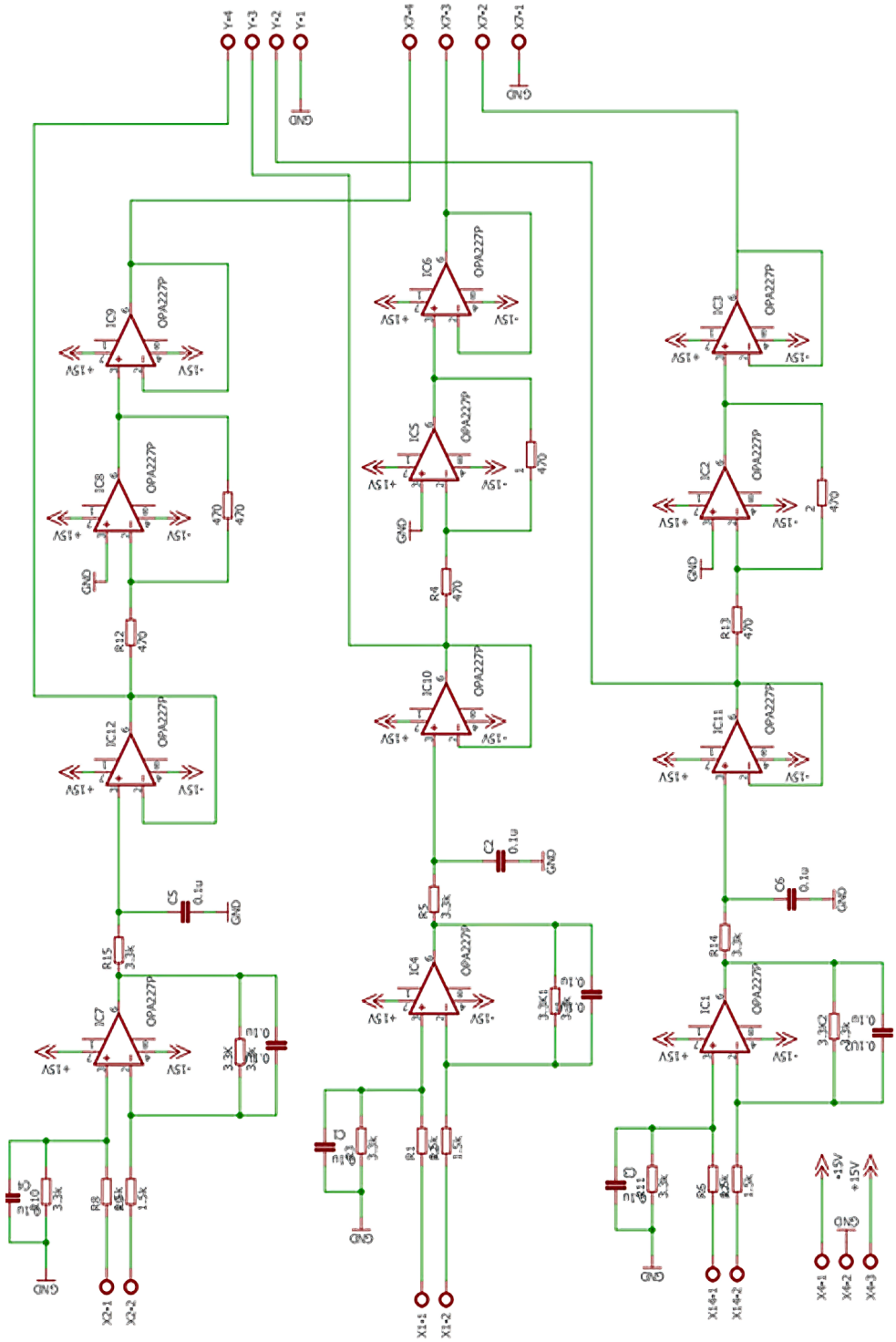

Figure 4.9: Schematic of scaling circuit

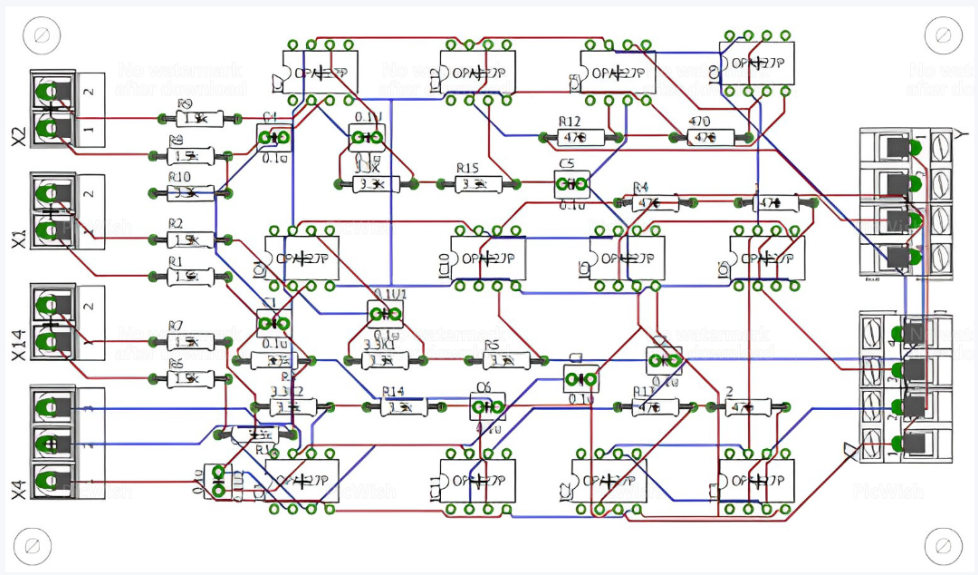

Figure 4.10: PCB layout of scaling circuit

and current sensor unit is 3.19 V and 1.74 V respectively. The switching frequency of the converter is considered as 2.5 kHz. In order to remove the switching noise, both the filters are designed at 3.3 kHz frequency. The PCB layout and schematic of the scaling circuit are shown in Figure 4.9 and Figure 4.10, respectively.

4.2.5 Encoder Interface

A differential encoder, JENCODER 260-ND-SL is used which is placed on the shaft of the PMSG to perform the sensor based field oriented control operation (FOC). The encoder gives six output signals namely A, $\overline{A}$, B, $\overline{B}$, Z, $\overline{Z}$ as shown in Figure 4.11. The encoder used is of 1024 PPR i.e. for one rotation A, $\overline{A}$, B, $\overline{B}$ will give 1024 pulses. Z, $\overline{Z}$ are taken as the reference for counting the pulse per rotation. Z, $\overline{Z}$ will give one pulse per revolution. A and B signals gives the information regarding the direction of rotation. If A leads B, speed is positive i.e. motor is rotating in the anticlockwise direction and if B leads A the speed is negative i.e. the motor is rotating in the clockwise direction. The encoder signals are received and strengthened by the IC AM26LS33ACN. It is a 16 pin IC. The signals can be verified by connecting output pins of the IC to the scope. The pin details of the IC are given in Table 4.4. A, B and Z signals are given to controller to obtain the speed and position information of the motor. The schematic and PCB layout of encoder interface are shown in Figure 4.12 and Figure 4.13 respectively.

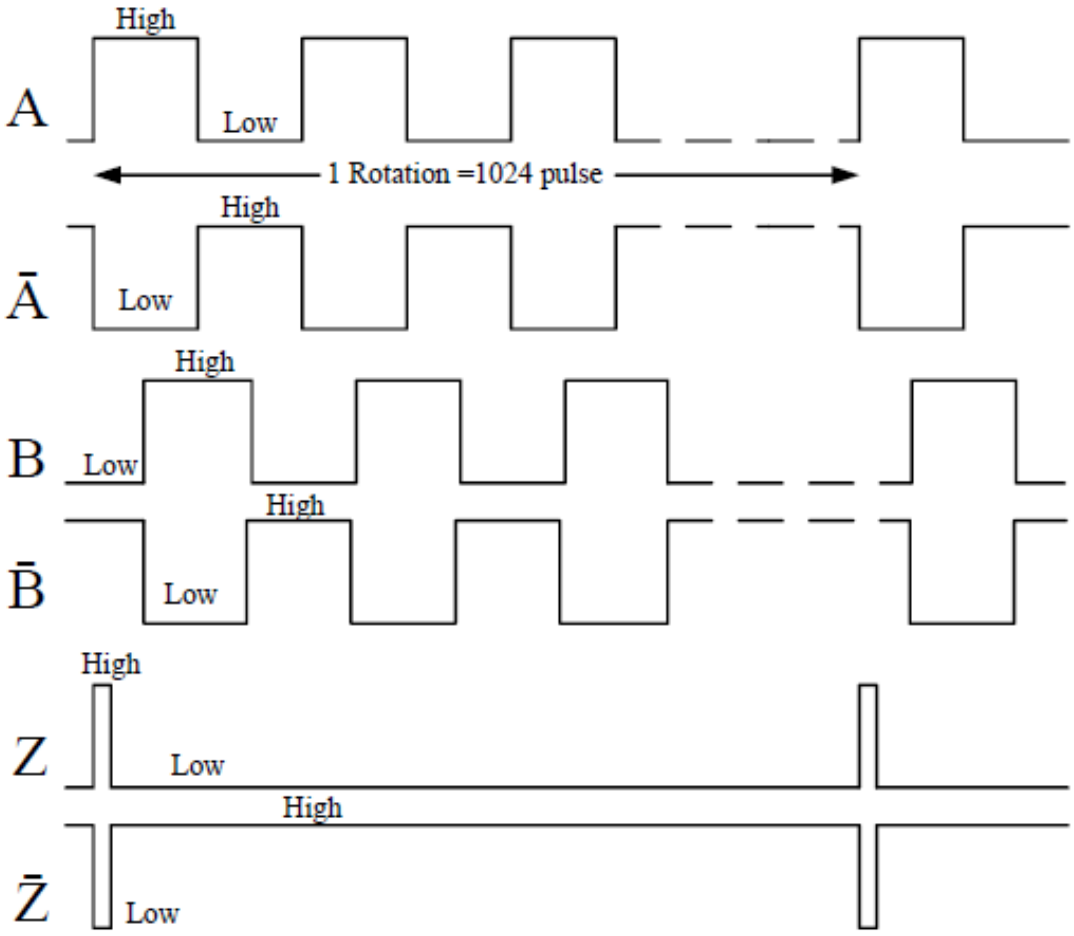

Figure 4.11: Speed Encoder Output

4.2.6 PWM scaling circuit

The schematic and layout of PCB for PWM amplification circuit are shown in Figure 4.14 and Figure 4.15 respectively. The output signals from the Dspace board (5V) are amplified by the IC ULN2003AN before being given to the SEMIKRON DRIVER card (skyper 32 pro) (15V). It is a 16 pin IC with an input impedance of 10 kΩ and an output impedance of 1 kΩ. The high value of impedance at the input side and low impedance at the output side is chosen to eliminate the loading effect on the driver card and also to connect more than one device at the output. The voltage supply is given to the 9th pin of the IC and the 8th pin is connected to the ground. This IC provides the inverted outputs. So, necessary precautions have to taken while connecting IC outputs to the driver card.

Table 4.4: Pin details of AM26LS33ACN

Pin No.	Function
1	Inverting signal ($\overline{A}$)
2	Non-Inverting signal (A)
3	Logic level output of (A/ $\overline{A}$)
6	Non-Inverting signal (B)
7	Inverting signal ($\overline{B}$)
5	Logic level output of (B/ $\overline{B}$)
10	Non-Inverting signal (Z)
9	Inverting signal ($\overline{Z}$)
11	Logic level output of (Z/$\overline{Z}$)
16	+5V supply
8	GND
12	Active low select
4	Active high select

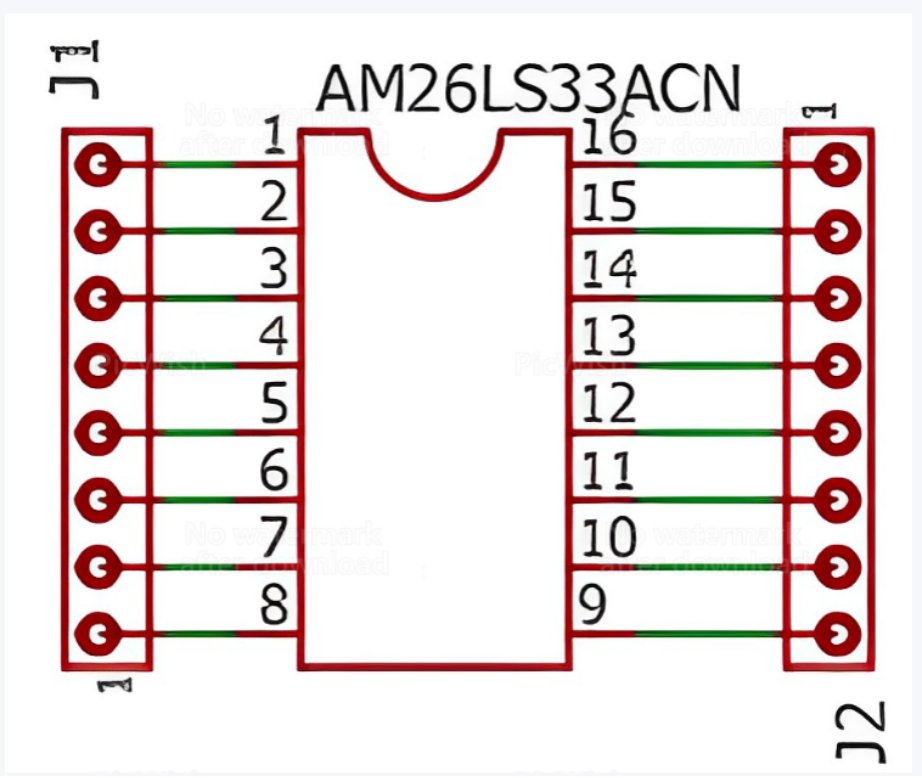

Figure 4.12: Schematic of encoder interface

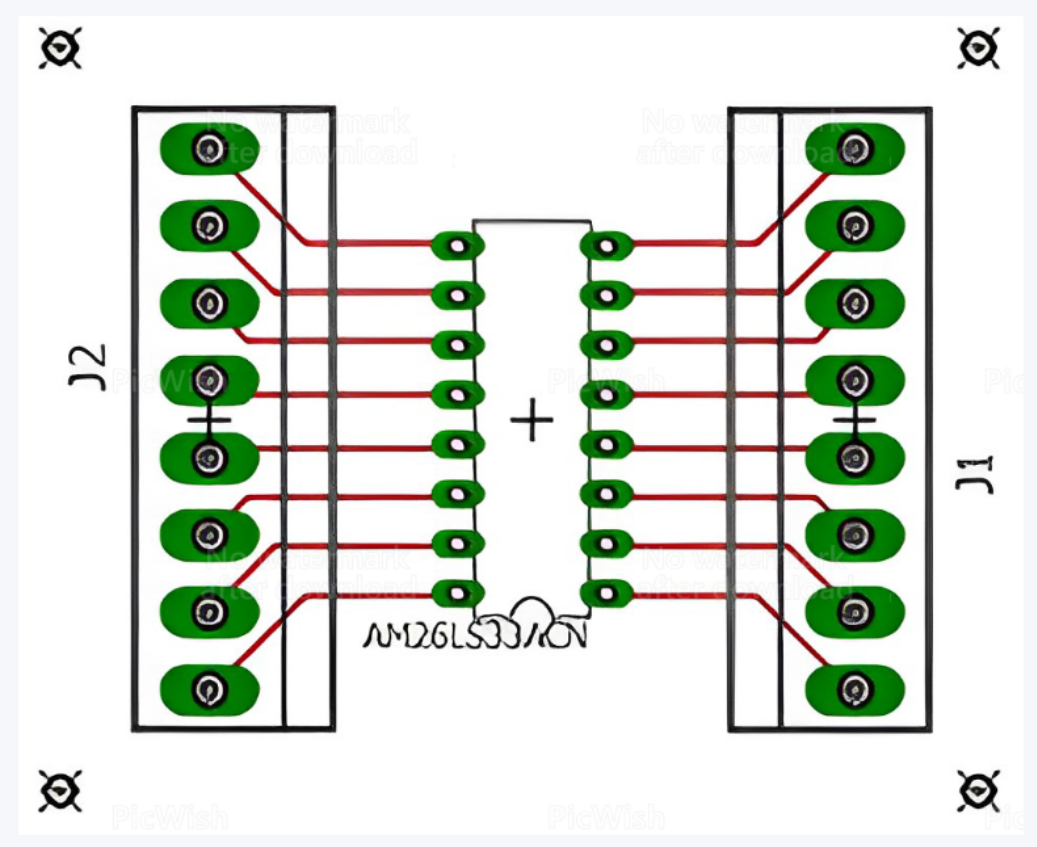

Figure 4.13: PCB layout of encoder interface

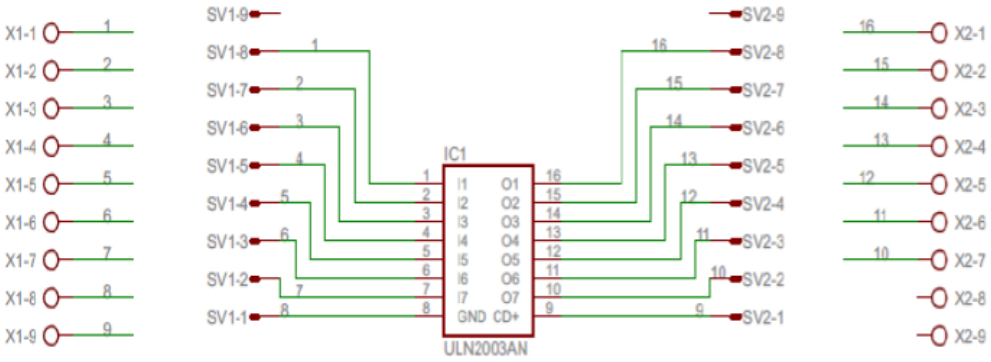

Figure 4.14: Schematic of PWM amplification

4.2.7 Gate driver card

The PWM signals are connected to the gate and emitter terminals of the IGBT through gate driver card, which provides isolation and sufficient current drive ability for operating

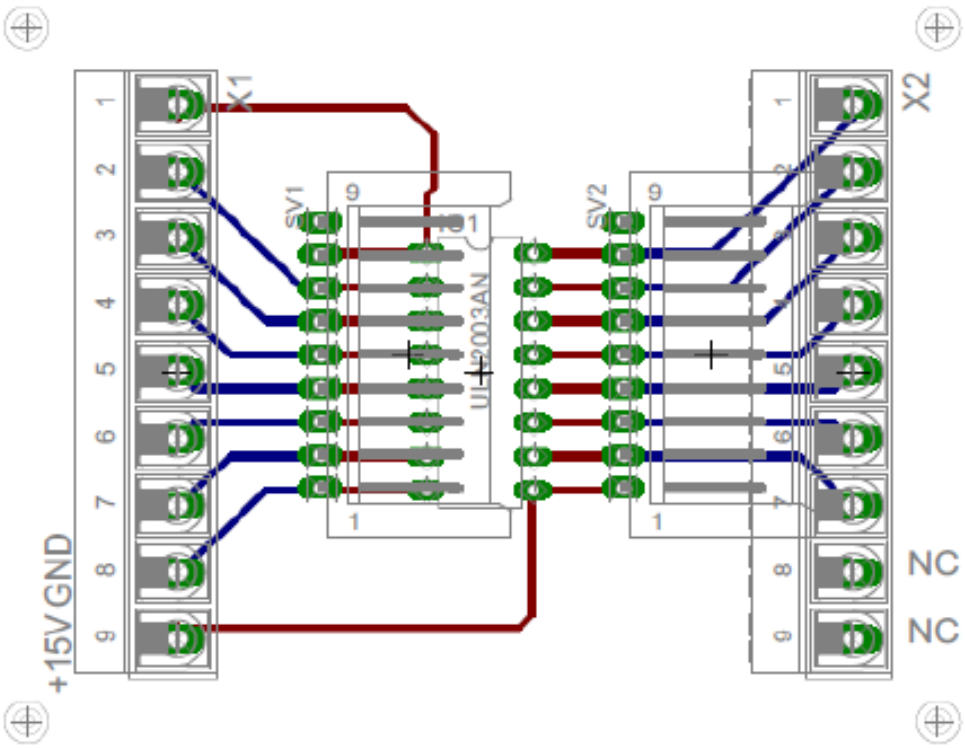

Figure 4.15: PCB layout of PWM amplification

the IGBT of proposed converter. The SEMIKRON made gate driver (SKYPER-32 Pro) is used in the proposed system experimental setup. The connection diagram of SKYPER-32 Pro is shown in Figure 4.16. The DC power supply of 15 V with current rating of 1 Amp is used for powering of driver card. Further, grounds are common for 15 V power supply and switching pulse. During normal/healthy condition of driver card, the error status is low (LED status is OFF) and the driver current should be around 120 mA.

4.3 Scenario 1: Constant input and variable load conditions

At constant rotor speed of 1500 rpm (wind input) and a constant solar irradiation level of $1000 W/m^2$, two step changes at the load port is applied from high level to low level and then back to high level. Herein, load voltage is maintained constant(=reference value) at different load conditions for constant inputs. The reference value of load side voltage is

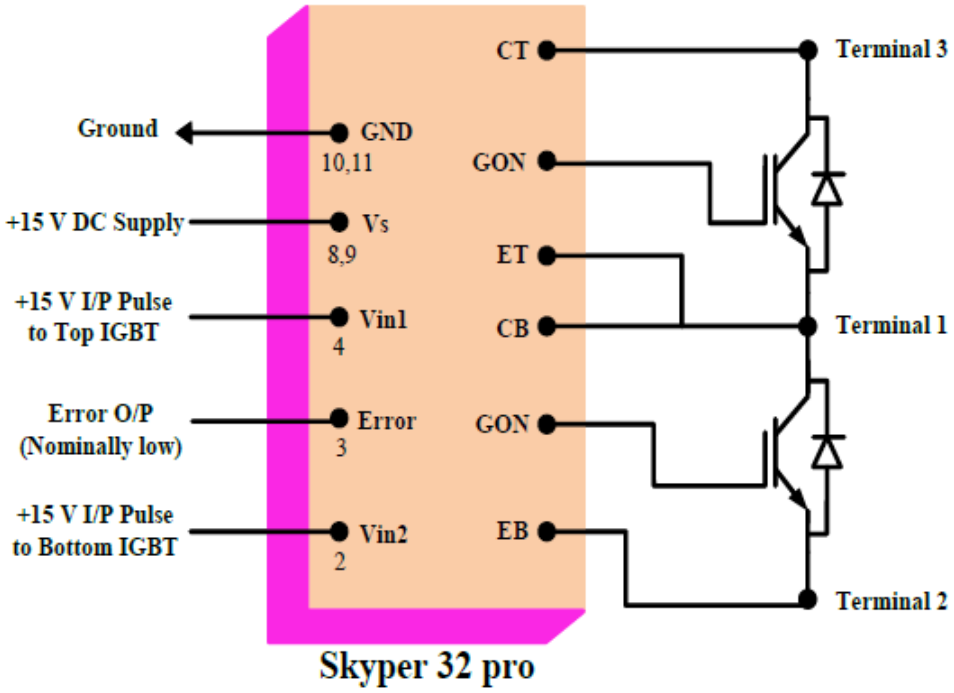

Figure 4.16: Skyper-32Pro driver card

750 V. This implies that irrespective of changes occurring in load resistances, load side voltage has to be maintained constant at 750 V DC.

Figure 4.17- 4.20 shows the both source side and load side performance waveforms pertaining to case study of the load change. In this case, two-step perturbations of load resistance have been considered. Initially, from time t = 0 sec. to t = 6 sec., the system is operating at a high load (125 Ω, 94 % of the rated load). Then, at time t = 6 sec., step load change is applied, and load resistance is changed to 750 Ω (which is 15.65 % of the rated load). Lastly, the load resistance is made to undergo step change of high load (125 Ω, which is 94% of the rated load).

- **Load port** : Figure 4.17 shows the load side waveforms pertaining to load variations at constant inputs. It can be observed that during the instance of high load, the mean value of load voltage is 746 V [during t = 0 to 6 sec. and during t = 12 to 18 sec.] while during the case of low load, the mean value of load voltage is 738 V. Therefore, it can be stated that the load voltage is maintained nearly constant during variable load conditions.

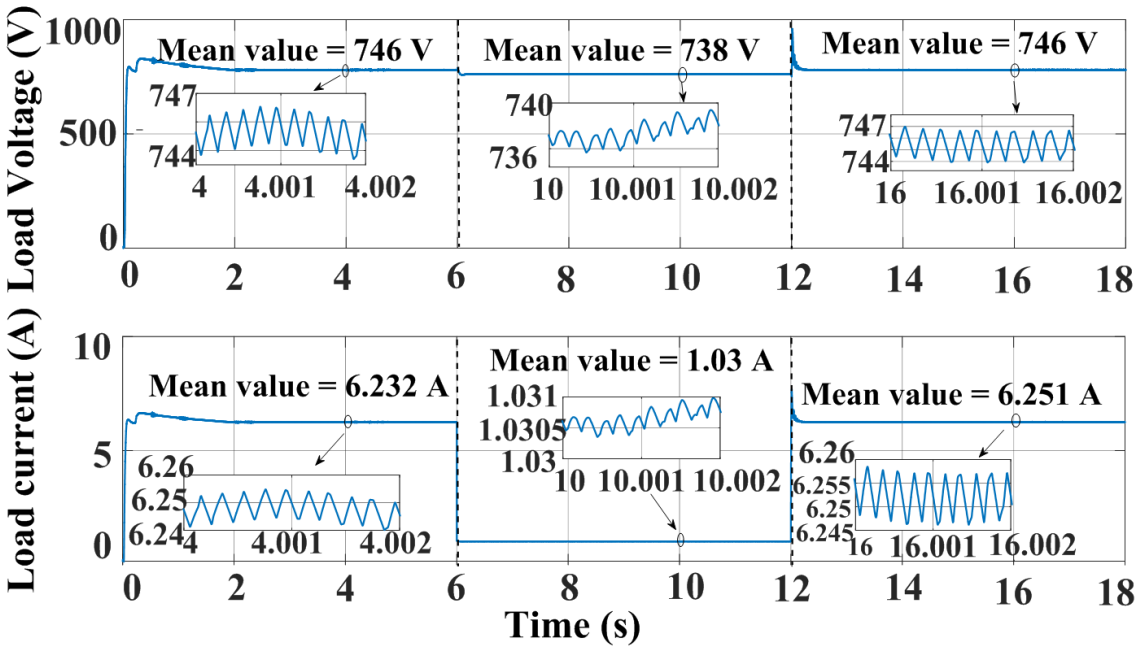

(a)

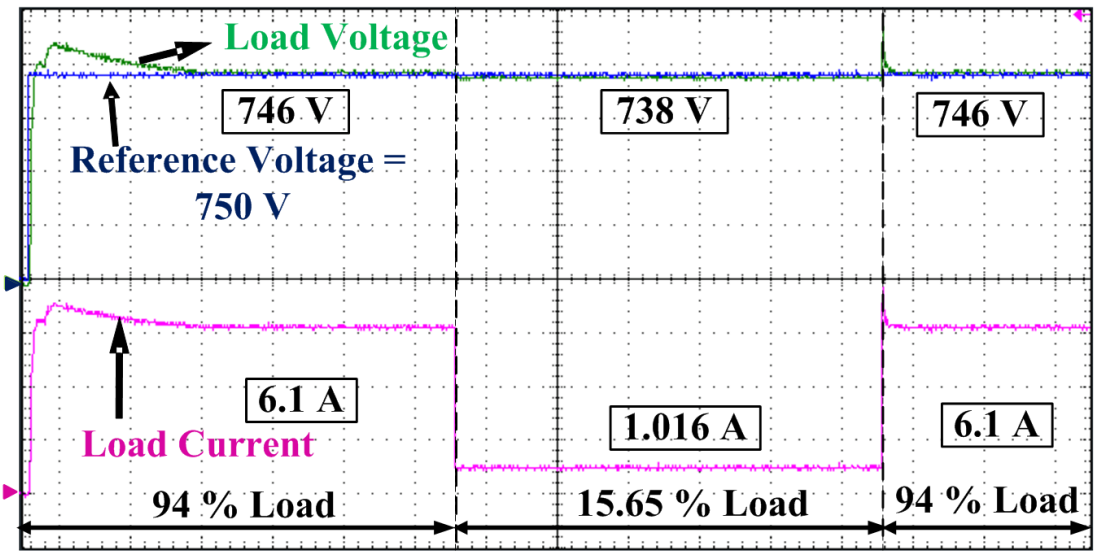

(b)

Figure 4.17: Load port waveforms under variable load conditions:(a) Simulation waveforms and (b) Experimental waveforms

Thereupon, with regard to load current, the magnitude of the load current will change in concurrence to the load level variation while the load voltage remains constant. During the case of high load, load current magnitude is around 6.1 A while magnitude of load current changes to 1.03 A during the scenario of low load. Furthermore, the load power is 4.5 kW during the scenario of high load and then at the scenario of low load the load power is 750 W.

Henceforth, it can be concluded that the proposed system is able to maintain constant load voltage when undergoing load step perturbations of 80 % change (both step-up load change and step-down load change).

- **PV array port** : Figure 4.18 illustrates the PV array voltage and current waveforms for variable load levels at constant irradiation of 1000 W/m^2. It can be perceived that in response to load change, PV array voltage and current waveforms will be changing in accordance to the constant load voltage and necessary load power requirement.

Herein, during the case of high load, the PV array voltage and current is 391 V and 8 A respectively. Then, the load level is decreased to 15.65 %(of rated load) and thereby the PV array voltage and current is 473.5 V and 1 A, respectively. Further, when load level is change to high level thereby the PV array voltage and current is restored to 391 V and 8 A, respectively. The PV array power during high load demand condition is 3.128 kW and during the case of low load demand condition the PV array power is 473 W.

It can be stated that during the case of high load, the PV array is operating nearly at maximum power point condition while during the case of low load power demand of 15.65 %, the PV array switches to Non-MPP mode of operation. Henceforth, it can be concluded that PV array is able to operate in accordance with dynamic load change requirements from high load (MPP) to low load (Non-MPP).

- **PMSG port** : Figure 4.19 depicts the PMSG phase voltage and current waveforms for variable load levels at constant rotor speed of 1500 rpm (or 157 rad/s). It is ob-

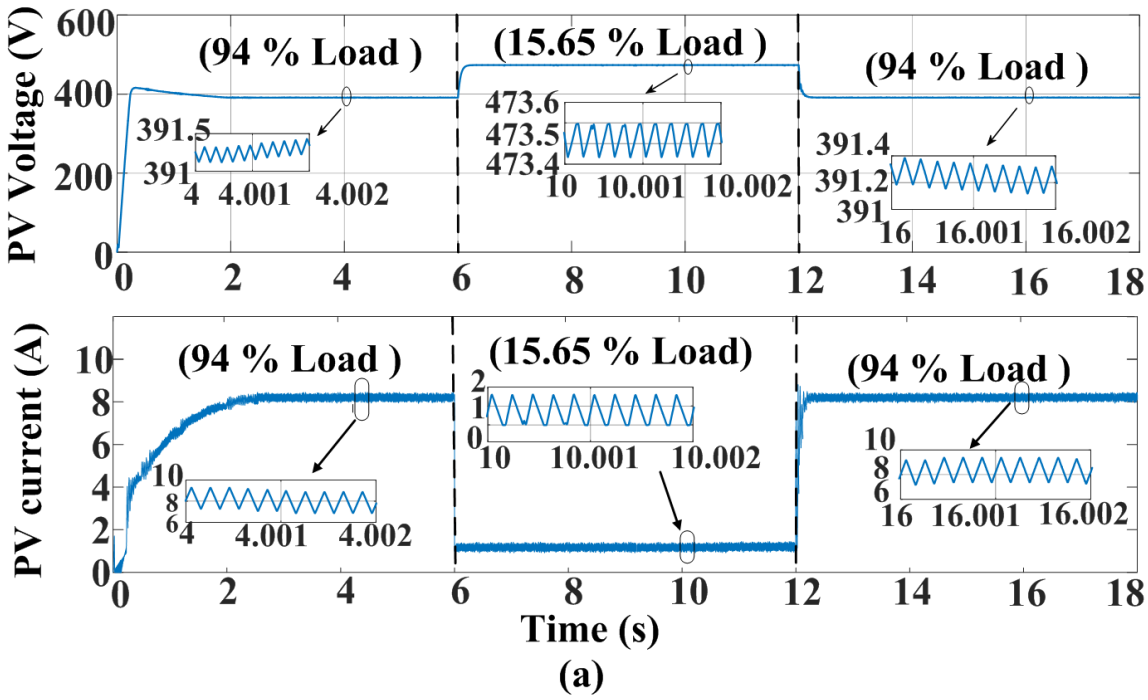

(a)

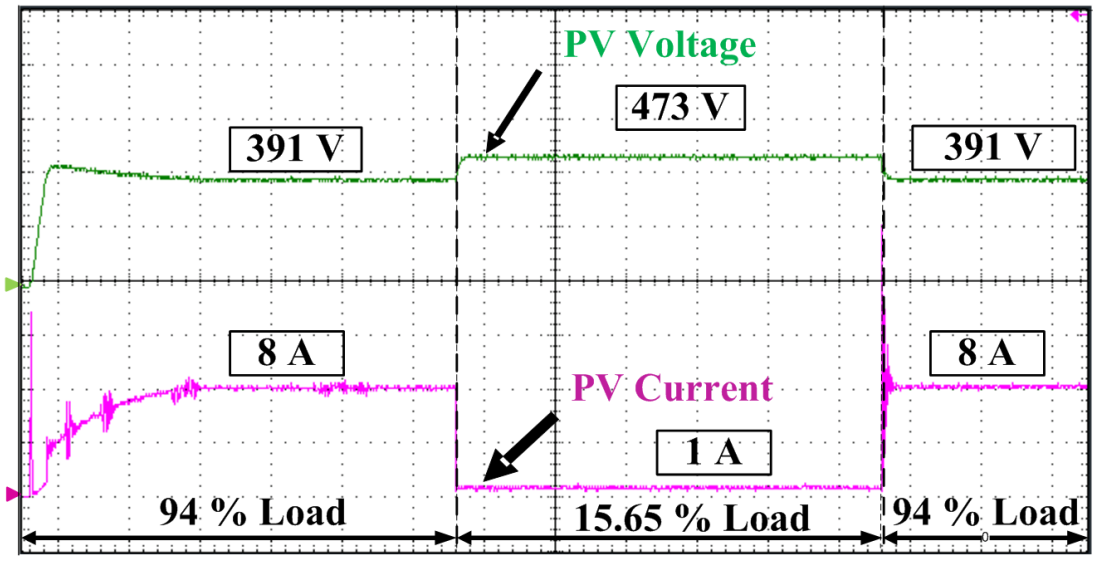

(y-axis: PV voltage : 200 V/div. & PV current : 4 A/div. ,
x-axis: Time scale= 1 s/div.)

(b)

Figure 4.18: PV port waveforms under variable load conditions:(a) Simulation waveforms and (b) Experimental waveforms

served that the voltage and current waveforms of the PMSG will vary in response to a change in the load, and these changes are in compliance with the constant load voltage requirement and the necessary load power demand.

In this case, the peak value of phase voltage and phase current of the PMSG is 265 V and 4 A, respectively corresponding to the case of high load level. Then, when the load demand drops down then the peak value of PMSG phase voltage and current is 310 V and 1.2 A, respectively. Further, when load demand rises again thereby the PMSG voltage and current is restored to previous peak value 265 V and 4 A, respectively.

With varying load levels, the load voltage will tend to deviate that will result in disturbing the load voltage from the reference value. In this case, when the load level changes from high level to low level thereby there will be tendency for load voltage to dip with respect to the reference voltage. However, as both the sources are contributing together in maintaining the constant load voltage operation as illustrated in section 2.5, therefore, the hybrid sources will try to increase their voltage levels to ensure the load voltage to be operating at constant level. As it is observed in Figure 4.18 that there is a rise in the PV voltage during the scenario of step-down load level. On the other hand, there is rise in the PMSG phase voltage occurring concurrently in this scenario as illustrated in the Figure 4.19 (both simulation and experimental waveforms). Further, as there is a decrease in the load level thereby it will result in the simultaneous decrement in the current injection from both PV and PMSG sources as detailed in Figure 4.18 and Figure 4.19. Therefore, it can be indicated that in order to meet the overall new load demand, then the power output from these sources drops down in comparison to its previous level.

Ultimately, when the load demand rises again then the load voltage will be disrupted again with the magnitude tending to rise with respect to the reference value. However, both the sources voltage level will be undergoing simultaneous decrement and henceforth the load voltage can be maintained at the same value equal to the reference voltage. In addition to this, in response to increase in the load demand, the injected PV and PMSG current rises simultaneously as can be perceived in Figure 4.18 and Figure 4.19, henceforth both the sources are able to realize the overall power

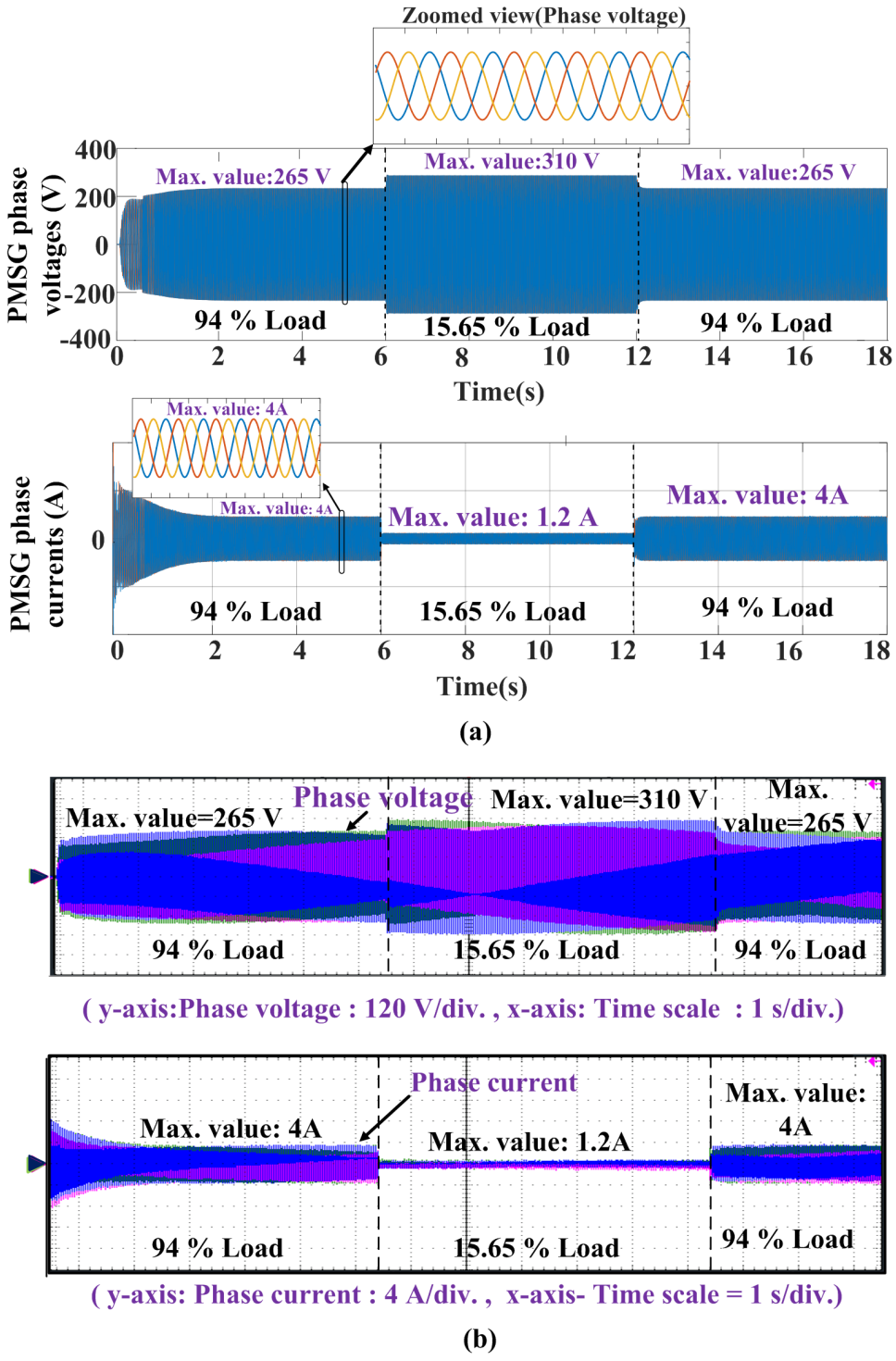

Figure 4.19: PMSG port voltage and current waveforms under variable load conditions:(a) Simulation waveforms and (b) Experimental waveforms

balance at this high load demand scenario.

- **PMSG port torque and speed**: Figure 4.20 presents the waveforms pertaining to the PMSG rotor speed and electromagnetic torque under the scenario of varying load levels at constant rotor speed. Herein, as observed, the rotor speed is constant at 1500 rpm (or 157 rad/s).

  Then with regard to the change in the load level, the changes in the electromagnetic torque is apparent as the rotor speed remains constant. During the case of high load demand, the magnitude of electromagnetic torque is 9.52 Nm and when the load demand is low thereby the magnitude of electromagnetic torque is 3.1 Nm. Thereupon, the PMSG power levels are 1.5 kW at high-load scenario and 486.7 W at low-load scenario.

  It can be stated that during the case of high load, PMSG is operating at maximum power point condition while during the case of low load power demand, the PMSG switches to Non-MPP mode of operation. Henceforth, it can be concluded that wind-PMSG is able to operate in accordance with dynamic load change requirements varying from high load (MPP) to low load (Non-MPP) and vice-versa.

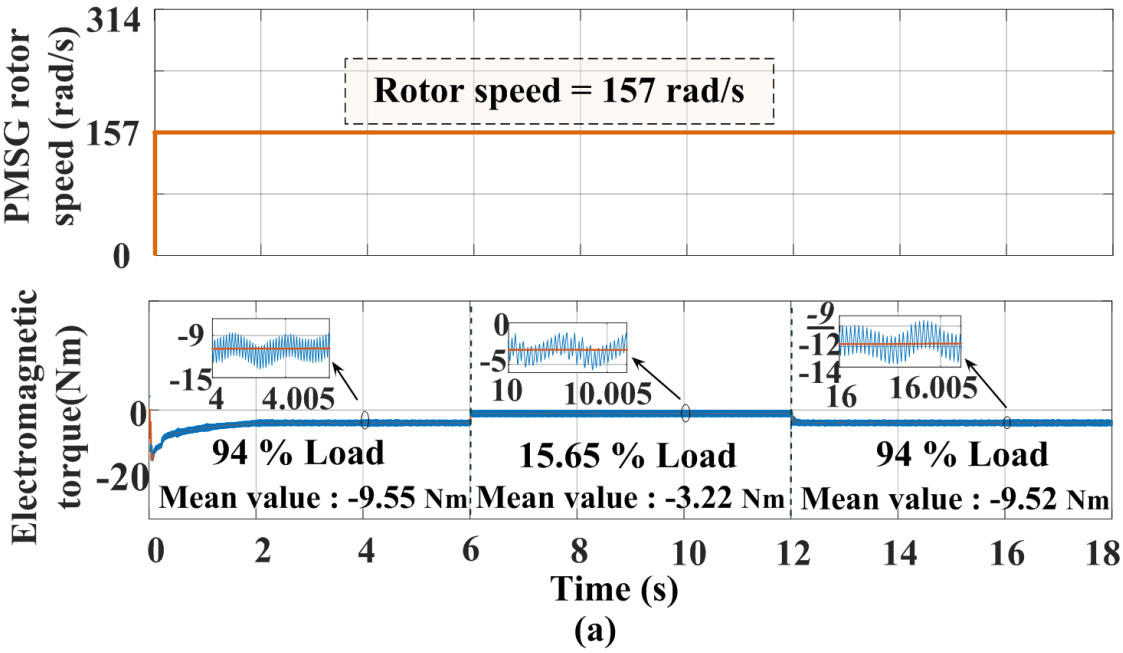

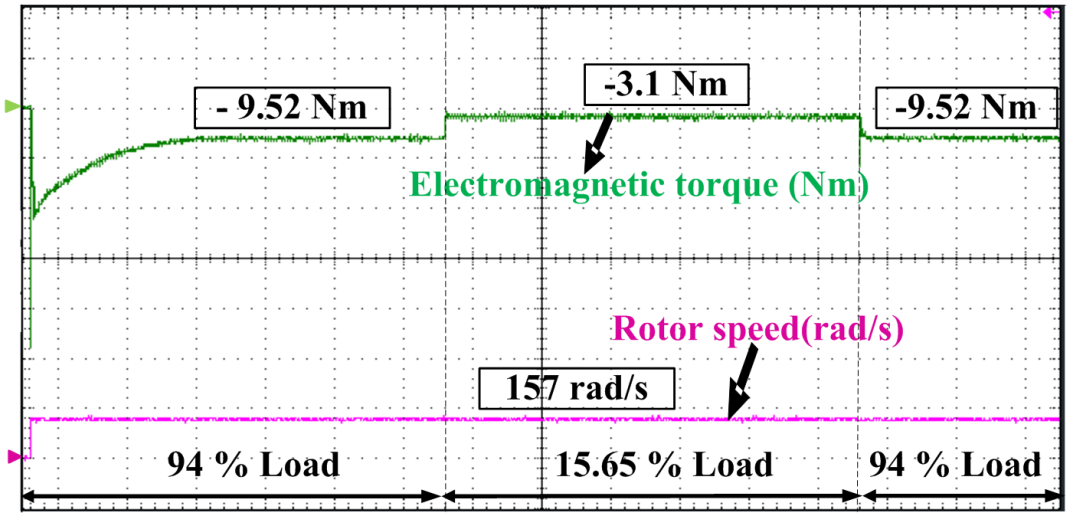

Figure 4.20: PMSG rotor speed and electromagnetic torque waveforms under variable load conditions:(a) Simulation waveforms and (b) Experimental waveforms

4.4 Scenario 2: Variable source and constant load conditions

In this section, proposed system is undergoing source side variations at constant load level and thereby the performance investigation of the proposed converter in this scenario is detailed. Herein, two cases of PV irradiation level variations alone and rotor speed variations alone at constant load level have been considered.

4.4.1 Only PV irradiation level variations

Figure 4.21- reftorquespeedsidewaveformspvcase shows the both the source side and load side performance waveforms pertaining to case study of the PV irradiation level change. In this case, two-step perturbations of irradiation level change have been considered. Initially, from time t = 0 sec. to t = 6 sec., the system is operating at an irradiation level of $1kW/m^2$. Then, at time t = 6 sec., step down in irradiation level is applied to an irradiation level of $500W/m^2$. And finally at t = 12 sec., the irradiation level is changed to $1kW/m^2$. In this case study, load level is constant at 70 % load level and rotor speed is constant at 1500 rpm(or 157 rad/s).

- **Load port** : Figure 4.21 shows the load port voltage and current waveforms pertaining to irradiation level variations at constant load level. It can be observed that during the instance of irradiation level of $1kW/m^2$, the mean value of load voltage is 755 V [during t = 0 to 6 sec. and during t = 12 to 18 sec.] while during the case of irradiation level of 500 W/m^2, mean value of load voltage is 753 V. Therefore, it can be concluded that the load voltage is maintained constant during varying irradiation level conditions.

  Thereupon, with regard to load current, the magnitude of the load current is staying constant at 3.8 A as load demand is same throughout irrespective of variations in the irradiation level. Thus, the load power is remain constant at magnitude of 2.8 kW. Henceforth, it can be concluded that the proposed system is able to maintain constant load voltage and necessary load power when undergoing irradiation level step perturbations (both step-up change and step-down change) at constant rotor speed and the constant load demand.

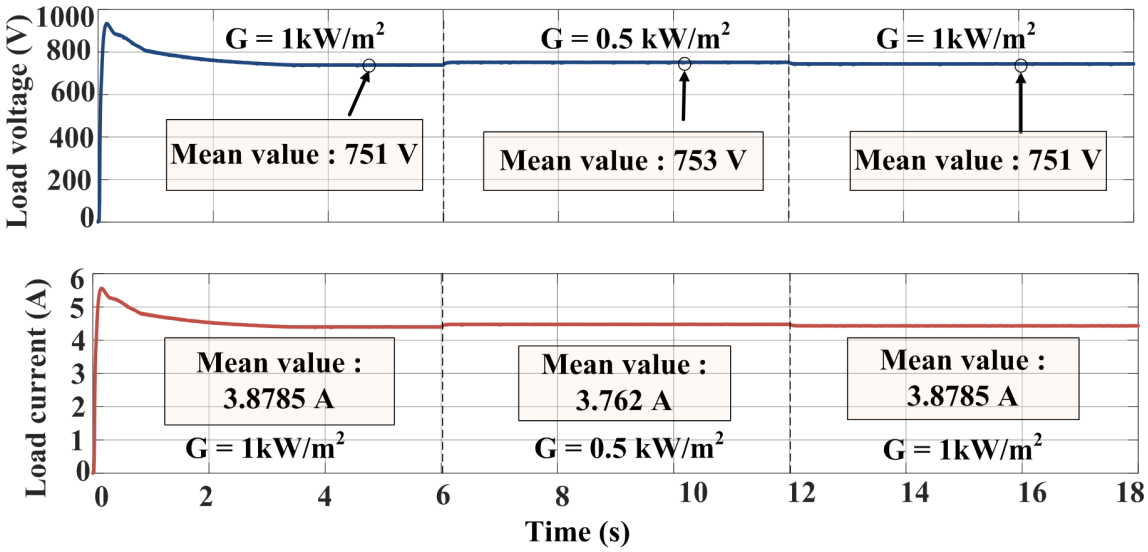

(a)

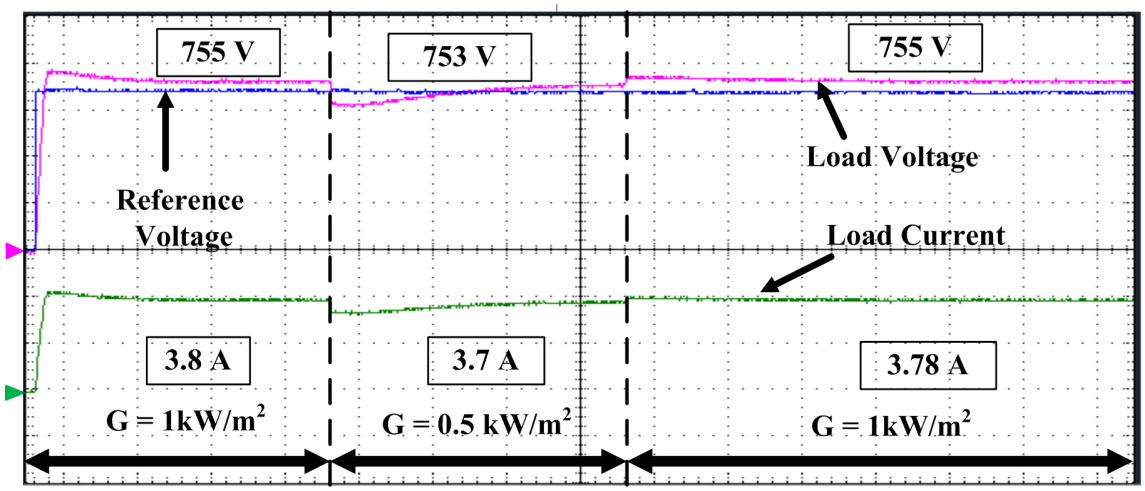

(y-axis: Load voltage : 200 V/div. , Load current : 2 A/div. ,
x-axis: Time scale : 2 s/div.)

(b)

Figure 4.21: Load voltage and current waveforms under variable irradiation conditions:(a) Simulation waveforms and (b) Experimental waveforms

- **PV port** : Figure 4.22 shows the PV array voltage and current waveforms for varying irradiation level scenario. It can be observed that in response to irradiation level change, PV array voltage and current waveforms will be undergoing changes in order to meet the constant load voltage and necessary load power requirement.

  In this case, during the case of irradiation level of $1kW/m^2$, the PV array

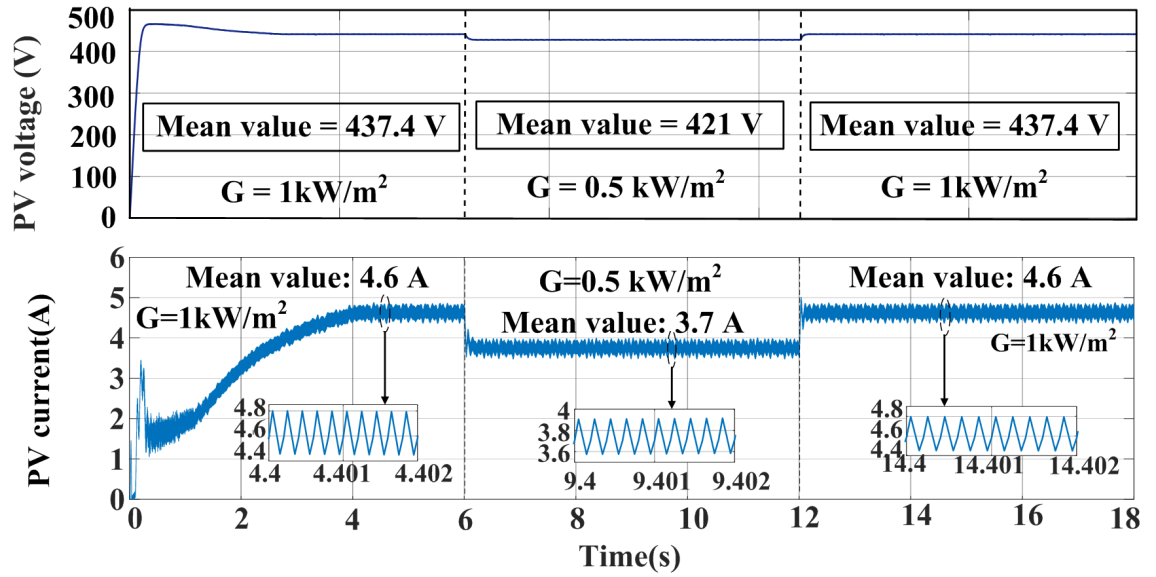

(a)

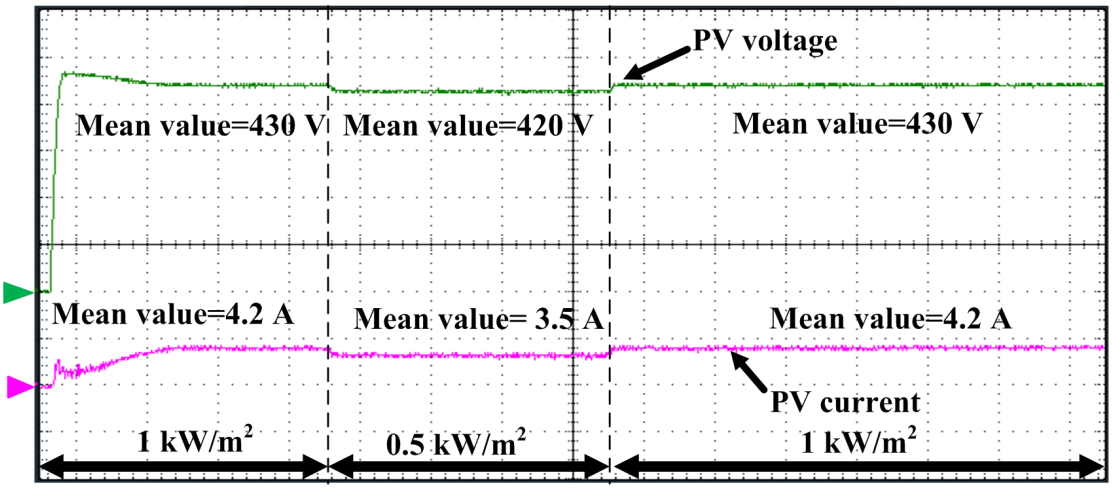

(y-axis-PV voltage : 100 V/div. , PV current : 5 A/div. ,
x-axis- Time scale : 1 s/div.)

(b)

Figure 4.22: PV port voltage and current waveforms under variable irradiation conditions: (a) Simulation waveforms and (b) Experimental waveforms

voltage and current is 430 V and 4.2 A ,respectively. Then, at an irradiation level of 0.5 kW/m^2 the PV array voltage and current level is decreased to 420 V and 3.5 A ,respectively. Further, when irradiation level is changed to $1kW/m^2$ thereby the PV array voltage and current is restored to 430 V and 4.2 A, respectively. Therefore,

the PV power at an irradiation level of $1kW/m^2$ is 1.8 kW and during the case of irradiation level of $500W/m^2$, the PV power is 1.47 kW.

Herein, it can be inferred that with the decrement in the PV irradiation level (from $1kW/m^2$ to $500W/m^2$), then the PV voltage and PV current decreases, thereby resulting in a decrease in the PV power magnitude. And when the irradiation level rises (from $500W/m^2$ to $1kW/m^2$), then both the PV voltage and PV current increases and thus resulting in a increase in the PV power magnitude.

- **PMSG port** : Figure 4.23 depicts the PMSG phase voltage and current waveforms for variable irradiation levels at constant load level and constant rotor speed. It is observed that the voltage and current waveforms of the PMSG will vary in response to a change in the irradiation level and thereby acting as power balancer in the system.

  At an irradiation level of $1kW/m^2$, the peak value of phase voltage and phase current is 280 V and 3 A, respectively while corresponding to the irradiation level of 500 W/m^2 the peak value of phase voltage and phase current is 270 V and 4 A. Further, when the irradiation level rises the peak value of phase voltage and current is restored to previous value of 280 V and 3 A, respectively.

  As irradiation level is changed from high level to the low level, the load voltage will tend to fluctuate, thereby in order to ensure the constant load voltage the PMSG voltage will tend to decrease in order to retain the load voltage level at its reference value. As there is constant load demand to be fulfilled the injected PMSG current rises.

  With varying irradiation level, the PV voltage will change that will result in disturbing the load voltage from the reference value. In this scenario, as there is step down change in the irradiation level from 1000 W/m^2 to 500 W/m^2 , the PV voltage will decrease and thereby the PV power magnitude also dips down with the decrease in the PV current level. As a result, the load voltage will tend to undergo reduction from the reference value. Now, in order to ensure the constant load voltage level operation and fulfilling the necessary load power requirement, the PMSG source will act as a power balancer therein. As PMSG is running at a constant rotor speed, the phase current injection from the PMSG will rise in order to satisfy the necessary load current because there is a decrement in the PV current magnitude. This will result in a decrease in the PMSG phase terminal voltage with a rise in the PMSG current,

however, there is an increase in the PMSG power level to realize the overall power balance in the system and henceforth achieving the constant voltage level operation.

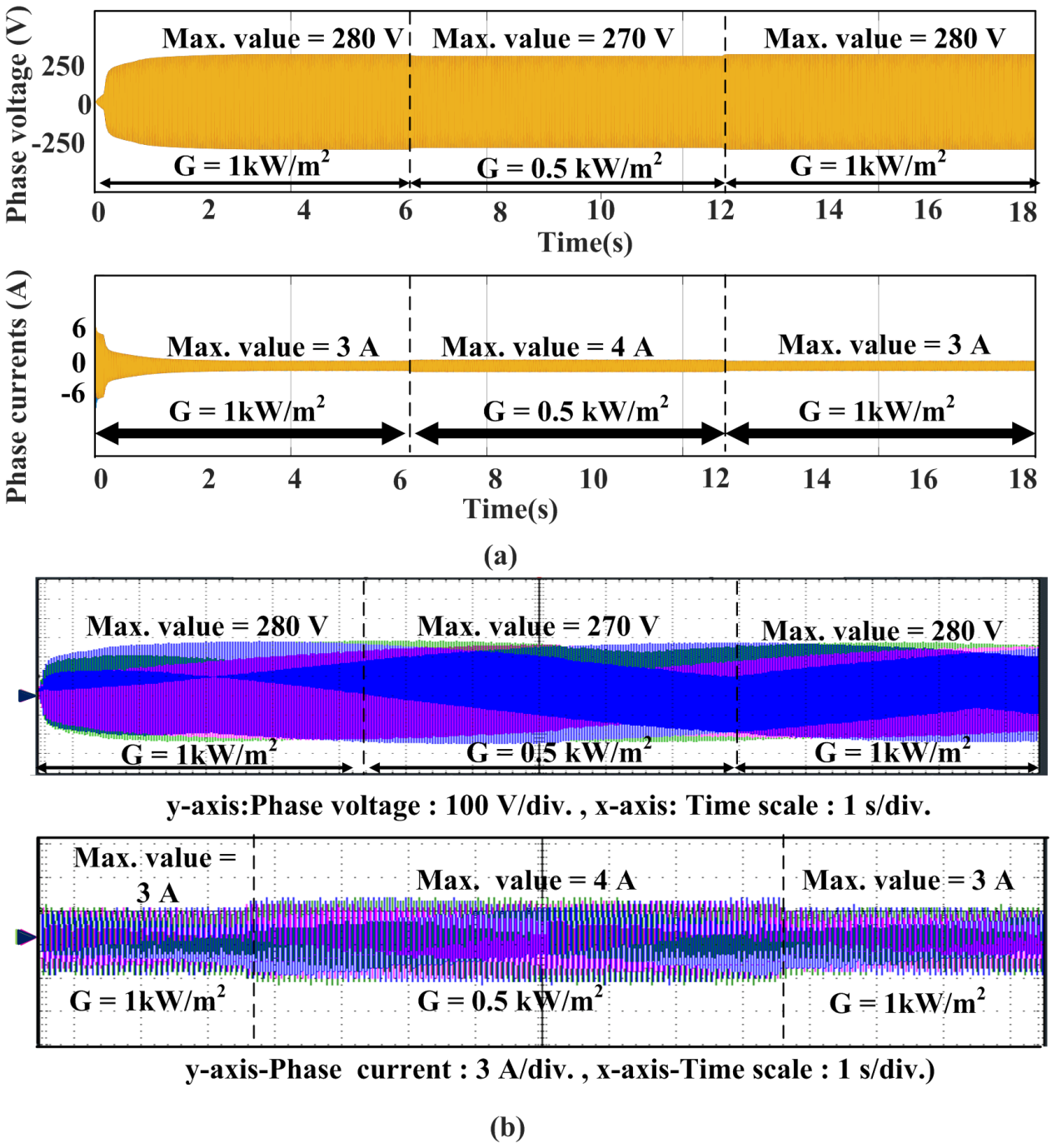

Figure 4.23: PMSG port voltage and current waveforms under variable irradiation conditions:(a)Simulation waveforms and (b) Experimental waveforms

Finally, in the scenario of step up in the irradiation level from 500 W/m^2 to 1000 W/m^2 , the PV voltage increases and thereby the PV power magnitude also rises with the increase in the PV current level. Consequently, the load voltage will tend to rise from its reference value. Thereupon, in order to maintain the constant load voltage level and meeting the necessary the load power requirement, the PMSG source again will act as a power balancer herein. As the PMSG is running at a constant rotor speed, the phase current injection from the PMSG will reduce because there is a rise in the PV current magnitude. This will result in a increase in the PMSG phase terminal voltage with a decrement in the PMSG current, however, there is a decrease in the PMSG power level to realize the overall power balance in the system and henceforth achieving the constant voltage level operation.

- **PMSG port torque and speed**: Figure 4.24 presents the waveforms pertaining to the PMSG rotor speed and electromagnetic torque under the scenario of varying irradiation levels at a constant rotor speed. Herein, as observed, the rotor speed is constant at 1500 rpm (or 157 rad/s). It is observed that with regard to the change in the irradiation level, the changes will occur in the electromagnetic torque as the rotor speed remains constant. During the case of $G = 1kW/m^2$, the magnitude of electromagnetic torque is 7.5 Nm and when the irradiation level is low thereby the magnitude of electromagnetic torque is 9.11 Nm.

Thereupon, the PMSG power levels are 1.177 kW at high-irradiation level scenario and 1.43 kW at low-irradiation level scenario. Because the rotor speed is constant the electromagnetic torque will be undergoing necessary adjustment with regard to change in irradiation level and thereby acting as power balancer in order to fulfil the load requirements of the proposed system.

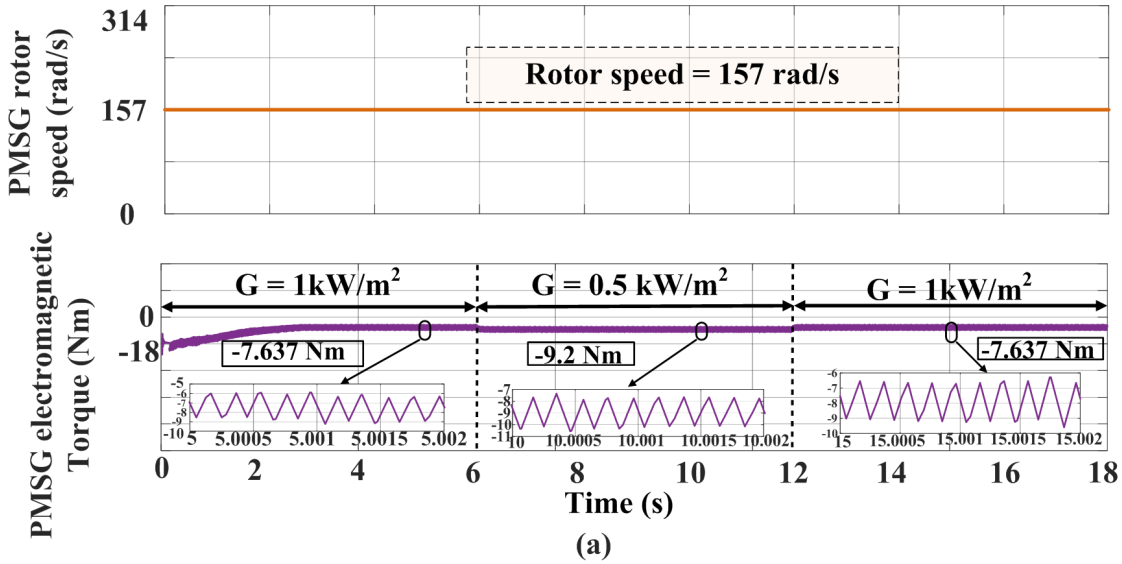

(a)

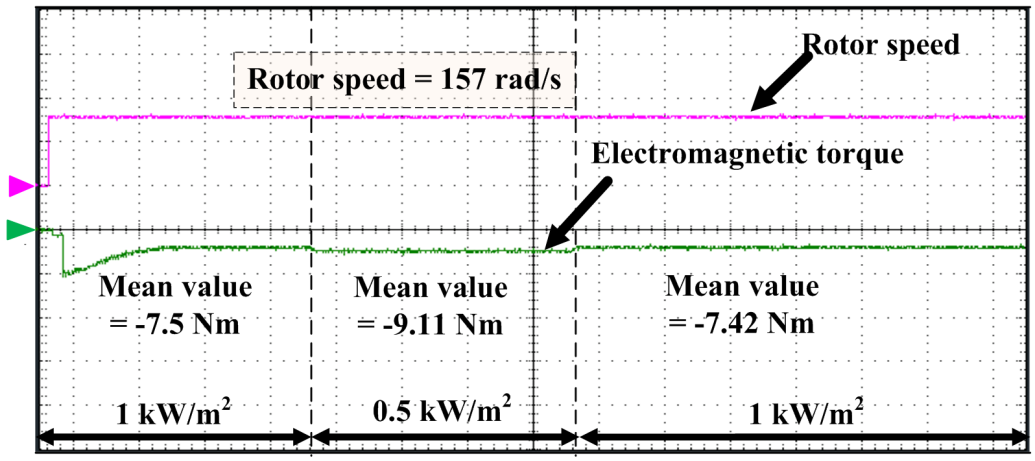

(y-axis- Speed : 100 rads/div., Electromagnetic torque : 18 Nm/div. , x-axis- Time scale : 1 s/div.)

(b)

Figure 4.24: PMSG rotor speed and electromagnetic torque waveforms under variable irradiation conditions:(a)Simulation waveforms and (b) Experimental waveforms

4.4.2 Only PMSG rotor speed variation

Figure 4.25- 4.28 shows both the source side and load side performance waveforms pertaining to case study of the PMSG rotor speed level variations. In this case, two-step perturbations of rotor speed level change have been imposed. Initially, from time t = 0 sec. to t = 6 sec., the system is operating at a rotor speed of 750 rpm (50% of rated speed).

Then, at time t = 6 sec., step change in rotor speed level level is applied to 1125 rpm(75% of rated speed). And finally at t=12 sec., the rotor speed level is changed to 1500 rpm(rated speed).. In this case study, irradiation level is constant at $G = 1kW/m^2$ and at constant 70% load level.

- **Load port** : Figure 4.25 shows the load port voltage and current waveforms pertaining to rotor speed level variations at constant load level and constant irradiation level. It can be observed that during the instance of rotor speed level of 750 rpm(50% of rated speed), the mean value of load voltage is 742 V [during t = 0 to 6 sec.) and while during the case of rotor speed level of 1500 rpm(100% of rated speed), the mean value of load voltage is 751.2 V. Therefore, it can be concluded that the load voltage is maintained constant during varying rotor speed level conditions.

  Thereupon, with regard to load current, the magnitude of the load current is staying constant at 4.4 A as load demand is same throughout irrespective of variations in the rotor speed level. Thus, the load power is constant at 3.38 kW. Henceforth, it can be concluded that the proposed system is able to maintain constant load voltage and necessary load power when undergoing rotor speed level changes perturbations at constant irradiation level and constant load demand.

- **PV port** :Figure 4.26 shows the PV array voltage and current waveforms for varying rotor speed level scenario. It can be observed that in response to rotor speed level change, PV array voltage and current waveforms will be undergoing changes in order to meet the constant load voltage and necessary load power requirement.

  In this case, during the case of rotor speed level of 750 rpm (50% of rated speed), the PV array voltage and current is 390 V and 7.2 A ,respectively. Then, at an rotor speed level of 1500 rpm(100% of rated speed) the PV array voltage and current level is decreased to 436 V and 4.6 A ,respectively. Therefore, the PV power at rotor speed level of 750 rpm (50% of rated speed) is 2.808 kW and during the case of rotor speed level of 1500 rpm (100% of rated speed), the PV power is 2.0056 kW.

  Herein, it can be inferred that with the rise in rotor speed level, the PV voltage and PV current decreases thereby resulting in a decrease in the PV power magnitude.

- **PMSG port** : Figure 4.27 depicts the PMSG phase voltage and current waveforms for variable rotor speed levels at constant irradiation level and constant load. It is

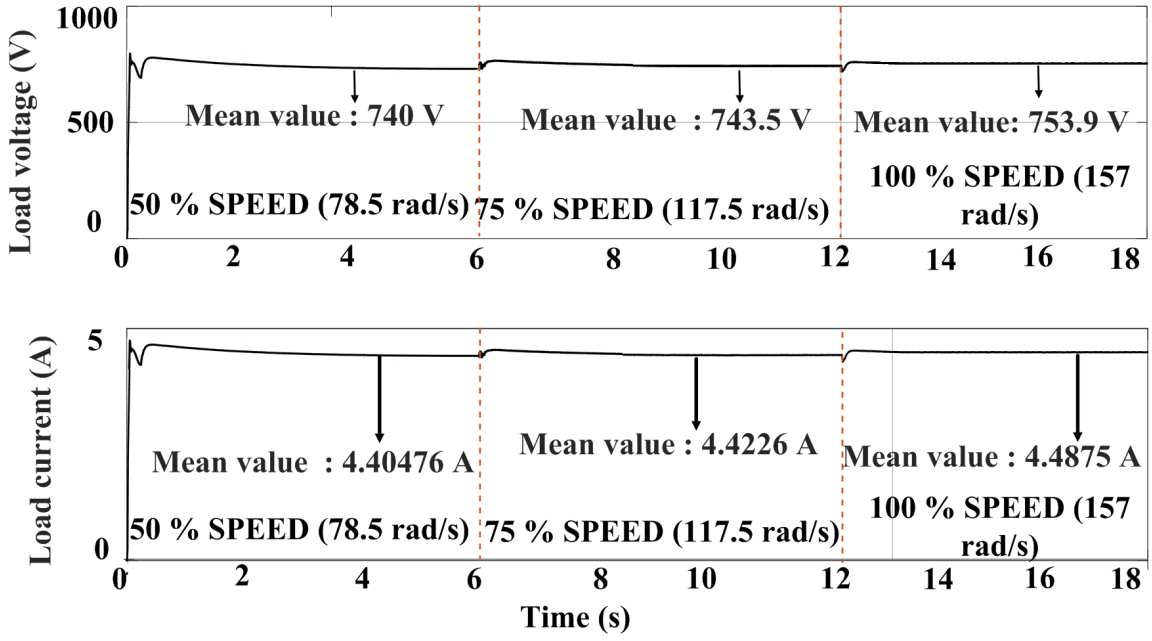

(a)

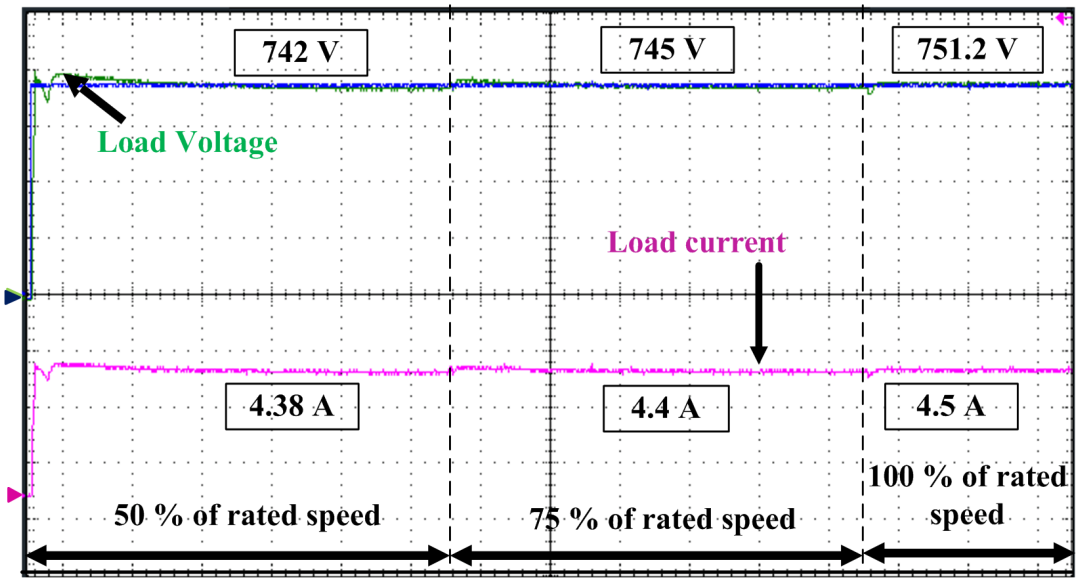

(y-axis-Load voltage : 200 V/div. , Load current : 2 A/div. , x-axis- Time scale : 1 s/div.)

(b)

Figure 4.25: Load voltage and current waveforms under variable rotor speed conditions:(a) Simulation waveforms and (b) Experimental waveforms

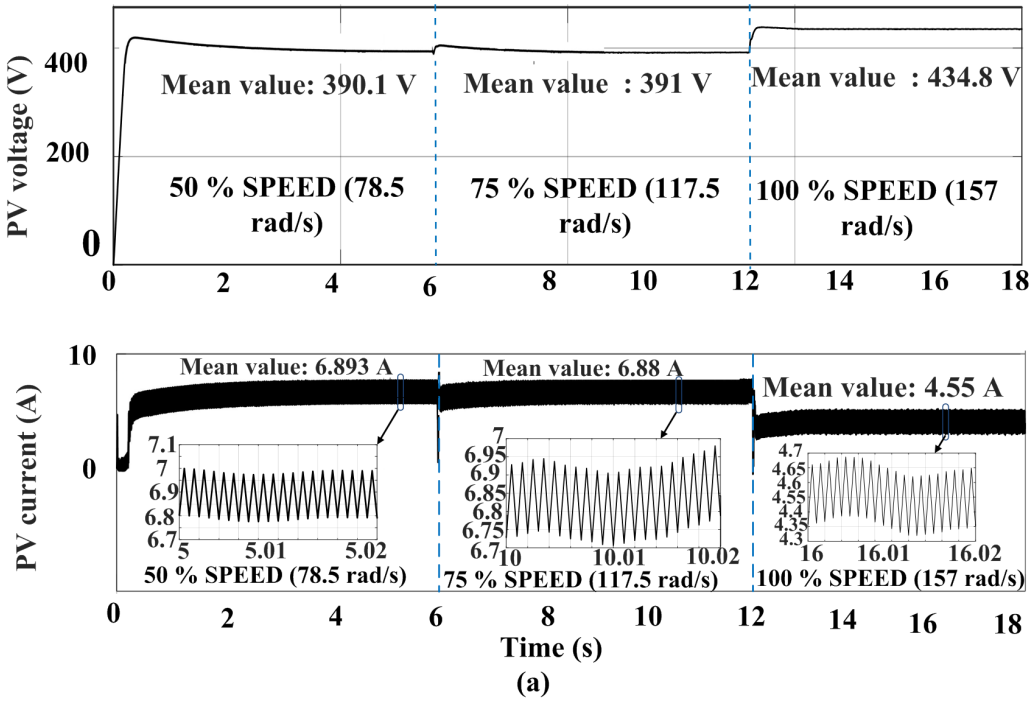

(a)

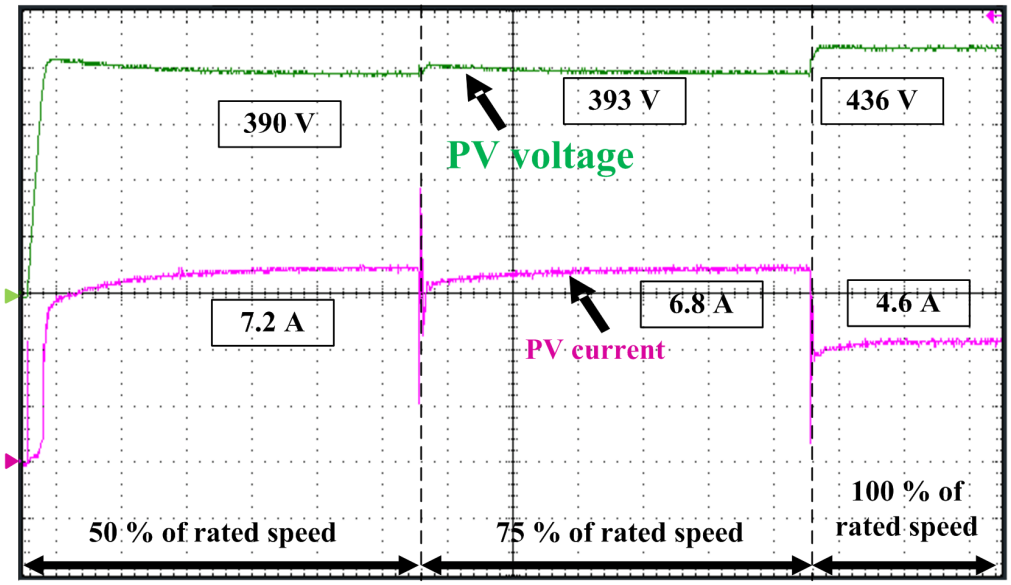

(y-axis-PV voltage : 100 V/div. , PV current : 2 A/div. ,
x-axis- Time scale : 1 s/div.)

(b)

Figure 4.26: PV port voltage and current waveforms under variable rotor speed conditions: (a) Simulation waveforms and (b) Experimental waveforms

observed that the voltage and current waveforms of the PMSG will vary in response to a change in the rotor speed level.

At rotor speed of 750 rpm, the peak value of phase voltage and phase current is 150 V and 2.8 A, respectively while corresponding to the rotor speed level of 1500 rpm, the peak value of phase voltage and phase current is 270 V and 4 A.

As there is a rise in rotor speed (or wind input), there is a rise in PMSG phase voltage and thereby there is increment in the PMSG power along with the increase in the PMSG phase current magnitude. This will lead to disruption in the load voltage with the magnitude tend to rise with respect to the reference value. However, as the load is maintained at the constant level, thereupon with regard to rise in the PMSG power the PV source will act as power balancer. Therefore, despite under constant irradiation level the PV source current will be undergoing reduction in the magnitude which is leading to rise in the PV voltage magnitude and consequently there is a dip in the PV power level to achieve the overall power balance in the system.

- **PMSG port torque and speed**: Figure 4.28 presents the waveforms pertaining to the PMSG rotor speed and electromagnetic torque under the scenario of varying rotor speed levels at a constant irradiation levels and constant load. Herein, as observed, the rotor speed is varying from 750 rpm (or 78.5 rad/s) to 1500 rpm (or 157 rad/s). It is observed that with regard to the change in the rotor speed level, the changes will occur in the electromagnetic torque.

  During the case of 50 % of rated speed, the magnitude of electromagnetic torque is 7 Nm and when the rotor speed rises to 100 % of rated speed the magnitude of electromagnetic torque is 9.5 Nm. With regard to change in the the rotor speed level the electromagnetic torque will be undergoing necessary adjustment in order to fulfil the load requirements of the proposed system.

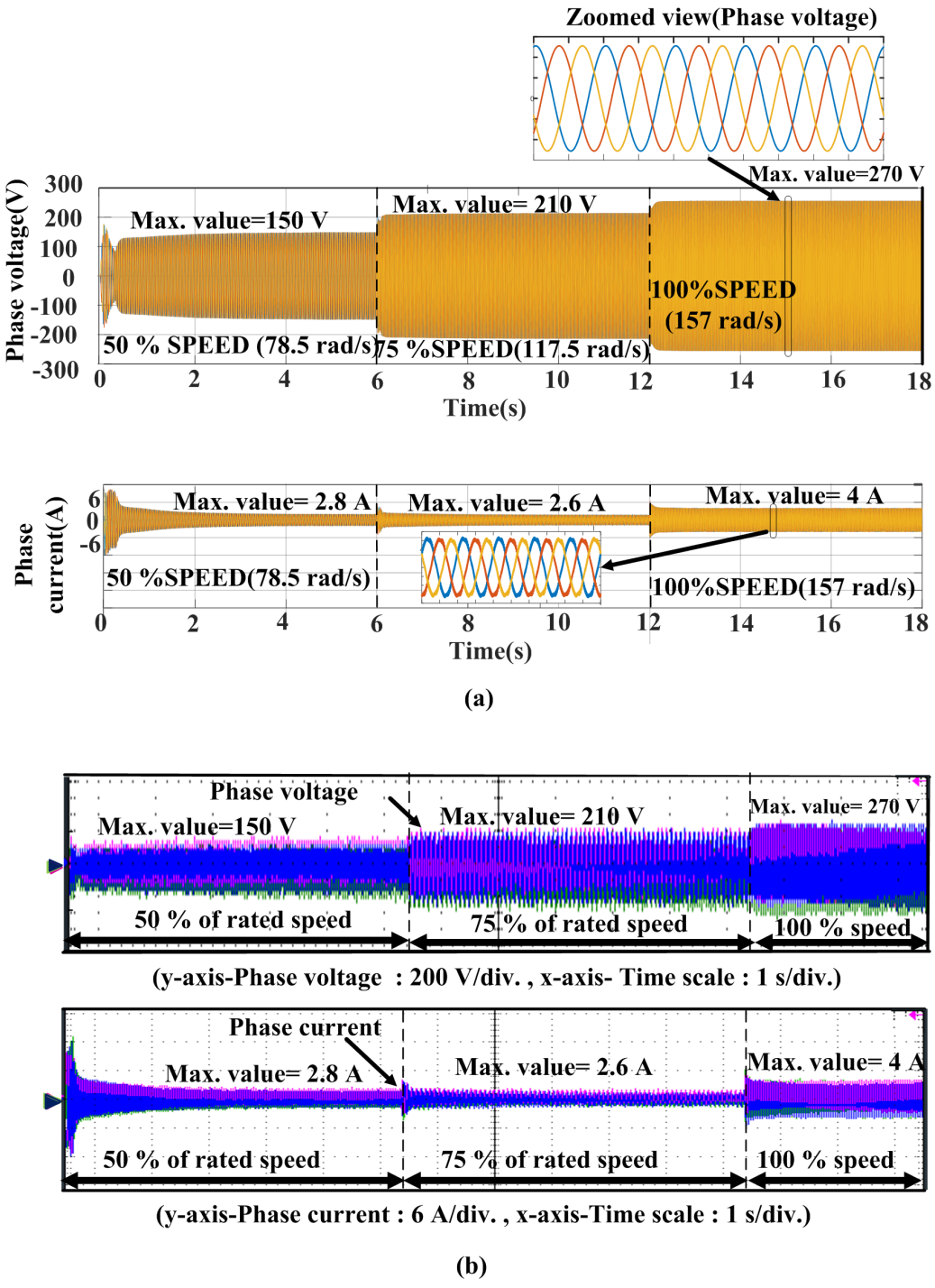

Figure 4.27: PMSG port voltage and current waveforms under variable rotor speed conditions: (a) Simulation waveforms and (b) Experimental waveforms

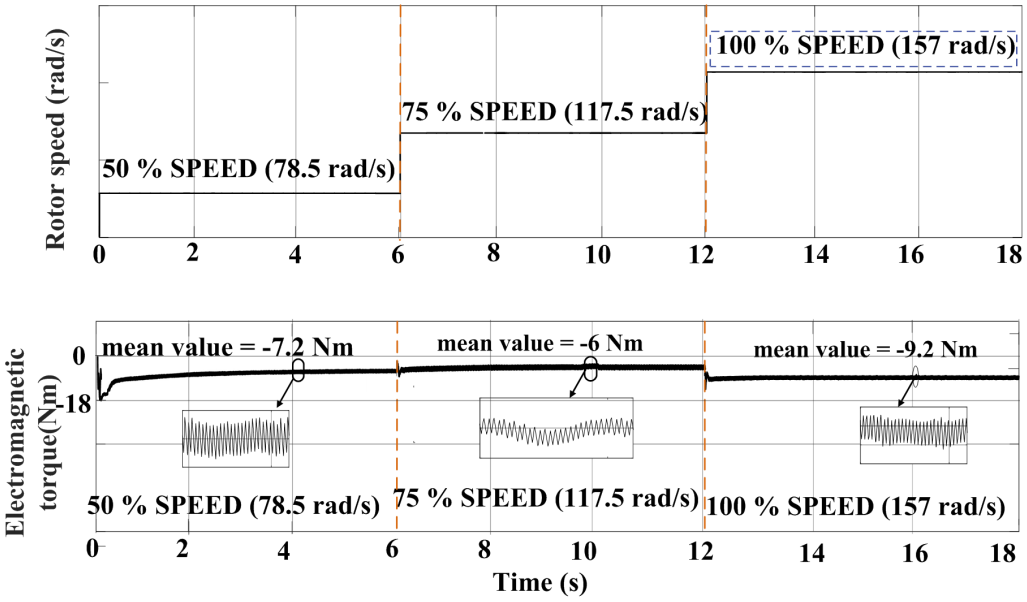

(a)

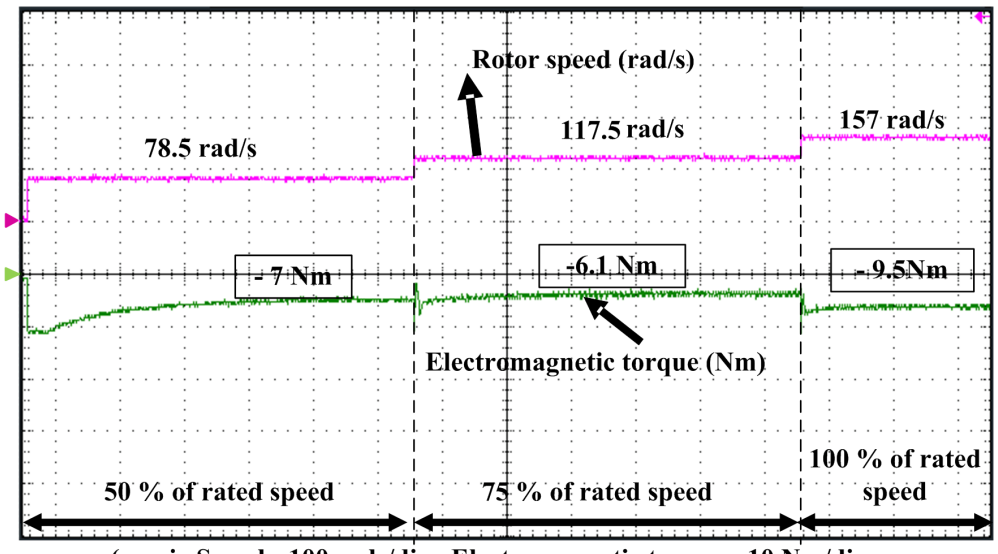

(y-axis-Speed : 100 rads/div., Electromagnetic torque : 10 Nm/div. ,
x-axis- Time scale : 1 s/div.)

(b)

Figure 4.28: PMSG rotor speed and electromagnetic torque waveforms under variable rotor speed conditions:(a) Simulation waveforms and (b) Experimental waveforms

4.5 Loss Analysis of the proposed hybrid power converter

4.5.1 Power losses-relations of the IGBT and diode in the proposed converter

The conduction-state power loss in the IGBT is represented as

$$P_{IGBT} = R_f.(i_{rms}^2) + V_T.i_{avg} \tag{4.1}$$

where P_{IGBT} is the average power losses of the IGBT during one switching period, i_{rms} is the root mean square(RMS) value of the current,i_{avg} is the average value of the current, R_f is the equivalent resistance of the IGBT and V_T is the voltage drop of the IGBT.

Similarly, the conduction-state power loss in the diode is represented as

$$P_{diode} = R_d.(i_{rms}^2) + V_d.i_{avg} \tag{4.2}$$

where P_{diode} is the average power losses of the diode during one switching period, i_{rms} is the root mean square(RMS) value of the current, i_{avg} is the average value of the current, R_d is the equivalent resistance of the diode and V_d is the voltage drop of the diode.

4.5.2 Switching losses-equations of the IGBT in the proposed converter

During switching processes, the transistor current and voltage do not abruptly change. As a result, in order to calculate the average power losses in these operations, an integral of the product of transistor current and voltage values is need to be considered. During the switching processes, the current and voltage of the specific transistor can vary in different manner. Therefore, switching losses during the turn-on process and switching losses during the turn-off process should be calculated separately.

The average losses in the turn-on process:

$$P_{on} = \frac{1}{6} f_{sw} V_{load} I_{C_{max}} t_r \tag{4.3}$$

The average losses in turn-off process:

$$P_{on} = 0.135 f_{sw} I_{load} V_{CE_{max}} t_f \tag{4.4}$$

The relationships 4.3 and 4.4 provides an estimate of switching losses in one transistor during one switching period. Therefore, the total switching losses can be estimated as :

$$P_{sw} = P_{on} + P_{off} \tag{4.5}$$

Power Loss in the converter for high load level scenario	
Loss distribution	Values
Conduction losses in switches(a)	16.606 W
Switching losses in the switches(b)	12.11 W
Conduction losses in load diode(c)	5.0396 W
Conduction losses in PV side diode(d)	8.0704 W
Ohmic losses in PMSG inductances(e)	16.34 W
Ohmic losses in PV side inductance(f)	11.97 W

Table 4.5: Loss distribution for high load scenario

Power Loss in the converter for PMSG rotor speed level variations scenario	
Loss distribution	Values
Conduction losses in switches(a)	15.0848 W
Switching losses in the switches(b)	11.65 W
Conduction losses in load diode(c)	9.0222 W
Conduction losses in PV side diode(d)	10.0522 W
Ohmic losses in PMSG inductances(e)	27.736 W
Ohmic losses in PV side inductance(f)	24.2 W

Table 4.6: Loss distribution for PMSG rotor speed level variations scenario

The loss distribution in the converter is presented in Table 4.5-4.6 and Figure 4.29 while the corresponding case studies's power distribution is shown in Table 4.7-4.8. Efficiency calculated in the above case study has also been presented in Table 4.7-4.8.

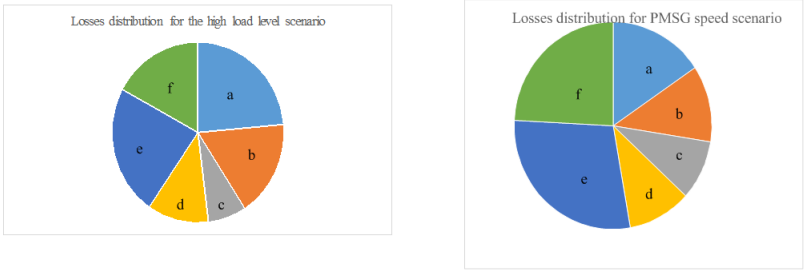

(a) (b)

Figure 4.29: Loss distribution in the converter

Power distribution in the converter for high load level scenario	
Power distribution	Values
Total Power Input	3128 + 1492 = 4620 W
Power Output	4550 W
Power losses	70.136 W
Efficiency	98.46 %

Table 4.7: Power distribution in the converter for for the high load level scenario

Power distribution in the converter for PMSG speed variation scenario	
Power distribution	Values
Total Power Input	2808 + 555 = 3362 W
Power Output	3249.96 W
Power losses	97.7452 W
Efficiency	96.67 %

Table 4.8: Power distribution in the converter for the PMSG rotor speed level variations scenario

4.6 Summary

In this chapter, performance investigation of the proposed system under varying source level or at varying load level is discussed. Herein, it can be inferred that despite either source variation or load variation the load voltage is maintained constant equal to the reference voltage. Also, the sources are undergoing dynamic changes in their voltage and current levels in accordance with the load requirements. Therefore, it can stated that the proposed converter is capable of integrating hybrid sources in single stage configuration with dynamic output capabilities while fulfilling the requirements of standalone DC system.

Chapter 5

Conclusion and future scope

Constraints in the isolated areas has made the AC grid connection not feasible. This prompted researchers to look for an alternative solution for combating the electrification issues prevailing in these isolated areas. In this regard, renewable energies based solutions have garnered widespread attention and thereby offered an alternative that can alleviate the deficit in electrification issues. However, these renewable energy sources require an appropriate power conversion circuitry and control that can ensure the reliability of the power supply as well as meeting the power requirements at the consumer side.

In the present thesis work, PV-wind hybrid sources based single stage multi-port power converter is presented. This converter can integrate the hybrid sources, viz. solar and wind in the single stage circuitry. The main focus of this thesis is the investigation of this single stage multiport converter in standalone DC system that implies the validation of the converter to be able to operate at the constant load voltage level irrespective of the sources level or load level variations. In this regard, firstly the principle of operation of this single stage converter with the incorporation of the hybrid sources is elaborated. The simultaneous conversions operation pertaining to both the sources affirms that both the sources are operating dynamically with regard to the requirements of the standalone DC load. This implies that either with source level variations or load level variations, both the sources are concurrently supplying power towards load side while maintaining the constant load voltage operation. Then, the closed-loop control architecture is discussed for the present system that ensures the load voltage regulation of the converter in addition to ensuring the dynamic power output from both the sources. Herein, the control architecture comprises of the common load voltage constraint on both the AC-DC conversion control and DC-DC conversion control loops that ensures the both the sources to supply the power levels such that the constant

load voltage operation and the necessary load power requirement can be satisfied. In relation to the PV DC-DC conversion control, the load voltage regulator will generate the duty ratio control signal to regulate the PV operating voltage and current for meeting the load requirements. While in wind-PMSG-based 3-phase AC-DC conversion control, dual loop control strategy is utilized. The load voltage regulator is employed as an outer loop to generate the inner current control reference value, i.e., q-axis current($i_{qs,ref.}$). And then, $i_{qs,ref.}$ and $i_{ds,ref.} = 0$ will actuate the inner loop control. Thus, in order to achieve the overall power balance and ensuring the load voltage to be constant under all operating situations, this integrated control based on load voltage regulation should be able to govern the dynamic output capabilities of hybrid sources. Further, to incorporate the simultaneous power conversion process in the converter, the process of generating the pulse width modulation signals is depicted that combines the sinusoidal pulse width modulation signals pertaining to AC-DC conversion with the pulses pertaining to the DC-DC conversion. This PWM scheme comprises of same switching frequency for both the sinusoidal PWM pulses and DC-DC conversion pulses. The presented PWM scheme ensures that the presented hybrid power converter should be able to operate with concurrent AC-DC conversion and DC-DC conversion process without affecting each other.

Lastly, in order to validate the operational aspects of the proposed converter, various operational scenario has been considered and thereby the investigation focusing on the load voltage regulation (of 750 V (DC)) and meeting necessary power balance has been carried out both in the simulation and experimental investigations. With regard to the presented results, it can be concluded that the presented converter is capable of maintaining constant load voltage at varying source or varying load conditions both in the simulation and experimental investigations. Also, at any conditions there is a dynamic power output perceived from the hybrid sources based on the load requirements, thus the process of simultaneous power conversion process is validated under various test scenarios. Finally, it can be concluded that the proposed single stage multi-port hybrid power converter can offer simple and reliable solution in the hybrid input systems based standalone DC system.

5.1 Future scope

The future scope of the present thesis is as follows:

- The present work can be extended with the integration of energy storage systems with input from the hybrid renewable sources (viz., solar and wind) with different

control strategies.

- The presented topology can be considered for wide-band-gap devices that allows higher switching frequency operation to make the converter more compact and overall reduce the system bulkiness.

- In continuation of endeavour of designing and developing the single-stage converter, an investigation of another topology with reduced switches can be explored in the future work.

Bibliography

Ahmed, T., Nishida, K., and Nakaoka, M. (2005). A novel stand-alone induction generator system for ac and dc power applications. In *Fourtieth IAS Annual Meeting. Conference Record of the 2005 Industry Applications Conference, 2005.*, volume 4, pages 2950–2957. IEEE.

Alagu, M., Ponnusamy, P., Pandarinathan, S., and Mohamed Ali, J. S. (2021). Performance improvement of solar pv power conversion system through low duty cycle dc-dc converter. *International Journal of Circuit Theory and Applications*, 49(2):267–282.

Amin, M. M. and Mohammed, O. (2011). Dc-bus voltage control technique for parallel-integrated permanent magnet wind generation systems. *IEEE Transactions on Energy Conversion*, 26(4):1140–1150.

Anand, S. and Fernandes, B. (2010). Optimal voltage level for dc microgrids. In *IECON 2010-36th Annual Conference on IEEE Industrial Electronics Society*, pages 3034–3039. IEEE.

Arriaga, M., Cañizares, C. A., and Kazerani, M. (2014). Northern lights: Access to electricity in canada's northern and remote communities. *IEEE Power and Energy Magazine*, 12(4):50–59.

Arutchelvi, M. and Daniel, S. A. (2006). Voltage control of an autonomous hybrid generation scheme based on pv array and wind-driven induction generators. *Electric power components and systems*, 34(7):759–773.

Chen, Y.-M., Cheng, C.-S., and Wu, H.-C. (2006). Grid-connected hybrid pv/wind power generation system with improved dc bus voltage regulation strategy. In *Applied Power Electronics Conference and Exposition, 2006. APEC'06. Twenty-First Annual IEEE*, pages 7–pp. IEEE.

Chiang, H., Ma, T., Cheng, Y. H., Chang, J., and Chang, W. (2010). Design and implementation of a hybrid regenerative power system combining grid–tie and uninterruptible power supply functions. *IET Renewable Power Generation*, 4(1):85–99.

Chiang, S., Shieh, H.-J., and Chen, M.-C. (2009). Modeling and control of pv charger system with sepic converter. *IEEE Transactions on industrial electronics*, 56(11):4344–4353.

Coelho, R. F., Concer, F. M., and Martins, D. C. (2010). A Simplified Analysis of DC-DC Converters Applied as Maximum Power Point Tracker in Photovoltaic Systems. In *Power Electronics for Distributed Generation Systems (PEDG), 2010 2nd IEEE International Symposium on*, pages 29–34. IEEE.

Daniel, S. A. and AmmasaiGounden, N. (2004). A novel hybrid isolated generating system based on pv fed inverter-assisted wind-driven induction generators. *IEEE Transactions on energy conversion*, 19(2):416–422.

Dash, S. S. and Nayak, B. (2015). Control analysis and experimental verification of a practical dc–dc boost converter. *Journal of Electrical Systems and Information Technology*, 2(3):378–390.

de Freitas, T. R., Menegáz, P. J., and Simonetti, D. S. (2016). Rectifier topologies for permanent magnet synchronous generator on wind energy conversion systems: A review. *Renewable and Sustainable Energy Reviews*, 54:1334–1344.

Dragičević, T., Lu, X., Vasquez, J. C., and Guerrero, J. M. (2015). Dc microgrids—part i: A review of control strategies and stabilization techniques. *IEEE Transactions on power electronics*, 31(7):4876–4891.

Finance, B. N. E., Global, L., et al. (2016). Off-grid solar market trends report 2016. *THe World Bank. https://www. lightingglobal. org/wpcontent/uploads/2016/03/20160301_OffGridSolarTrendsReport-1. pdf*.

González-Castaño, C., Restrepo, C., Kouro, S., and Rodriguez, J. (2021). Mppt algorithm based on artificial bee colony for pv system. *IEEE Access*, 9:43121–43133.

Gugulothu, R., Nagu, B., and Pullaguram, D. (2023). Energy management strategy for standalone dc microgrid system with photovoltaic/fuel cell/battery storage. *Journal of Energy Storage*, 57:106274.

Gundavarapu, A., Misra, H., and Jain, A. K. (2017). Direct torque control scheme for DC Voltage Regulation of the Standalone DFIG-DC System. *IEEE Transactions on Industrial Electronics*, 64(5):3502–3512.

Hazzab, A., Gouabi, H., Habbab, M., Rezkallah, M., Ibrahim, H., and Chandra, A. (2023). Wind turbine emulator control improvement using nonlinear pi controller for wind energy conversion system: Design and real-time implementation. *International Journal of Adaptive Control and Signal Processing*.

Iacchetti, M. and Marques, G. (2015). Voltage control in a dfig-dc system connected to a stand-alone dc load. In *Compatibility and Power Electronics (CPE), 2015 9th International Conference on*, pages 323–328. IEEE.

Jacob, E. and Farzaneh, H. (2022). Dynamic modeling and experimental validation of a standalone hybrid microgrid system in fukuoka, japan. *Energy Conversion and Management*, 274:116462.

Kant, K., Jain, C., and Singh, B. (2017). A hybrid diesel-windpv-based energy generation system with brushless generators. *IEEE Transactions on Industrial Informatics*, 13(4):1714–1722.

Krishna, K. S. and Kumar, K. S. (2015). A review on hybrid renewable energy systems. *Renewable and Sustainable Energy Reviews*, 52:907–916.

Kumar, D., Zare, F., and Ghosh, A. (2017). Dc microgrid technology: System architectures, ac grid interfaces, grounding schemes, power quality, communication networks, applications, and standardizations aspects. *Ieee Access*, 5:12230–12256.

Kumar, M., Singh, S., and Srivastava, S. (2012). Design and control of smart dc microgrid for integration of renewable energy sources. In *2012 IEEE Power and Energy Society General Meeting*, pages 1–7. IEEE.

Kumar, N., Tatabhatla, V. M. R., and Agarwal, A. (2021). Design of novel universal converter for integration of solar and wind energy for ac and dc load. *International Journal of Circuit Theory and Applications*, 49(12):4088–4119.

Kurohane, K., Uehara, A., Senjyu, T., Yona, A., Urasaki, N., Funabashi, T., and Kim, C.-H. (2011). Control strategy for a distributed dc power system with renewable energy. *Renewable Energy*, 36(1):42–49.

Li, L., Li, K.-J., Sun, K., Liu, Z., and Lee, W.-J. (2022). A comparative study on voltage level standard for dc residential power systems. *IEEE Transactions on Industry Applications*, 58(2):1446–1455.

Mahajan, S., Subramaniam, S., Natarajan, K., Gounder, A. G. N., and Borru, D. V. (2017). Analysis and control of induction generator supplying stand-alone ac loads employing a matrix converter. *Engineering Science and Technology, an International Journal*, 20(2):649–661.

Mangu, B., Akshatha, S., Suryanarayana, D., and Fernandes, B. (2016). Grid-connected pv-wind-battery-based multi-input transformer-coupled bidirectional dc-dc converter for household applications. *IEEE journal of emerging and selected topics in power electronics*, 4(3):1086–1095.

Merabet, A., Ahmed, K. T., Ibrahim, H., Beguenane, R., and Ghias, A. M. (2016). Energy management and control system for laboratory scale microgrid based wind-pv-battery. *IEEE transactions on sustainable energy*, 8(1):145–154.

Mishra, R., Banerjee, U., Sekhar, T. N., and Saha, T. K. (2019). Development and implementation of control of stand-alone pmsg-based distributed energy system with variation in input and output parameters. *IET Electric Power Applications*, 13(10):1497–1506.

Misra, H. and Jain, A. K. (2017). Analysis of stand-alone dfig-dc system and dc voltage regulation with reduced sensors. *IEEE Transactions on Industrial Electronics*, 64(6):4402–4412.

Misra, H. and Jain, A. K. (2018). Mathematical modeling and control of standalone dfig-dc system in rotor flux reference frame. *IEEE Transactions on Industrial Electronics*, 65(5):3708–3719.

Mohan, N., Undeland, T. M., and Robbins, W. P. (2003). *Power electronics: converters, applications, and design*. John wiley & sons.

Nayanar, V., Kumaresan, N., and Gounden, N. A. (2015). A single-sensor-based mppt controller for wind-driven induction generators supplying dc microgrid. *IEEE Transactions on Power Electronics*, 31(2):1161–1172.

Oliver, S. and Line, V. C. P. (2012). High-voltage DC distribution is key to increased system efficiency and renewable-energy opportunities. *Vicor White Paper*.

Prabhakaran, K., Karthikeyan, A., Varsha, S., Perumal, B. V., and Mishra, S. (2020). Standalone single stage pv-fed reduced switch inverter based pmsm for water pumping application. *IEEE Transactions on Industry Applications*, 56(6):6526–6535.

Prabhakaran, P. and Agarwal, V. (2018). Novel four-port dc–dc converter for interfacing solar pv–fuel cell hybrid sources with low-voltage bipolar dc microgrids. *IEEE Journal of Emerging and Selected Topics in Power Electronics*, 8(2):1330–1340.

Pradhan, S., Singh, B., Panigrahi, B. K., and Murshid, S. (2018). A composite sliding mode controller for wind power extraction in remotely located solar pv–wind hybrid system. *IEEE transactions on industrial electronics*, 66(7):5321–5331.

Prakash, S. L., Arutchelvi, M., and Jesudaiyan, A. S. (2016). Autonomous pv-array excited wind-driven induction generator for off-grid application in india. *IEEE Journal of Emerging and Selected Topics in Power Electronics*, 4(4):1259–1269.

Priyadarshi, N., Ramachandaramurthy, V. K., Padmanaban, S., and Azam, F. (2019). An ant colony optimized mppt for standalone hybrid pv-wind power system with single cuk converter. *Energies*, 12(1):167.

Radwan, A. A. A. and Mohamed, Y. A.-R. I. (2019). Grid-connected wind-solar cogeneration using back-to-back voltage-source converters. *IEEE Transactions on Sustainable Energy*, 11(1):315–325.

Ravada, B. R., Tummuru, N. R., and Ande, B. N. L. (2020). Photovoltaic-wind and hybrid energy storage integrated multi-source converter configuration for dc microgrid applications. *IEEE Transactions on Sustainable Energy*, 12(1):83–91.

Ravada, B. R., Tummuru, N. R., and Ande, B. N. L. (2021). A grid-connected converter configuration for the synergy of battery-supercapacitor hybrid storage and renewable energy resources. *IEEE Journal of Emerging and Selected Topics in Industrial Electronics*, 2(3):334–342.

Rezkallah, M., Chandra, A., Ibrahim, H., Ghandour, M., Taoufik, S., Feger, Z., and Savard, J.-f. (2022). Hardware implementation of cooperative multitasking control and stability analysis for dc off-grid system. *IEEE Transactions on Industry Applications*.

Rezkallah, M., Hamadi, A., Chandra, A., and Singh, B. (2017). Design and implementation of active power control with improved p&o method for wind-pv-battery-based

standalone generation system. *IEEE Transactions on Industrial Electronics*, 65(7):5590–5600.

Rezkallah, M., Singh, S., Chandra, A., Singh, B., Tremblay, M., Saad, M., and Geng, H. (2019). Comprehensive controller implementation for wind-pv-diesel based standalone microgrid. *IEEE transactions on industry applications*, 55(5):5416–5428.

Rodriguez-Diaz, E., Savaghebi, M., Vasquez, J. C., and Guerrero, J. M. (2015). An overview of low voltage dc distribution systems for residential applications. In *2015 IEEE 5th International Conference on Consumer Electronics-Berlin (ICCE-Berlin)*, pages 318–322. IEEE.

Saafan, A. A., Khadkikar, V., Edpuganti, A., El Moursi, M. S., and Zeineldin, H. H. (2023). A novel non-isolated four-port converter for flexible dc microgrid operation. *IEEE Transactions on Industrial Electronics*.

Samrat, N. H., Ahmad, N., Choudhury, I. A., and Taha, Z. (2015). Technical study of a standalone photovoltaic–wind energy based hybrid power supply systems for island electrification in malaysia. *PloS one*, 10(6):e0130678.

Sekhar, N. and Kumaresan, N. (2021). Operation and control of a stand-alone power system with integrated multiple renewable energy sources. *Wind Engineering*, page 0309524X211024126.

Sekhar, N. and Kumaresan, N. (2022). Operation and control of a stand-alone power system with integrated multiple renewable energy sources. *Wind Engineering*, 46(1):221–239.

Shanthi, P., Uma, G., and Keerthana, M. S. (2017). Effective power transfer scheme for a grid connected hybrid wind/photovoltaic system. *IET Renewable Power Generation*, 11(7):1005–1017.

Sharma, B., Dahiya, R., and Nakka, J. (2019). Effective grid connected power injection scheme using multilevel inverter based hybrid wind solar energy conversion system. *Electric Power Systems Research*, 171:1–14.

Singaravel, M. R. and Daniel, S. A. (2015). Mppt with single dc–dc converter and inverter for grid-connected hybrid wind-driven pmsg–pv system. *IEEE Transactions on Industrial Electronics*, 62(8):4849–4857.

Singh, S. et al. (2017). Selection of Non-Isolated DC-DC CONVERTERS for Solar PHOTOVOLTAIC SYSTEM. *Renewable and Sustainable Energy Reviews*, 76:1230–1247.

Solanki, C. S. (2015). *Solar Photovoltaics: Fundamentals, Technologies And Applications*. PHI Learning Pvt. Ltd.

Villalva, M., De Siqueira, T., and Ruppert, E. (2010). Voltage regulation of photovoltaic arrays: Small-signal analysis and control design. *IET Power Electronics*, 3(6):869–880.

Wandhare, R. G. and Agarwal, V. (2014). Novel integration of a pv-wind energy system with enhanced efficiency. *IEEE Transactions on Power Electronics*, 30(7):3638–3649.

Wu, B., Lang, Y., Zargari, N., and Kouro, S. (2011). *Power conversion and control of wind energy systems*. John Wiley & Sons.

Xiao, W., Dunford, W. G., Palmer, P. R., and Capel, A. (2007). Regulation of Photovoltaic Voltage. *IEEE Transactions on Industrial Electronics*, 54(3):1365–1374.

Yaramasu, V., Dekka, A., Durán, M. J., Kouro, S., and Wu, B. (2017). PMSG-based wind energy conversion systems: survey on power converters and controls. *IET Electric Power Applications*, 11(6):956–968.

Zhang, W., Liang, H., Bin, Z., Li, W., and Guo, R. (2012). Review of DC technology in Future Smart Distribution Grid. In *Innovative Smart Grid Technologies-Asia (ISGT Asia), 2012 IEEE*, pages 1–4. IEEE.

Zia, M. F., Nasir, M., Elbouchikhi, E., Benbouzid, M., Vasquez, J. C., and Guerrero, J. M. (2022). Energy management system for a hybrid pv-wind-tidal-battery-based islanded dc microgrid: Modeling and experimental validation. *Renewable and Sustainable Energy Reviews*, 159:112093.

Publications based on the thesis

International Journals

1. Anvit Khare and Karthikeyan Anabalagan, "A Single-Stage, Multi-Port Hybrid Power Converter Integrating PV and Wind Sources for a Standalone DC System",*MDPI-Energies-SI: Modeling, Topologies, and Modulation Techniques of Power Converters (DC/DC and DC/AC) for the Grid-Integration with Renewable Energy Sources)*, Aug. 2023.

CURRICULUM VITAE

Full Name: Anvit Khare
Date of Birth: 16-08-1993
E-mail: anvitkhare@yahoo.co.in
Mobile: +91-8238422816

Address
Research Scholar,
Department of Electrical & Electronics Engineering,
National Institute of Technology Karnataka (NITK),
Surathkal,
Srinivasnagar P.O.,
Surathkal, Mangalore–575 025, INDIA.

Educational Qualification

Degree	Specialization	Institute/University	Year
B.E.	Electrical Engineering	VGEC,Ahmedabad (Gujarat Technological University)	2011-2015
M.Tech	Power and Energy Systems	NITK, Surathkal	2015-2017
Pursuing Ph.D.	Power Electronics	NITK-Surathkal	2017-till date

Research Interests :

- Power electronics and control
- Renewable Energy systems

Society Memberships

- Student Member of IEEE

Software and Computer Proficiency

- Operating Systems: Windows .
- Simulation Packages: MATLAB/Simulink, PSIM/LTspice.

Interest and Activities

- Football
- Music